Dinoflagellate Cysts from the Upper Cretaceous (Upper Campanian to Lowermost Maastrichtian) of the Middle Vistula River Section, Poland

Taylor & Francis
Taylor & Francis Group

OPEN ACCESS   Check for updates

Dinoflagellate cysts from the Upper Cretaceous (upper Campanian to lowermost Maastrichtian) of the Middle Vistula River section, Poland

Mariusz Niechwedowicz [ID]

S.J. Thugutt Geological Museum, Faculty of Geology, University of Warsaw, Warsaw, Poland

ABSTRACT

In this article, the most representative dinoflagellate cyst genera and species recognised in the rich palynomorph assemblages of the upper Campanian–lowermost Maastrichtian succession of the Middle Vistula River section (central Poland) are treated taxonomically: in particular, six genera and 16 species are considered. *Oligosphaeridium araneum* sp. nov., which possesses processes with relatively long and slim stems and perforate or fenestrate terminations, is described as new. *Glaphyrocysta pala* comb. nov. and *Hystrichosphaeridium brevispinum* stat. nov. are proposed. *Glaphyrocysta pala* comb. nov. has a dorso-ventrally compressed central body and lacks mid-ventral processes connecting the central body with the membrane, suggesting its affinity with *Glaphyrocysta*, rather than *Riculacysta*; and *H. brevispinum* stat. nov. is raised to species rank on the basis of the distinct morphology of its processes. The tabulation pattern and plate arrangement are determined for the first time in *Amphorosphaeridium* and revised in *Callaiosphaeridium*. Both genera have a sexiform hypocystal configuration, L-type ventral organisation, and neutral torsion, which indicates their inclusion in the subfamily Leptodinioideae. The species-level taxonomy of the genera *Hystrichosphaeridium* and *Samlandia* is discussed. The transfer of *Hystrichosphaeridium proprium* to *Hystrichokolpoma* is rejected, and *Hystrichosphaeridium? recurvatum* is questionably left in *Hystrichosphaeridium*, although it is characterised by a commonly larger number of processes per plate and the lack of a preapical process.

1. Introduction

The rich and well-preserved organic-walled dinoflagellate cyst assemblages recovered from the Middle Vistula River section were found to include many biostratigraphically critical forms, which enabled the development of a refined dinoflagellate cyst-based biostratigraphical framework (Niechwedowicz and Walaszczyk 2021). The dinoflagellate cyst record, based on a dense sample set, revealed a narrow interval, immediately below the Campanian–Maastrichtian boundary, characterised by a distinctive taxonomic turnover in dinoflagellate cyst assemblages. This interval is marked by the extinction of a number of typically Campanian (and pre-Campanian) genera and species (*Xenascus* and some species of *Odontochitina*), and the appearance of typically Maastrichtian and younger (Paleogene) forms (of the genera *Cladopyxidium* and *Glaphyrocysta*). The documented Middle Vistula River dinoflagellate cyst succession (Niechwedowicz and Walaszczyk 2021) is consistent with both Boreal (Belgium and the Netherlands) and Tethyan Realm successions (southern Germany, south-west France, the northern Apennines), enabling reliable correlations. Of particular importance is the correspondence of the Polish material with the dinoflagellate cyst record documented in Tercis les Bains, south-west France [the Global Stratotype Section and Point (GSSP) for the base of the Maastrichtian Stage; see Odin and Lamaurelle

(2001)], supporting the correlation between the Boreal and Tethyan Realms inferred from macrofossils (Walaszczyk et al. 2002; Walaszczyk 2004; Machalski 2012a).

In total, 129 species- or subspecies-level dinoflagellate cyst taxa have been identified from the upper Campanian–lowermost Maastrichtian interval of the Middle Vistula River section (see Niechwedowicz and Walaszczyk 2021). Not all are treated herein. The present paper focuses on those species or genera that, in light of the present material, appear new to science, are in need of supplementary taxonomic treatment, or represent biostratigraphically critical forms. The 16 species and six genera discussed herein include the description of a new species, *Oligosphaeridium araneum* sp. nov., a discussion on some stratigraphically important species of the genus *Samlandia*, the transfer of a *Riculacysta* species to *Glaphyrocysta*, a discussion on tabulation patterns and systematic positions in the genera *Amphorosphaeridium* and *Callaiosphaeridium*, and species-level taxonomy in the genus *Hystrichosphaeridium*. Three additional new dinoflagellate cyst species from the Campanian–Maastrichtian boundary interval of the Middle Vistula section, *Odontochitina dilatata*, *Callaiosphaeridium bicoronatum*, and *Samlandia paucitabulata*, were recently described (Niechwedowicz 2018a, and in Niechwedowicz and Walaszczyk 2021).

CONTACT Mariusz Niechwedowicz   niechwedowicz.m@uw.edu.pl   S.J. Thugutt Geological Museum, Faculty of Geology, University of Warsaw, ul. Żwirki i Wigury 93, 02-089 Warszawa, Poland.
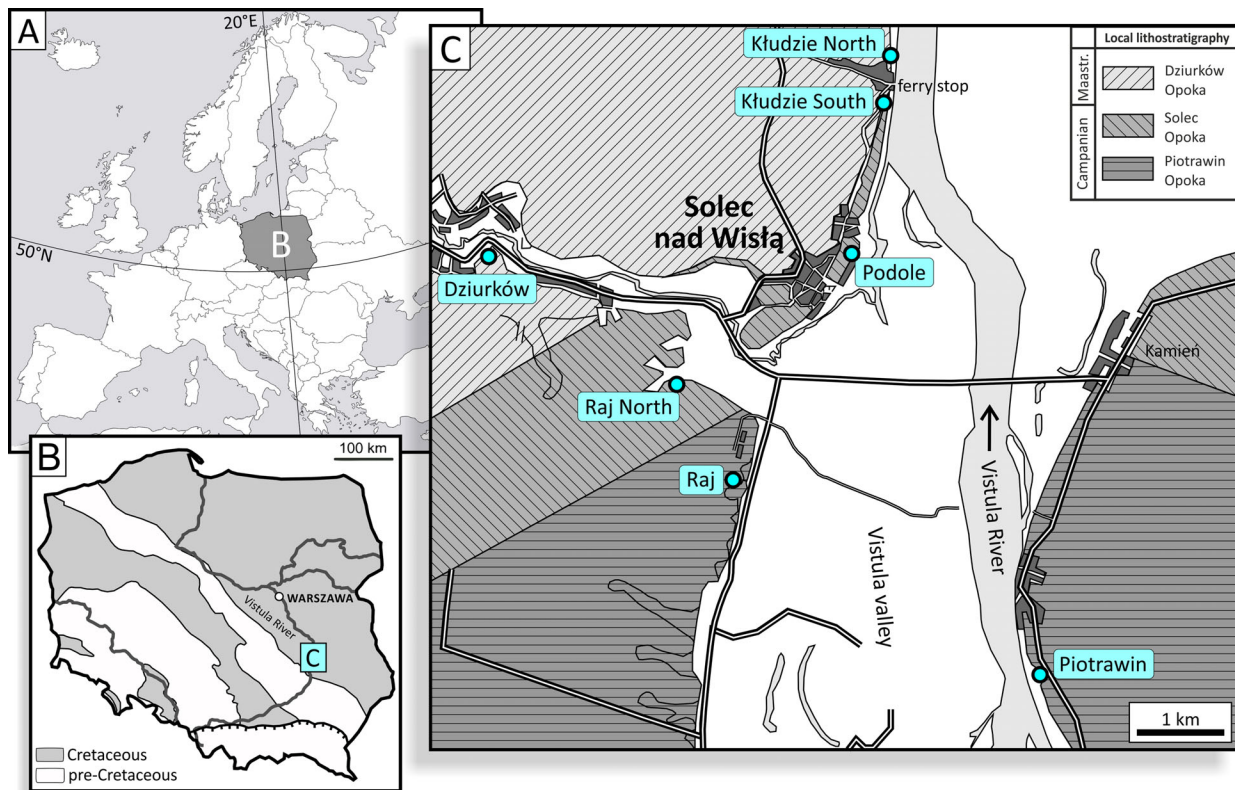
Figure 1. Middle Vistula River section in Europe (A), and Poland (B; geological sketch map of Poland without Cenozoic cover after Pożaryski (1974)), and locations of the studied sections (C) within a geological map of the upper Campanian–lowermost Maastrichtian part of the Middle Vistula River section (modified from Walaszczyk 2004).

2. Stratigraphical framework

The Middle Vistula River composite section consists of middle Albian to Danian strata and is accessible in a series of outcrops located along the Middle Vistula River valley (Pożaryski 1938; Marcinowski and Radwański 1983; Walaszczyk 1992, 2004). The Upper Cretaceous succession is quite complete, with small hiatuses mostly present in the lower part (Marcinowski 1980; Walaszczyk 1987). The upper Campanian–lowermost Maastrichtian interval treated in this study is exposed near the town of Solec nad Wisłą (Figure 1). Due to the rather monotonous siliceous marl (referred to locally as opoka; see Jurkowska et al. 2019) facies development of the succession, lithological correlations between particular sections in this interval are not reliable: the sole exception is a single marly layer, the so-called 'boundary marl' at the Campanian/Maastrichtian boundary (Figure 2; Walaszczyk 2004). Fortunately, the succession is highly fossiliferous, yielding a variety of biostratigraphically significant groups, including both macro- and microfossils (Walaszczyk 2012, 2015). The modern biozonal schemes developed for the section, based on inoceramid bivalves (Walaszczyk 2004), ammonites (Machalski 2012b), belemnites (Keutgen et al. 2012; Remin 2012, 2015), foraminifers (Dubicka and Peryt 2012; Dubicka in Walaszczyk et al. 2016), and dinoflagellate cysts (Niechwedowicz and Walaszczyk 2021), provide reliable stratigraphical control (Figure 2). Beyond biostratigraphy, the succession also contains good $\delta^{13}C$ (Voigt in Keutgen et al.

2012) and palaeomagnetic signals (Plasota et al. 2015). For a more detailed historical review of stratigraphical studies conducted in the area, the reader is referred to Walaszczyk (2004, 2012).

3. Material and methods

The sampled portion of the Campanian–Maastrichtian boundary interval of the Middle Vistula River composite section consists of the following exposures (in ascending stratigraphical order): Piotrawin, Raj, Podole, Raj North, Kłudzie North, Kłudzie South, and Dziurków (Figures 1C and 2). Their characteristics are summarised in Table 1. A total of 183 samples were collected, taken at 1 m intervals on average; denser sampling (down to 25 cm resolution) was conducted in the Campanian–Maastrichtian boundary interval and in strata critical for the inter-section correlation of particular exposures (Figure 2).

The palynological material was extracted from 95–105 g of dry sediment; in rare cases, only 20–50 g of sample were available. The samples were processed using a standard palynological preparation technique, including 30% hydrochloric and 70% hydrofluoric acid treatments, with repeated decantation; oxidation, ultrasonic treatment, and heavy-liquid separation were not used. The extracted organic residues were sieved through a 15 µm nylon mesh and concentrated via centrifugation. A drop of residue from each sample was mounted on a slide using glycerin jelly, overlain with a
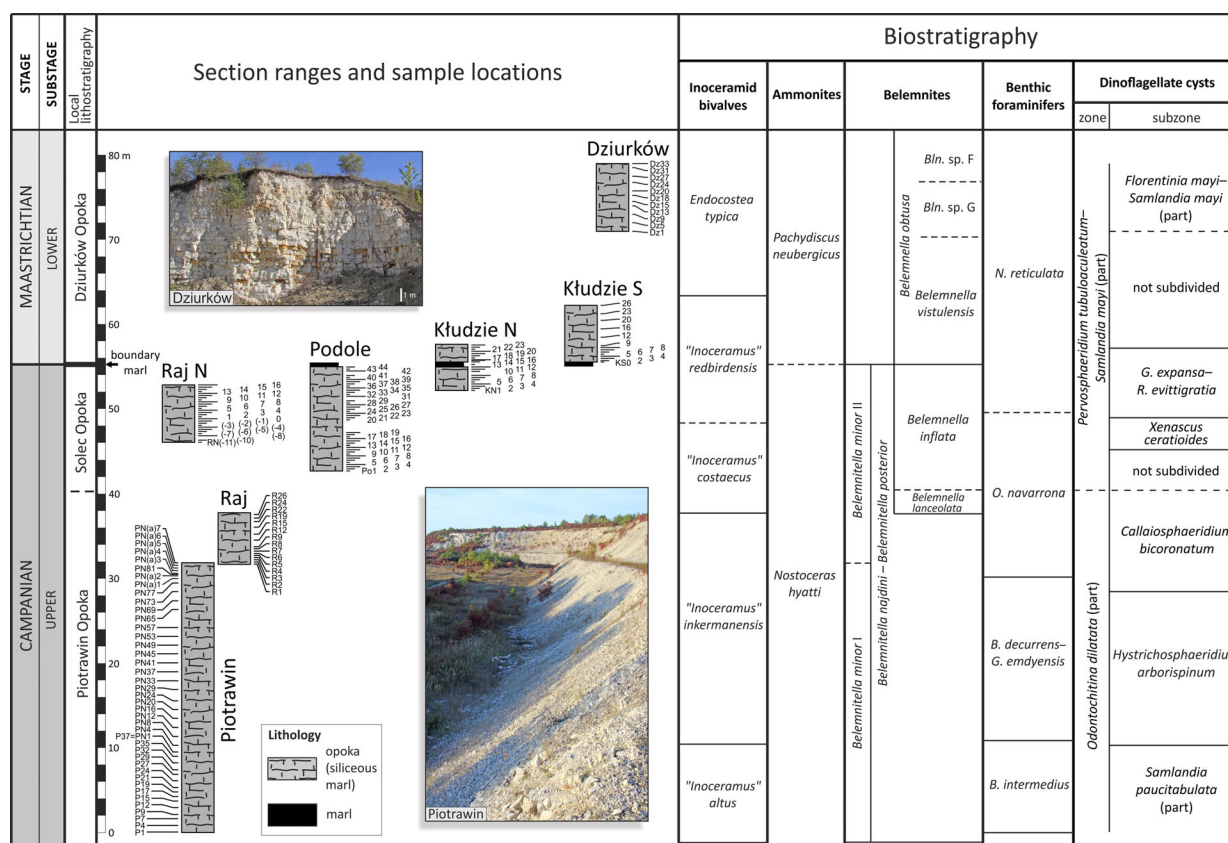
Figure 2. Stratigraphy of the upper Campanian–lowermost Maastrichtian succession of the Middle Vistula River composite section. Lithostratigraphy after Walaszczyk (2004); ranges of sections studied and sample locations after Niechwedowicz and Walaszczyk (2021). Biostratigraphy: inoceramid bivalves (after Walaszczyk 2004), ammonites (Machalski 2012b), belemnites (Remin 2012, 2015), benthic foraminifers (Dubicka in Walaszczyk et al. 2016), and dinoflagellate cysts (Niechwedowicz and Walaszczyk 2021). Position of the Campanian–Maastrichtian boundary as defined at the Global Stratotype Section and Point in Tercis.

20 × 20 mm coverslip, and sealed with clear varnish; at least two slides per sample were prepared. Identification of palynomorphs was conducted under a transmitted light microscope (TLM). The most important specimens were documented using both a TLM (equipped with a digital video camera) and scanning electron microscopy (SEM), where possible; SEM was performed at the NanoFun Cryo-SEM Laboratory (Faculty of Geology, University of Warsaw, Warsaw, Poland), with Zeiss AURIGA 60 and Zeiss SIGMA VP scanning electron microscopes. The captions for each illustrated specimen include both slide number and microscope coordinates. The coordinates were provided from the vernier scale of the microscope (0.1 mm accuracy), consisting of a pair of horizontal/vertical coordinates measured from the 0/0 reference point (the bottom left corner of the coverslip marked on each slide). England Finder (EF) coordinates were computed using the England Finder Calculator (see González 2012). For specimens mounted on SEM stubs, only EF coordinates are provided. The taxonomy is after Fensome et al. (1993) and Fensome et al. (2019a), with additions from Pearce and Williams (2018) and Niechwedowicz and Walaszczyk (2021). The descriptive terminology follows Evitt (1985), Williams et al. (2000), and Fensome et al. (2009). The 'para' terminology is not used here for the reasons suggested by Fensome et al. (2009, p. 8). The organic residues, palynological slides, and SEM stubs are lodged at the S.J. Thugutt Geological Museum, Faculty of Geology, University of Warsaw, Warsaw, Poland (MWGUW).

4. Systematic palaeontology

Division **DINOFLAGELLATA** (Bütschli 1885) Fensome et al. 1993
Subdivision **DINOKARYOTA** Fensome et al. 1993
Class **DINOPHYCEAE** Pascher 1914
Subclass **PERIDINIPHYCIDAE** Fensome et al. 1993
Order **GONYAULACALES** Taylor 1980
Suborder **GONYAULACINEAE** (autonym)
Family **GONYAULACACEAE** Lindemann 1928
Subfamily **LEPTODINIOIDEAE** Fensome et al. 1993

Genus *Amphorosphaeridium* Davey 1969 emend. nov.

Synonymy.
1969 *Amphorosphaeridium* Davey: p. 30.
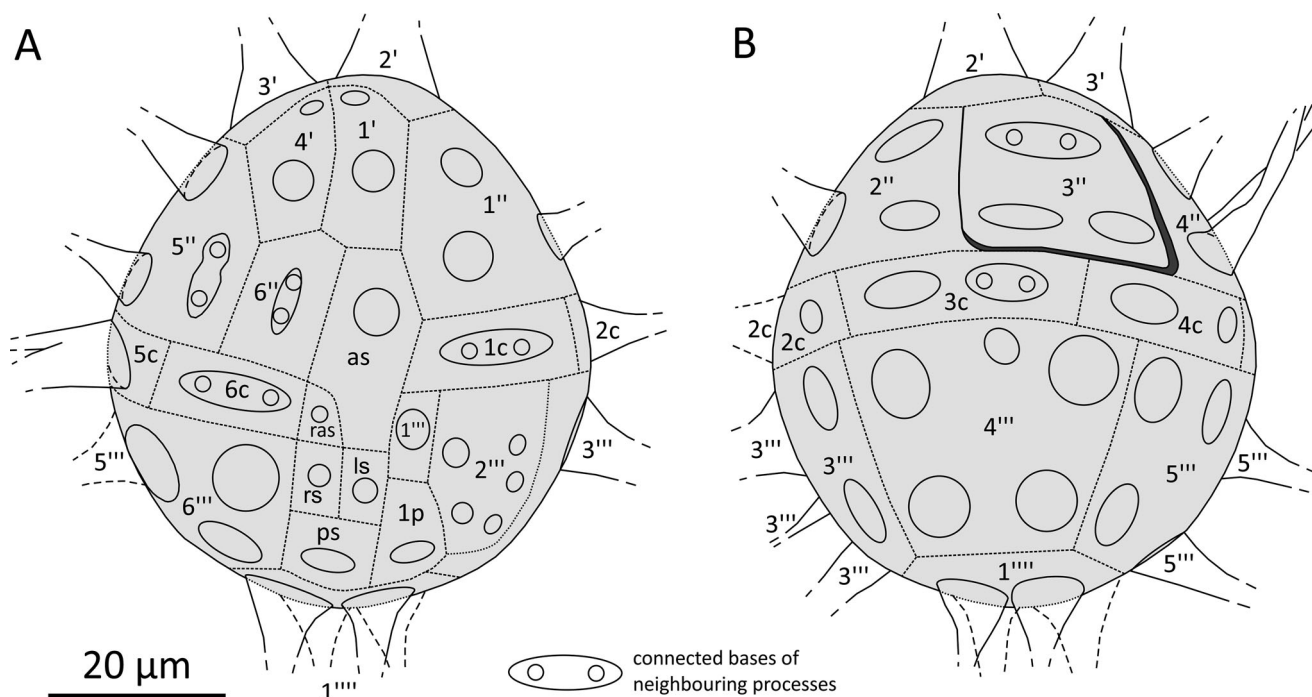1978 *Amphorosphaeridium* Davey 1969 – Stover & Evitt: p. 140, 141.

Type. *Amphorosphaeridium fenestratum* Davey 1969.

Emended diagnosis. Gonyaulacacean (leptodinioid) chorate cysts of intermediate size, with subspheroidal to ovoidal central body and numerous processes. Central body and process walls are more or less fibrous. The processes are relatively

Table 1. Characteristics of the exposures studied herein (listed in descending stratigraphical order), belonging to the Middle Vistula River composite section.

Exposure	Location	Exposure type	Local lithostratigraphy (succession thickness)	Biostratigraphy		
				Inoceramid bivalves (Walaszczyk 2004)	Belemnites (Remin 2012, 2015)	Dinoflagellate cysts (Niechwedowicz and Walaszczyk 2021)
Dziurków (51°08′18″N, 21°42′54″E)	Near the eastern end of the village of Dziurków	Small working quarry	Dziurków Opoka (c. 8 m)	*E. typica* Zone	Middle *B. obtusa* Zone (= *B.* sp. G and *B.* sp. F subzones)	*F. mayi–S. mayi* Subzone
Kłudzie South (51°09′09″N, 21°46′44″E)	Western bank of the Vistula River, about 100 m south of the Kłudzie Ferry stop	Cliff section	Dziurków Opoka (c. 8 m); the 'boundary marl' is located in the basal part of the section	Upper part of the '*I.*' *redbirdensis* Zone	Lower part of the *B. vistulensis* Subzone	Basal part of exposure corresponds to uppermost *G. expansa–R. evittigratia* Subzone
Kłudzie North (51°09′18″N, 21°46′45″E)	Western bank of the Vistula River, 50 m north of the Kłudzie Ferry stop	Cliff section	Solec and Dziurków Opoka (c. 6 m), separated by the 'boundary marl'	Middle part of the '*I.*' *redbirdensis* Zone	Uppermost *B. inflata* Zone and lowermost *B. vistulensis* Subzone	Upper part of the *G. expansa–R. evittigratia* Subzone
Raj North (51°07′33″N, 21°44′51″E)	Southern bank of the Krępianka River, c. 1.5 km south-east of the town of Solec nad Wisłą	Small working quarry	Solec Opoka (7 m)	'*I.*' *costaecus* and '*I.*' *redbirdensis* zones	Upper part of the *B. inflata* Zone	*X. ceratioides* and lower *G. expansa–R. evittigratia* subzones
Podole (51°08′15″N, 21°46′22″E)	Western bank of the Vistula River, 200 m south of the village of Podole	Cliff section	Solec Opoka (13 m); the 'boundary marl' is present at the topmost part of the exposure	Upper part of the '*I.*' *costaecus* Zone and lower part of the '*I.*' *redbirdensis* Zone	*B. inflata* Zone	*X. ceratioides* and *G. expansa–R. evittigratia* subzones
Raj (51°06′52″N, 21°45′19″E)	Western bank of the Vistula River, c. 100 m south of the southern end of the village of Raj	Small abandoned quarry	Piotrawin Opoka (6 m)	Upper part of the '*I.*' *inkermanensis* Zone	Lower third of the *B. minor* II Zone	Upper part of the *C. bicoronatum* Subzone
Piotrawin (51°05′37″N, 21°48′06″E)	Eastern bank of the Vistula River, c. 500 m south of the village of Piotrawin	Large abandoned quarry with three exploitation levels	Piotrawin Opoka (c. 32 m)	'*I.*' *altus* (lower level), and '*I.*' *inkermanensis* (middle and upper levels) zones	*B. minor* I Zone	*S. paucitabulata* to lower *C. bicoronatum* subzones

Figure 3. *Amphorosphaeridium fenestratum* Davey 1969 (specimen also illustrated in Plate 1, figures 1–8) with attached operculum (plate 3″), showing the distribution of processes and inferred tabulation. A, ventral view; B, dorsal view. Note the sexiform antapex, L-type ventral arrangement, and neutral torsion of the hypocyst (the boundaries between plates 3″/4″ and 4‴/5‴ are more or less in line), indicating a leptodinioid pattern.

robust, generally tapering and hollow, occasionally solid (or partially solid), intratabular, one to five per plate area; neighbouring processes sometimes are joined proximally or are completely fused. Apical and antapical prominences are occasionally present, expressed by enlarged (widened or fused) processes. The tabulation formula is 4′, 6″, 6c, 6‴, 1p, 5 s, 1‴′, more or less clearly expressed by distribution of the processes, indicating sexiform antapex, L-type ventral plate arrangement, and neutral torsion of the hypocyst. The archaeopyle is precingular, type 1 P (3″), operculum is free or attached.

Remarks. The diagnosis of the genus is here emended to emphasise the leptodinioid tabulation pattern recognised in the type species (see Figure 3; Plate 1, figures 1–12). Although Davey (1969) did not recognise the tabulation pattern in *A. fenestratum*, and it cannot be clearly inferred from illustrations of the holotype alone (Davey 1969, pl. 3, figs 1, 2), he noticed some process alignment in the type species (Davey 1969, p. 31). In overall morphology, *Amphorosphaeridium* most resembles *Exochosphaeridium* Davey et al. 1966, which, however, belongs to the subfamily Cribroperidinioideae (see Helenes 2000, p. 137, 138, 140; Fensome et al. 2009, p. 31). Peyrot (2011, p. 284) synonymised *Amphorosphaeridium fenetratum* of Davey 1969, pl. 3, figs 1, 2 (the holotype of the species and the type species of the genus) with *Exochosphaeridium majus* (Lejeune-Carpentire 1940) Peyrot 2011, indicating the synonymy of the two genera, although not *expressis verbis*. However, the two species differ significantly: the processes in *E. majus* are solid or hollow (more commonly solid), whereas *A. fenestratum* generally bears hollow processes (only the slimmest, mainly sulcal processes may be solid distally, but proximally they are hollow). Furthermore,

in *E. majus* the antapical prominence is never developed, while *A. fenestratum* may bear prominences at both poles.

Comparison. Similarly to *Amphorosphaeridium*, the genus *Exochosphaeridium* has fibrous (or fibro-pitted) central body wall and processes, but the two genera differ in the development of processes and their distribution. In *Exochosphaeridium* the processes are generally more slender; they are commonly acuminate or hair-like and generally solid. Hollow processes, when present, are usually hollow only proximally. Occasionally, *Exochosphaeridium* possesses an enlarged apical process, sometimes irregularly branched distalward (see Plate 1, figure 16). Furthermore, the processes in *Exochosphaeridium* are generally nontabular, rarely contabular, vaguely indicating the tabulation (recognised in only single species, *E. alisitosense*; see Helenes 2000). In contrast, processes in *Amphorosphaeridium* are more robust, distinctly hollow, and less fibrous, and their arrangement more clearly indicates tabulation. Moreover, *Amphorosphaeridium* may possess prominences at both poles. *Fibrocysta* Stover & Evitt 1978 has an ellipsoidal central body, generally horn-like protrusions at the cyst poles, and more slender processes. *Cordosphaeridium* Eisenack 1963b has fewer processes (1 meso- to obtabular process per plate; Fensome et al. 2009). *Operculodinium* Wall 1967 has generally solid processes, which usually are uniform in size and shape, and tend to be isolated. *Turbiosphaera* Archangelsky 1969a has fewer, intratabular (one per plate), wider, and taeniate processes.

Amphorosphaeridium fenestratum Davey 1969 emend. nov.
Figure 3; Plate 1, figures 1–12

Synonymy.
1969 *Amphorosphaeridium fenestratum* Davey: p. 30–32, pl. 1, fig. 6, pl. 2, figs 2, 4, pl. 3, figs 1–3, text-fig 1.2a–e.
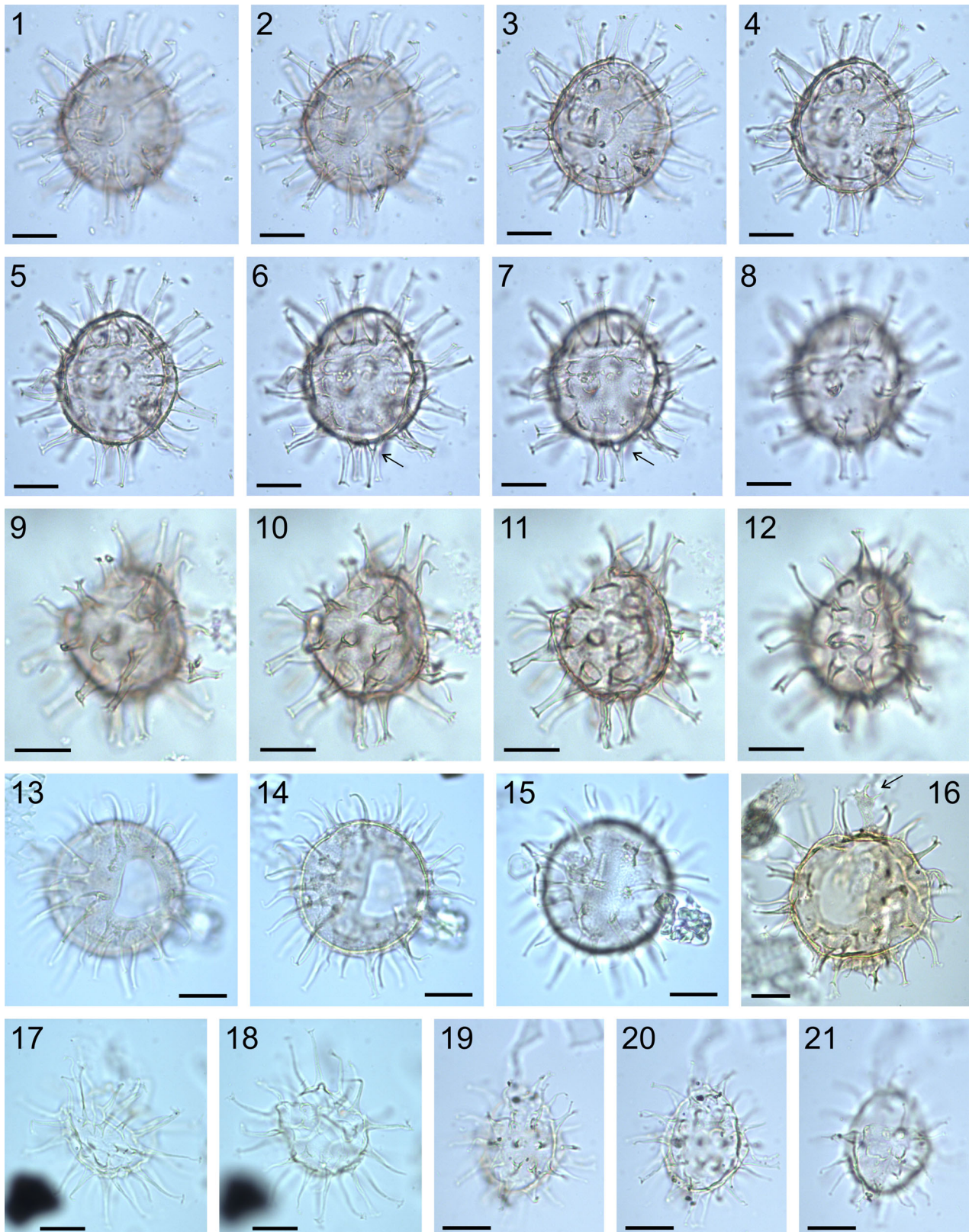
Plate 1. Dinoflagellate cysts from the upper Campanian–lowermost Maastrichtian of the Middle Vistula River section, central Poland. All photomicrographs taken with a transmitted light microscope; scale bars = 20 μm. 1–12. *Amphorosphaeridium fenestratum* Davey 1969. 1–8. MWGUW ZI/90/Dz5/0a, 14.5/18, EF F30/4; ventral view of ventral (1–3) and dorsal (6–8) surfaces, and optical section (4, 5), operculum attached (see also Figure 3); arrows indicate a partial fusion of antapical processes. 9–12. MWGUW ZI/90/Dz9/0a, 1/13.2, EF L17/0; right lateral view of right lateral (9, 10) and left lateral (12) surfaces, and optical section (11). 13–16. *Exochosphaeridium majus* (Lejeune-Carpentier 1940) Peyrot 2011. 13–15. MWGUW ZI/90/P9/0, 5.9/3.5, EF W21/2; oblique dorsal view of dorsal (13) and ventral (15) surfaces, and optical section (14); note the lack of a prominent apical process. 16. MWGUW ZI/90/Dz33/0a, 12.4/2.6, EF W28/1; dorsal view of optical section; note the prominent, distally branched apical process (indicated by arrow). 17, 18. *Pervosphaeridium elegans* Louwye 1997, MWGUW ZI/90/Po26/0, 14.2/3.2, EF W31/0; oblique ventral view of ventral (17) and dorsal (18) surfaces. 19–21. *Pervosphaeridium tubuloaculeatum* Slimani 1994, MWGUW ZI/90/Po12/0b, 6.7/10.2, EF O23/3; ventral view of ventral (19) and dorsal (21) surfaces, and optical section (20).

1969 *Amphorosphaeridium fenestratum* var. *dividum* Davey: p. 32, 33, pl. 2, figs 5, 6, text-fig. 2.
1973 *Amphorosphaeridium fenestratum* subsp. *fenestratum* (autonym) – Lentin & Williams: p. 13.
1973 *Amphorosphaeridium fenestratum* subsp. *dividum* (Davey 1969) Lentin & Williams: p. 13.

Emended diagnosis. Gonyaulacacean (leptodinioid) chorate cysts of intermediate size, with ovoidal central body, and numerous, relatively long and robust processes. Central body and process walls are more or less fibrous. The processes are generally hollow, intratabular, one to five per plate area; neighbouring processes may be joined. Apical and antapical prominences are occasionally present, expressed by enlarged processes. The tabulation is indicated by the archaeopyle and arrangement of the processes. The archaeopyle is precingular, type 1 P (3′′), operculum is free or attached.

Emended description. Chorate cysts of intermediate size, with ovoidal central body and numerous (c. 60) robust processes. Central body wall and process walls are more or less fibrous (or fibro-pitted). The processes are constant in length (c. 1/3–1/2 of central body diameter), but vary in width; generally tapering and hollow throughout entire length, rarely acuminate and distally solid (most commonly sulcal processes). The processes are relatively wide proximally, typically with circular bases, and tapering, distally only slightly expanded, terminating with aculeate tip. The processes are intratabular, commonly arranged in latitudinal and meridional rows. The processes arising from the larger pre- and postcingular plates are commonly penitabular. Process distribution is more or less uniform; the number of processes per plate (1–5) depends on the plate size and position on cyst: one process per 1p plate and each sulcal plate, 1–3 processes per smaller plate of other types (6′′, 1′′′, cingular, and apical plates), 3–5 processes per larger plate (rest of pre- and postcingulars, and antapical plate). Neighbouring processes occupying particular plates sometimes are connected proximally, or are completely fused. Apical and antapical prominences are occasionally evident, expressed by enlarged (widened) process. The tabulation formula is 4′, 6′′, 6c, 6′′′, 1p, 5 s (ps, ls, rs, ras, as), 1′′′′, more or less clearly expressed by the distribution of the processes, indicating leptodinioid pattern (sexiform antapex, L-type ventral plate arrangement, and neutral torsion of the hypocyst). The archaeopyle is precingular, type 1 P (3′′), operculum is free or attached.

Dimensions (minimum (mean) maximum).
Central body length: 49 (57.8) 65 µm, central body width: 43 (51.7) 59 µm, process length: 16 (20.9) 23 µm, total cyst length: 82 (95.4) 106 µm, total cyst width: 76 (87) 96 µm, process length/central body width ratio: 0.34 (0.42) 0.48 (11 specimens measured).

Remarks. The ovoidal shape of the central body, the presence of the 1 P archaeopyle and the distribution of processes (arranged in latitudinal and meridional rows, sulcal processes typically slimmer than others and distally solid, except for those occupying plates as and ps) make the cyst orientation easy to determine. The processes in *A. fenestratum* are of constant length, but occasionally exhibit significant variability

in width on a single specimen. Essentially, the processes have circular bases, and their number per particular plate is constant. However, some of the neighbouring processes occupying the same plate area may connect proximally or may be almost completely fused; such processes have wider bases (oval, elliptical, or subangular in cross-section), and have two or more tips (Plate 1, figures 9–11). The subspecies differentiation of Davey (1969) is confusing, since in both subspecies the processes may be branched/connected (see Davey 1969, p. 31–33). The degree of process fusion in *A. fenestratum* is considered intraspecifically variable and, consequently, the two subspecies are synonymised herein.

Peyrot (2011, p. 284, 289) included the specimens of *A. fenestratum* that lack enlarged antapical process (including the holotype – see Davey 1969, pl. 3, figs 1, 2) into *Exochosphaeridium majus*, significantly broadening its concept. The concept of *Amphorosphaeridium* refers to the presence of prominences at both poles (Davey 1969, p. 30), but this is not the most distinctive feature of *A. fenestratum*, in which the prominences may be absent or difficult to recognise. Based on the material studied herein, a single enlarged process at the apex may be one of the apical processes (e.g. the process occupying plate 2′, as in the specimen in Figure 3; Plate 1, figures 4–7), which does not occupy the central polar position. The antapical pole of the same specimen is characterised by the presence of four processes, none of which are enlarged (significantly wider) or occupy the central polar position. The distinction of the antapical prominence in this case may be marked by a partial fusion of processes (Plate 1, figures 6, 7). It appears that the processes occupying plate 1′′′′ may be completely fused, forming one relatively wide process. This would explain the presence or absence of an antapical prominence in the type material (see Davey 1969, pl. 1, fig. 6, pl. 2, fig. 4, pl. 3, figs 1–3). In contrast, *Exochosphaeridium* may bear only one prominence (an enlarged apical process, commonly branched or expanded distally; see Plate 1, figure 16); but, as in *Amphorosphaeridium*, it is not always present. Thus, the most characteristic feature of *A. fenestratum* is the development of processes and their arrangement, in which it clearly differs from *E. majus* (Plate 1, figures 13–16). Consequently, the synonymy proposed by Peyrot (2011) is rejected.

Comparison. *Exochosphaeridium majus* (Lejeune-Carpentier 1940) Peyrot 2011 (see Plate 1, figures 13–16) most resembles *Amphorosphaeridium fenestratum*, both in overall appearance and in its fibrous (or fibro-pitted) wall. What differentiates the two species is the process development. In *A. fenestratum*, processes are usually relatively wide and distinctly hollow throughout their entire length; by contrast, *E. majus* bears solid and hollow processes, but the latter are commonly acuminate, being hollow only proximally (if at all). Furthermore, the processes in *E. majus* are not arranged in a manner indicating tabulation. *Amphorosphaeridium fenestratum* may bear apical and antapical prominences, while *E. majus* may bear only the apical one. *Pervosphaeridium elegans* Louwye 1997 and *P. tubuloaculeatum* Slimani 1994 also resemble *A. fenestratum* in possessing hollow processes. *Pervosphaeridium elegans* (Plate 1, figures 17, 18) differs in having more slender and relatively longer (c. 3/4 of central
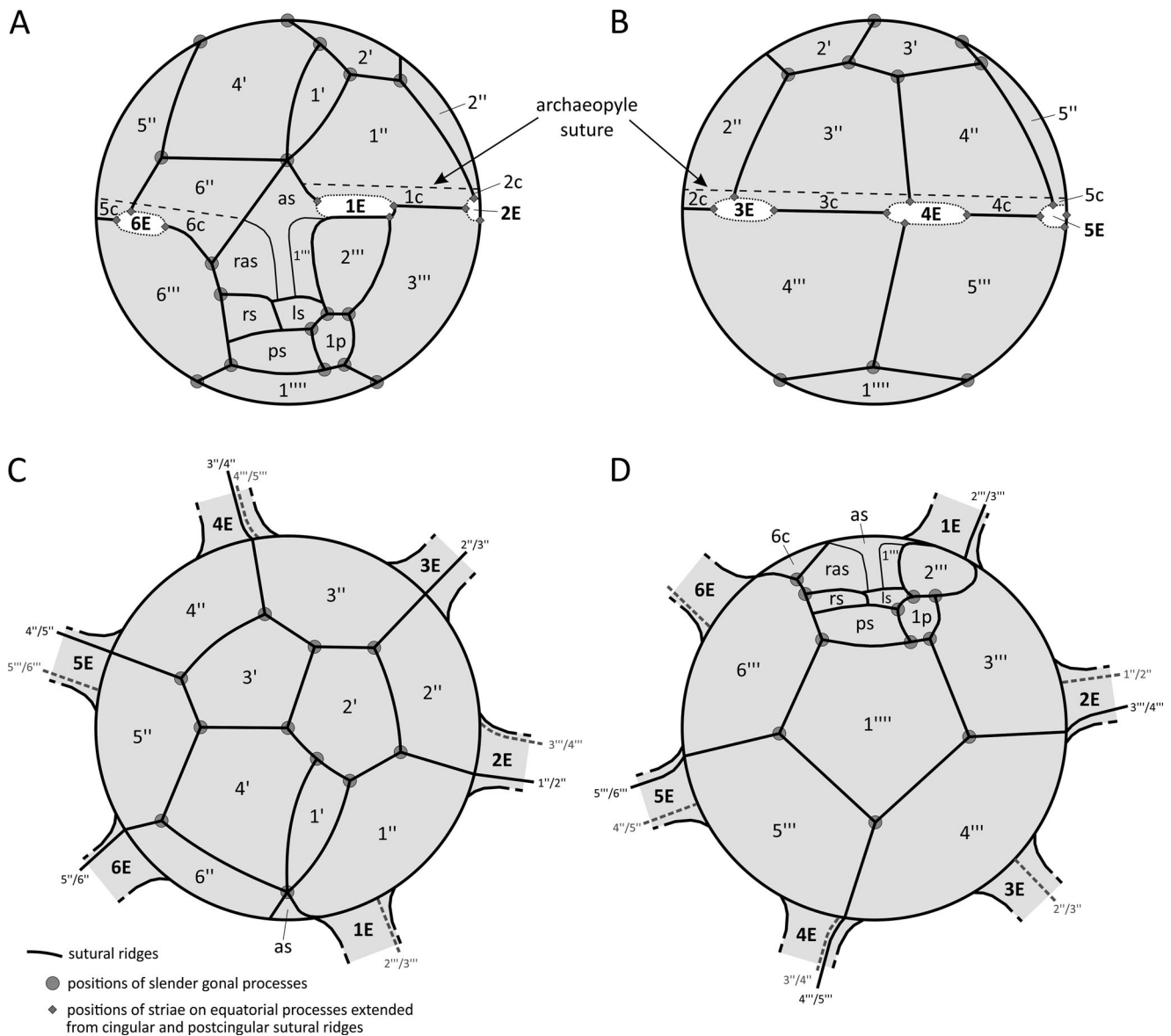
Figure 4. Tabulation in *Callaiosphaeridium asymmetricum* (Deflandre & Courteville 1939) Davey & Williams 1966. Note the leptodinioid pattern, indicated by the sexiform hypocystal plate arrangement, L-type ventral organisation, and neutral torsion of the hypocyst (sutures between plates 3″/4″ and 4‴/5‴ are in line); E = equatorial tubular processes. A, ventral view; B, dorsal view; C, apical view; D, antapical view.

body diameter) processes, constant in width on individual specimens (except for the sulcal processes) and never connected proximally. *Pervosphaeridium tubuloaculeatum* (Plate 1, figures 19–21) is significantly smaller, and it can be distinguished by the morphology of its processes (degree of tapering of the processes and their termination type). Furthermore, *Pervosphaeridium* has an archaeopyle of type 2 P.

Recorded stratigraphical range. Middle upper Campanian–lowermost Maastrichtian, '*Inoceramus*' *altus* Zone–lower *Endocostea typica* Zone (recorded in Piotrawin, Podole, Kłudzie North, Kłudzie South, and Dziurków).

Genus ***Callaiosphaeridium*** Davey & Williams 1966 emend. nov.

Synonymy.
1966 *Callaiosphaeridium* Davey & Williams: p. 103.
1967 *Hexasphaera* Clarke & Verdier: p. 42 (illegitimate name).

1978 *Callaiosphaeridium* Davey & Williams 1966 – Stover & Evitt: p. 202.
1980 *Callaiosphaeridium* Davey & Williams 1966 – Duxbury: p. 113.
1983 *Callaiosphaeridium* Davey & Williams 1966 – Duxbury: p. 40.
2009 *Callaiosphaeridium* Davey & Williams 1966 – Fensome, Williams, & MacRae: p. 17, 18.
2016 *Callaiosphaeridium* Davey & Williams 1966 – Fensome, Williams, & Nøhr-Hansen: p. 30.

Type. *Callaiosphaeridium asymmetricum* (Deflandre & Courteville 1939) Davey & Williams 1966.

Emended diagnosis. Gonyaulacacean (leptodinioid) chorate cysts with subspheroidal to ovoidal central body, bearing gonal (processes) and sutural (ridges, septa, processes) features, clearly reflecting plate arrangement. The processes are of two types: (i) six prominent equatorial processes (tubular,

broad, distally open) in gonal positions; and (ii) simple processes (solid, slender, or taeniate) in gonal or intergonal positions, located elsewhere on epi- and hypocyst excluding cingulum. Processes of both types commonly are connected by sutural septa of variable height (not higher than the processes), with distal margin entire or irregular; septa sometimes are distally supported by thickening (transverse ridge parallel to plate suture). The archaeopyle is epicystal.

Emended description. Chorate cysts with subspheroidal to ovoidal central body, bearing gonal (rarely intergonal) processes, sutural ridges and septa; suturocavate. Epi- and hypocyst are of similar size, or epicyst is slightly smaller. The central body surface is internally smooth, and externally it is smooth, scabrate, or rugulate, with plate margins smooth and often perforate in regular manner (lines of perforations parallel to plate boundaries); septa and processes are generally smooth. The processes are of two types: (i) six equatorial processes, tubular, broad, located in gonal positions between cingular and postcingular plate series; and (ii) slender processes, predominantly gonal, rarely intergonal, positioned elsewhere on epi- and hypocyst, except for the anterior and posterior margin of the cingulum. The equatorial processes are distinct, tubiform, distally flared, and open, terminating with few spines, or with low crests with incorporated numerous short spines. The equatorial processes bear more or less expressed longitudinal striae (three or four) extending from postcingular and cingular sutures. The slender gonal processes are generally solid (sometimes partially hollow), resulting from merging of sutural septa at gonal points; distally they are commonly furcate, occasionally with additional bifurcation of second order. The intergonal processes, if present, are taeniate. Equatorial and slender processes are connected by a more or less complete network of sutural ridges and septa of variable height (not higher than the processes); equatorial processes are sometimes interconnected basally by low septa or septum-like hollow membranous structures. Septa have entire or irregular distal margin, in the latter case forming taeniate intergonal processes; distally septa may be supported by thickening (transverse ridge parallel to plate suture), crowned with short spines incorporated into low crests. The tabulation formula is 4′, 6′′, 6c, 6′′′, 1p, 5 s, 1′′′′, expressed by the archaeopyle and arrangement of gonal and sutural features, indicating leptodinioid pattern (sexiform hypocystal configuration, L-type ventral organisation, and neutral torsion of the hypocyst; see Figure 4); sutural ridges between apical and sulcal plates may be reduced or absent. The archaeopyle is epicystal (formula $A_{1-4'} + P_{1-6''}$), operculum is free or attached ventrally.

Remarks. The present emendation emphasises the leptodinioid tabulation pattern, the gonal nature of the tubular processes, and variability in the development of septa and processes in *Callaiosphaeridium*. The sutural features indicating tabulation in *Callaiosphaeridium* may be present at almost all plate boundaries, but may be only partially developed or absent in the sulcal and apical regions (see also Duxbury 1983, pl. 5, fig. 12, text-fig. 18; Khowaja-Ateequzzaman and Garg 2004, pl. 1, fig. 7). The sutural ridge

is also absent from the anterior margin of the cingulum (the boundary between the precingular and cingular series is defined by the archaeopyle suture), but contrary to Davey and Williams (1966, p. 103) and Evitt (1985, p. 244), the posterior margin of the cingulum and the boundaries between particular cingular plates are clearly defined by low sutural ridges (Plate 2, figures 1–5; Plate 3, figures 5–7; Plate 4, figure 17; Plate 5, figures 3, 4, 7–10). These plate boundaries may, however, be poorly visible on specimens in apical or antapical views, which is quite common in the case of *Callaiosphaeridium* specimens lacking the operculum. The distribution of sutural and gonal features in *Callaiosphaeridium asymmetricum* (Deflandre & Courteville 1939) Davey & Williams 1966 clearly indicates the leptodinioid affinity of this genus. This is suggested by a sexiform hypocystal configuration (plate 1′′′′ is in contact with six plates, i.e. ps, 1p, 3′′′–6′′′; see Plate 2, figures 13, 16), L-type ventral organisation (longitudinal, more or less straight sulcus; Plate 2, figures 13, 14), and neutral torsion (boundaries between plates 3′′/4′′ and 4′′′/5′′′ are in line; Plate 2, figures 16, 17; Plate 3, figures 1, 2). A similar pattern was also observed in *C. bicoronatum* Niechwedowicz in Niechwedowicz & Walaszczyk 2021 (see Plate 5, figures 5–12, 16, 18).

The processes in *Callaiosphaeridium* are mainly gonal (including the large tubular ones), and rarely intergonal (these are present only in *C. trycherium*). The characteristic six equatorial processes in *Callaiosphaeridium* are not intratabular (as suggested before, e.g. Davey and Williams 1966, p. 103; Stover and Evitt 1978, p. 202; Below 1981, p. 27; Evitt 1985, p. 181, 188, 243, 245), but occupy gonal positions (compare also Duxbury 1980, p. 114; Fensome et al. 2009; p. 17, 2016, p. 30). This is indicated by the distribution of faint sutural ridges on the cyst surface: tubular processes arise at locations where three or four sutural ridges meet (see Figures 4 and 5; Plate 3, figures 5–7; Plate 5, figures 8–10). These ridges separate postcingular and cingular plates, and extend onto the tubular processes in the form of longitudinal striae (Plate 2, figures 7, 10; Plate 3, figure 11; Plate 4, figure 17). Since the tubular processes in *Callaiosphaeridium* are gonal and positioned between the cingular and postcingular series, they should rather be referred to as equatorial, not cingular. The gonal position of such processes is not an unusual feature; e.g. gonal, hollow, and distally open processes are known in *Spiniferites pseudofurcatus* (see Evitt 1985, p. 228; Riding and Lucas-Clark 2016, p. 45, pl. 8, figs 1, 2), and *S. procerus* (see Marheinecke 1992, p. 29).

What should also be emphasised is the variability in the development of septa and processes occupying the epi- and hypocyst and the presence of suturocavation. Suturocavation is commonly manifested in the presence of lines of perforations running along the sutures near plate margins, and it is visible under both SEM (Plate 2, figures 5–8; Plate 3, figures 5–7, 9; Plate 4, figures 8, 9, 17) and TLM (Plate 2, figure 2; Plate 5, figure 10). Suturocavation is recognised in *C. asymmetricum*, *C. bicoronatum* (see Niechwedowicz and Walaszczyk 2021), and most probably in *C. trycherium* (see Duxbury 1980, p. 114). In fact, the manifestation of
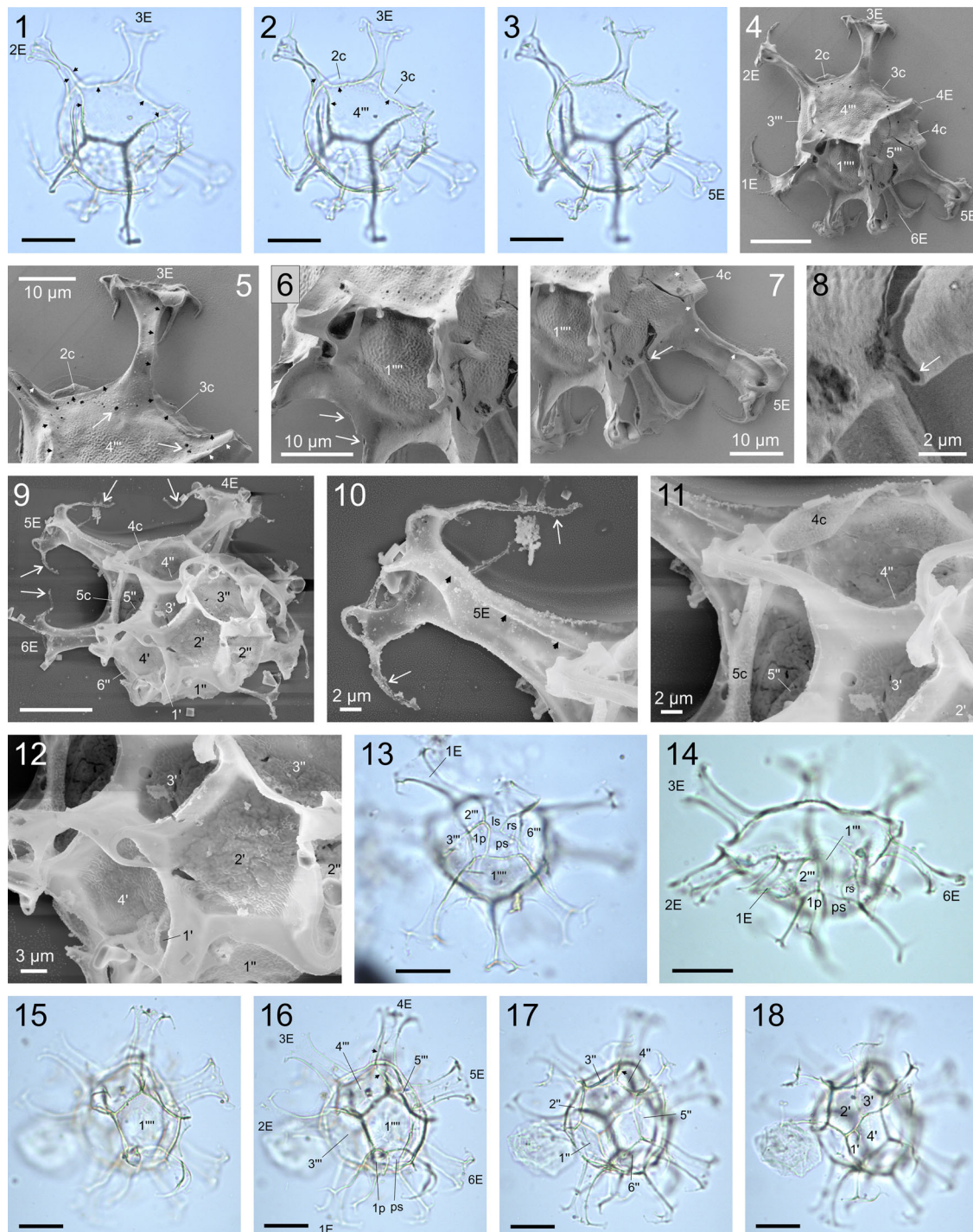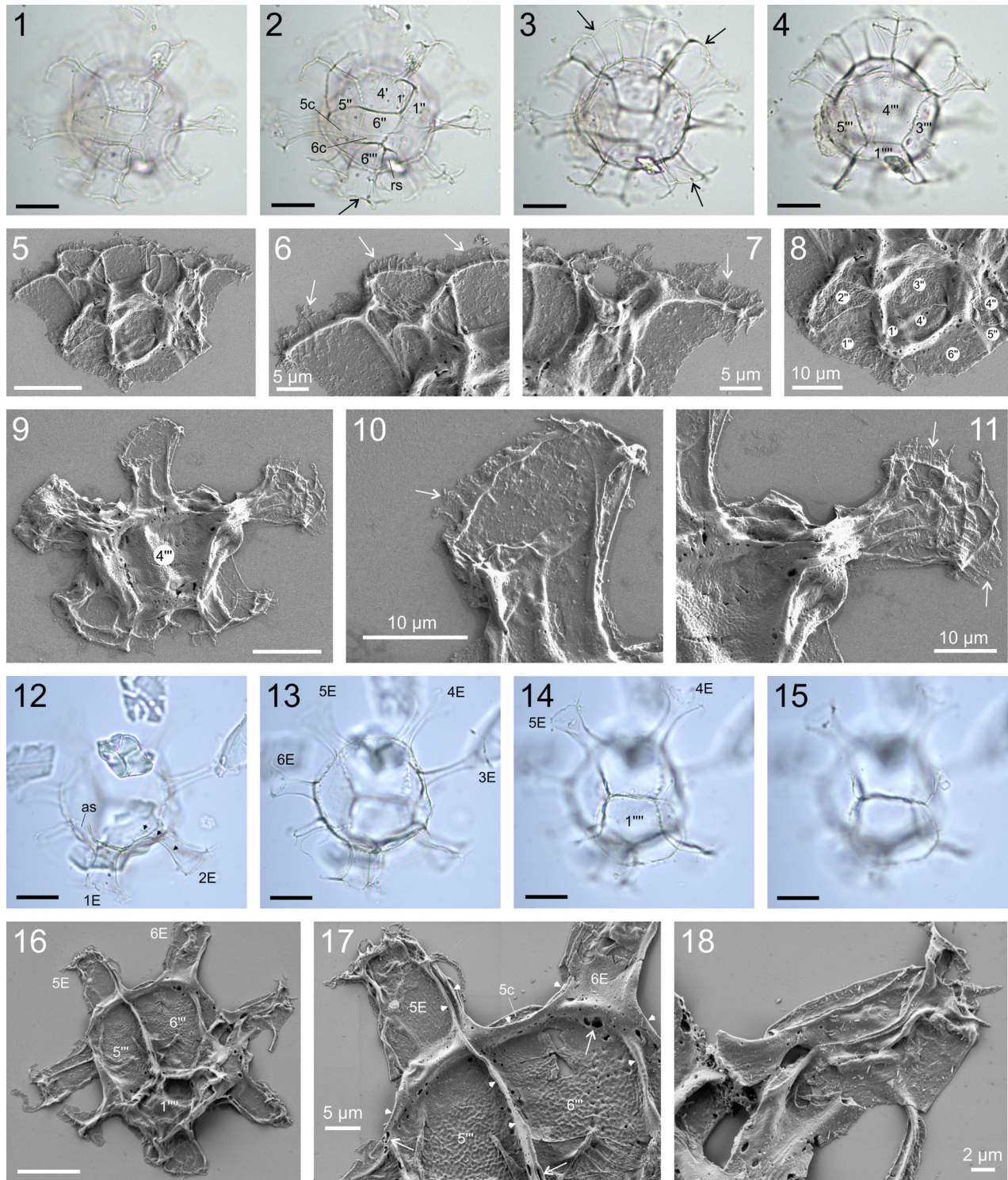
Plate 2. Dinoflagellate cysts from the upper Campanian–lowermost Maastrichtian of the Middle Vistula River section, central Poland. Photomicrographs 1–3, 13–18 taken with a transmitted light microscope; 4–12 taken by scanning electron microscopy; scale bars = 20 μm (unless otherwise specified). 1–18. *Callaiosphaeridium asymmetricum* (Deflandre & Courteville 1939) Davey & Williams 1966. 1–8. MWGUW ZI/90/Po11/0b, 17.9/16.7, EF G30/0; oblique dorso-antapical view, operculum detached; note the rugulate wall ornament covering most of the plate areas; arrowheads indicate sutural ridges corresponding to plate boundaries, arrows indicate suturocavations (E = equatorial processes). 9–12. MWGUW ZI/90/Po12/SEM/8, EF Q18/0; apical view, operculum attached; note the rugulate wall ornament covering most of the plate areas, and the aculeate spines (indicated by arrows) arising from the distal portion of equatorial processes (E). **13.** MWGUW ZI/90/RN(-7)/0, 8.5/19, EF F25/2; oblique dorso-apical view of ventro-antapical surface, operculum detached (E = equatorial process); note a sexiform antapex and L-type ventral arrangement. 14. MWGUW ZI/90/R7/0, 0.4/2, EF X15/4; oblique dorso-antapical view of ventral surface, operculum detached (E = equatorial processes). 15–18. MWGUW ZI/90/Po12/0a, 15.7/19.6, EF E33/3; antapical view of antapical (15) and apical (17, 18) surfaces, and optical section (16), operculum attached; note a neutral torsion of the hypocyst (sutures between plates 3″/4″ and 4‴/5‴ are in line), and sexiform antapex (16); arrowheads indicate sutural ridges corresponding to plate boundaries (E = equatorial processes).
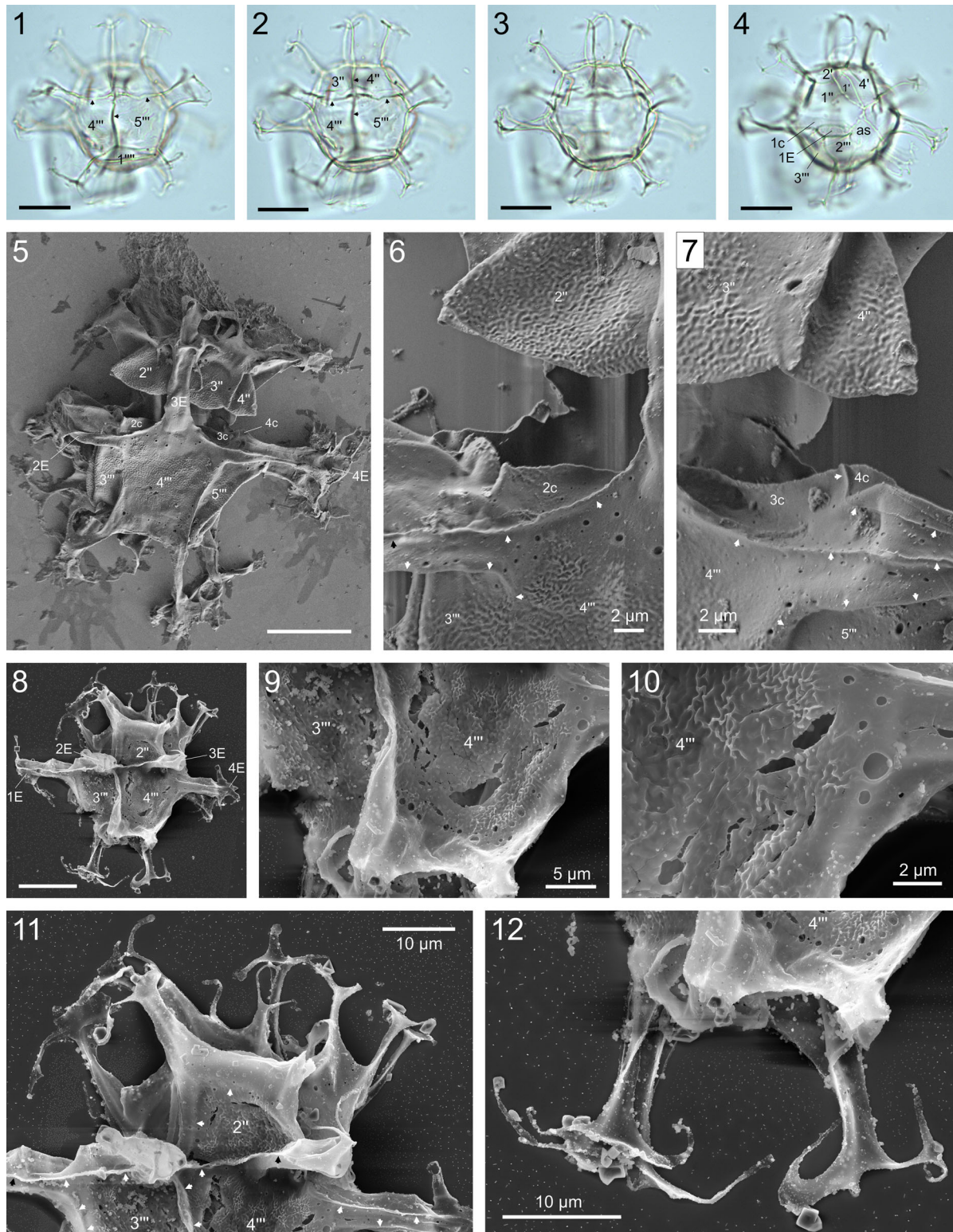
Plate 3. Dinoflagellate cysts from the upper Campanian–lowermost Maastrichtian of the Middle Vistula River section, central Poland. Photomicrographs 1–4 taken with a transmitted light microscope; 5–12 taken by scanning electron microscopy; scale bars = 20 μm (unless otherwise specified). 1–12. *Callaiosphaeridium asymmetricum* (Deflandre & Courteville 1939) Davey & Williams 1966. 1–4. MWGUW ZI/90/R4/0, 16.7/11.9, EF M34/3; dorsal view of dorsal (1, 2) and ventral (4) surfaces, and optical section (3), operculum attached; note a neutral torsion of the hypocyst (sutures between plates 3″/4″ and 4‴/5‴ are in line); arrowheads indicate sutural ridges corresponding to plate boundaries (E = equatorial processes), note also a subtriangular shape of plate 1′. 5–7. MWGUW ZI/90/Po12/SEM/10, EF D31/4; dorsal view, operculum attached; note a neutral torsion of the hypocyst; arrowheads indicate sutural ridges corresponding to plate boundaries (E = equatorial processes). 8–12. MWGUW ZI/90/Po12/SEM/8, EF P18/4; dorsal view, operculum attached; note the rugulate wall ornament covering most of the plate areas; arrowheads indicate sutural ridges corresponding to plate boundaries (E = equatorial processes).

Plate 4. Dinoflagellate cysts from the upper Campanian–lowermost Maastrichtian of the Middle Vistula River section, central Poland. Photomicrographs 1–4, 12–15 taken with a transmitted light microscope; 5–11, 16–18 taken by scanning electron microscopy; scale bars = 20 μm (unless otherwise specified). 1–18. *Callaiosphaeridium bicoronatum* Niechwedowicz in Niechwedowicz & Walaszczyk 2021. 1–4. MWGUW ZI/90/PN(a)2/0e, 17.4/7.3, EF R33/0; oblique ventro-apical view of ventro-apical (1, 2) and dorso-antapical (4) surfaces, and optical section (3), operculum attached; arrows indicate transverse ridges distally supporting septa. 5–8. MWGUW ZI/90/PN81/SEM/1, EF N23/0; isolated operculum in dorsal view; arrows indicate transverse ridges distally supporting septa, surmounted by low crests with incorporated spines. 9–11. MWGUW ZI/90/PN81/SEM/1, EF M23/4; dorsal view, operculum detached; close-ups (10, 11) show details of the equatorial process terminations (arrows indicate low crests with numerous incorporated short spines). 12–15. MWGUW ZI/90/PN81/0a, 7.9/6.6, EF S23/2; oblique ventro-apical view of optical section (12, 13), and dorso-antapical surface (14, 15), operculum detached (see also Figure 5). 16–18. MWGUW ZI/90/PN81/SEM/2, EF J18/1; antapical view, operculum detached; note the rugulate wall ornament covering most of the plate areas; arrowheads indicate sutural ridges (corresponding to plate boundaries) extending to equatorial processes (E); arrows indicate suturocavations.

suturocavation has been noticed in *C. asymmetricum* by prior workers, but identified previously as 'globular [structures], [present] especially along the ribs … [that refer] to small spherical spaces between the endophragm and the periphragm' (Davey and Williams 1966, p. 104) or 'strings of pearl-like cavities … at the base of the septa' (author's translation from Below 1981, p. 29) and illustrated by Harding (1990, pl. 21, fig. 4).

Comparison. The possession of an epicystal archaeopyle, and more broadly an overall similarity in appearance, make *Actinotheca* Cookson & Eisenack 1960a, *Avellodinium* Duxbury 1977, and *Heslertonia* Sarjeant 1966b very similar to *Callaiosphaeridium*. *Actinotheca* differs in having the equatorial processes, or rather 'intergrown membranes' or 'equatorial row of somewhat boxlike chambers' (Evitt 1985, p. 243, 244), extended more in the equatorial plane. Additionally, it is characterised by the absence or weak development of epi- and hypocystal sutural and gonal features (ridges, septa, processes), unlike *Callaiosphaeridium*. *Avellodinium*, similar to *Callaiosphaeridium*, has gonal and intergonal processes. However, its equatorial processes are not tubular, but are comparable in shape with other processes. *Heslertonia* has high and regularly developed sutural septa covering the entire cyst sutures. Morphologically, *Callaiosphaeridium* is a transitional form between *Avellodinium* and *Heslertonia*.

In ventral, dorsal, or lateral views, *Callaiosphaeridium* specimens with attached operculum resemble *Spiniferites* Mantell 1850. The gonal, distally furcate processes occupying the polar regions in *Callaiosphaeridium* (e.g. in *C. asymmetricum*) are very similar to those in *Spiniferites* (see Evitt 1985, p. 244). The latter genus, however, differs from *Callaiospharedium* in having S-type ventral organisation and a precingular archaeopyle.

Stratigraphical comments. *Callaiosphaeridium* is biostratigraphically important for the Campanian–Maastrichtian boundary; *C. asymmetricum* disappears in the uppermost Campanian (Habib and Miller 1989; Kurita and McIntyre 1994; Nøhr-Hansen 1996; Slimani 2001; Skupien and Mohamed 2008; Niechwedowicz and Walaszczyk 2021), and the genus finally disappears in the lowermost Maastrichtian in Poland with its youngest representative, *C. bicoronatum* (Niechwedowicz and Walaszczyk 2021).

Callaiosphaeridium asymmetricum (Deflandre & Courteville 1939) Davey & Williams 1966 emend. nov.
Figure 4; Plates 2, 3

Synonymy.
1939 *Hystrichosphaeridium asymmetricum* Deflandre & Courteville: p. 100, 101, pl. 4, figs 1, 2.
1966 *Callaiosphaeridium asymmetricum* (Deflandre & Courteville 1939) Davey & Williams: p. 104, pl. 8, figs 9, 10, pl. 9, fig. 2.
1967 *Hexasphaera asymmetrica* (Deflandre & Courteville 1939) Clarke & Verdier: p. 43, pl. 7, figs 1–3, text-fig. 17 (combination illegitimate).
1980 *Callaiosphaeridium asymmetricum* (Deflandre & Courteville 1939) Davey & Williams 1966 – Duxbury: pl. 8, figs 3, 6, 11.

1983 *Callaiosphaeridium asymmetricum* (Deflandre & Courteville 1939) Davey & Williams 1966 – Duxbury: pl. 5, figs 11, 12, text-fig. 18.

Emended diagnosis. Gonyaulacacean (leptodinioid) chorate cysts with subspheroidal to ovoidal central body, bearing gonal processes and sutural features (ridges, septa) reflecting plate arrangement; suturocavate. The processes are of two types: (i) six prominent equatorial processes, tubular, broad, distally open; and (ii) slender processes, solid, distally furcate, located elsewhere on epi- and hypocyst excluding cingulum. The slender processes are connected by sutural septa with U-shaped and entire distal margin; the equatorial processes are occasionally connected to each other and to the slender ones by low septa. The archaeopyle is epicystal.

Emended description. Chorate cysts with subspheroidal to ovoidal central body, bearing gonal (processes) and sutural (ridges and septa) ornament; suturocavate. Epi- and hypocyst are of similar size, or epicyst is slightly smaller. The central body surface is internally smooth, and externally bears rugulate ornament covering most of the plate areas; plate margins are smooth, and often regularly perforate (lines of perforations parallel to plate boundaries); septa and processes have smooth walls. The processes are of two types: (i) six equatorial tubular processes located in gonal positions between cingular and postcingular series; and (ii) slender gonal processes, positioned elsewhere on epi- and hypocyst, except for margins delimiting cingulum. The equatorial processes are distinct, tubiform, with oval to elliptical cross-sections (wider in equatorial plane), distally are flared and open, terminating with a few aculeate spines (c. 7–10 μm in length). The equatorial processes bear three to four longitudinal striae (faint, poorly expressed) extending from postcingular and cingular sutural ridges. The slender processes are generally solid (may be partially hollow), resulting from merging of sutural septa at gonal points; distally are furcate (usually trifurcate), with branches more or less perpendicular to process stem and parallel to sutures; occasionally with additional bifurcation of second order. The slender processes are connected by a network of U-shaped septa, variable in height, with entire distal margin; septa are equal in height to process length, with minimum height at half distance between the processes. Rarely, the equatorial processes are connected by low septa to the slender processes, or are interconnected basally by septa or septum-like hollow membranous structures. The tabulation formula is 4′, 6″, 6c, 6‴, 1p, 5 s (ps, ls, rs, ras, as), 1‴′, expressed by the archaeopyle and arrangement of gonal and sutural features, indicating leptodinioid pattern (sexiform hypocystal configuration, L-type ventral organisation, and neutral torsion of the hypocyst). Sutural ridge between plates 1′ and 4′ may be reduced; ridges outlining plate 1‴ and sulcal plates may be reduced or absent. The cingulum is relatively narrow, laevorotatory, shifted by one cingulum width. The archaeopyle is epicystal (formula $A_{1-4'} + P_{1-6''}$), operculum is free or attached ventrally.

Dimensions (minimum (mean) maximum).
Central body length (operculum attached): 40 (50.5) 62 μm, central body width: 37 (48) 60 μm, equatorial process length:
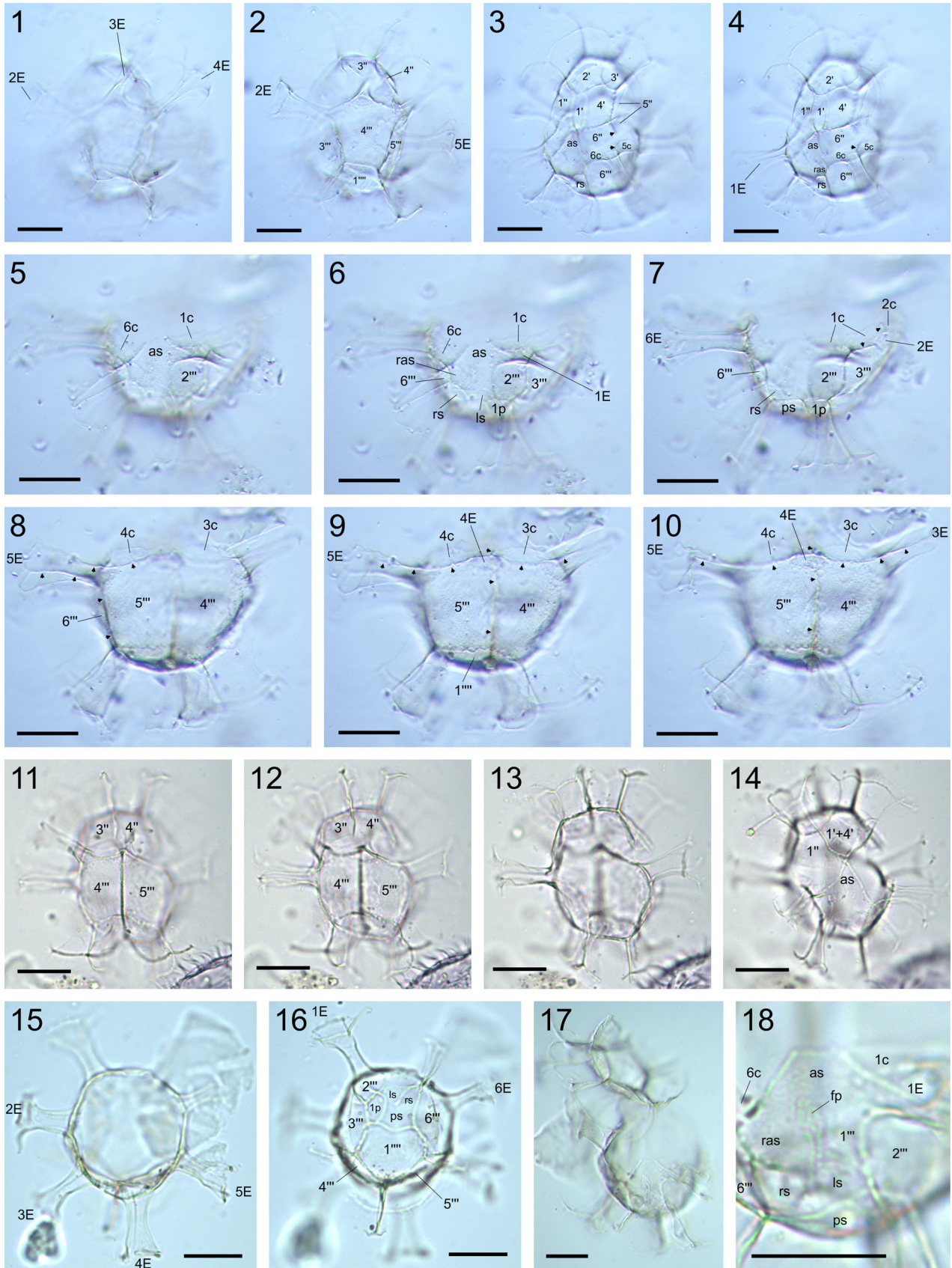
18 (24.6) 32 μm, slender process length: 13 (19.6) 25 μm, maximum septa height: 13 (19.6) 25 μm, minimum intergonal septa height: 2 (4.7) 9 μm (42 specimens measured).

Remarks. The present emendation defines more precisely the distribution of the sutural and gonal features on the cyst surface and their correspondence to the tabulation pattern (see also Figure 4). Additionally, it highlights the nature of tubular equatorial processes that are in gonal positions in the type species of the genus, as are the slender ones.

The central body wall in *C. asymmetricum* is relatively thin (c. 0.5–1 μm), but robust. It is homogeneous in structure with indistinguishable layering (Plate 2, figure 8). The surface of the central body wall is smooth, foveolate, or granular under TLM. SEM studies prove it to be rugulate, resembling the wrinkled skin of withered fruit (Plate 2, figures 5–7, 12; Plate 3, figures 6, 7, 9–12). Plate margins are smooth, with the characteristic lines of perforations, which is a manifestation of the suturocavate septal nature (Plate 2, figures 5–7; Plate 3, figures 5–7). The most characteristic features of this species are the epi- and hypocystal slender gonal processes connected by U-shaped sutural septa (Plate 2, figures 6, 7, 13). The slender processes are distally furcate (usually trifurcate), commonly with additional second-order bifurcation (Plate 2, figure 13; Plate 3, figure 12) similar to the processes in *Spiniferites ramosus* (Ehrenberg 1837) Mantell 1854. The six tubular (equatorial) processes in *C. asymmetricum* bear distally a few characteristic, aculeate spines (Plate 2, figures 5, 9, 10) that arise from the outer surface of the process wall. The spines arise perpendicularly to the process wall and curve distally towards the central body.

Recorded stratigraphical range. Middle upper Campanian–uppermost Campanian, upper-third '*Inoceramus*' *inkermanensis* Zone–lowermost '*Inoceramus*' *redbirdensis* Zone (recorded in Piotrawin, Podole, Raj, and Raj North).

Callaiosphaeridium bicoronatum Niechwedowicz in
Niechwedowicz & Walaszczyk 2021
Figure 5; Plates 4, 5

Synonymy.
?2000 *Callaiosphaeridium asymmetricum* (Deflandre & Courteville 1939) Davey & Williams 1966 – Slimani: pl. 7, figs 9, 10.
?2001 *Callaiosphaeridium asymmetricum* (Deflandre & Courteville 1939) Davey & Williams 1966 – Slimani: pl. 3, fig. 11.
?2011 *Callaiosphaeridium asymmetricum* (Deflandre & Courteville 1939) Davey & Williams 1966 – Slimani, Louwye, Dusar, Lagrou: fig. 5m.

2018b *Callaiosphaeridium* sp. A – Niechwedowicz: p. 63.
2021 *Callaiosphaeridium bicoronatum* Niechwedowicz in Niechwedowicz & Walaszczyk: figs 11, 12, pl. 4, figs 13–19, pl. 5, figs 1–18.

Dimensions (minimum (mean) maximum). Central body length (operculum attached): 43 (53.8) 64 μm, central body width: 39 (49.6) 61 μm, equatorial process length: 19 (25.7) 33 μm, slender process length: 12 (16.9) 24 μm, septa height: 12 (16.9) 24 μm, height of crests crowning septa: 3 (3.5) 5 μm (33 specimens measured).

Remarks. Similarly to *Callaiosphaeridium asymmetricum*, the sutural features (ridges and septa) are well expressed in *C. bicoronatum* and discernible under both TLM and SEM. The ridges bounding the cingular and postcingular plates are extended to six tubular (equatorial) processes (Figure 5; Plate 4, figures 16, 17; Plate 5, figures 8–10), with each bearing a constant number (three or four, depending on their position on the cyst) of longitudinal striae (Niechwedowicz and Walaszczyk 2021, pl. 4, figs 13, 18, pl. 5, fig. 18). The presence of these sutures proves that the equatorial processes occupy gonal positions. As in *C. asymmetricum*, the sutural ridges between plates 1′ and 4′ may be reduced, and the ridges outlining plate 1‴ and the sulcal plates may be reduced or absent (Plate 4, figure 2; Plate 5, figure 14). The tabulation formula in *C. bicoronatum* (4′, 6″, 6c, 6‴, 1p, ps, ls, rs, ras, as, 1‴′) is identical to that of *C. asymmetricum* (see Figure 4). The plate arrangement in *C. bicoronatum*, well demonstrated by the distribution of gonal processes, sutural ridges, and septa, reflects, as in the type species, a leptodinioid pattern (sexiform hypocystal configuration, L-type ventral organisation, and neutral torsion of the hypocyst; Plate 5, figures 5–12, 16, 18). The only difference in the plate arrangements is in the shape of the first apical plate: in both species, it is antero-posteriorly elongated, but in *C. bicoronatum* it is roughly rectangular (Plate 5, figure 4), while in *C. asymmetricum* it is subtriangular (with posteriorly directed acute angle; plate 1′ is not in contact with plate 6″; Plate 3, figure 4).

Callaiosphaeridium asymmetricum differs from *C. bicoronatum* in having relatively low and U-shaped sutural septa. In the latter species, septa are of constant height and are supported by distal ridges (parallel to plate sutures) surmounted with short spines incorporated into low crests. In *C. bicoronatum*, the equatorial processes distally bear crests with spines similar to those terminating septa, while *C. asymmetricum* lack this feature.

Plate 5. Dinoflagellate cysts from the upper Campanian–lowermost Maastrichtian of the Middle Vistula River section, central Poland. All photomicrographs taken with a transmitted light microscope; scale bars = 20 μm. 1–18. *Callaiosphaeridium bicoronatum* Niechwedowicz in Niechwedowicz & Walaszczyk 2021. 1–4. MWGUW ZI/90/PN(a)2/0a, 2.9/17.6, EF G18/3; oblique dorso-antapical view of dorso-antapical (1, 2) and ventro-apical (3, 4) surfaces, operculum attached; note a roughly rectangular shape of plate 1′; arrowheads indicate sutural ridges corresponding to plate boundaries (E = equatorial processes). 5–10. MWGUW ZI/90/PN(a)2/0, 12.5/12.6, EF M28/0; ventral view of ventral (5–7) and dorsal (8–10) surfaces, operculum detached; note that the fourth equatorial process (4E) lies at the boundary between the cingular and postcingular plate series; arrowheads indicate sutural ridges corresponding to plate boundaries (E = equatorial processes). 11–14. MWGUW ZI/90/PN(a)2/0e, 14.3/7.3, EF R30/1; dorsal view of dorsal (11, 12) and ventral (14) surfaces, and optical section (13), operculum attached; note a neutral torsion of the hypocyst (sutures between plates 3″/4″ and 4‴/5‴ are in line). 15, 16. MWGUW ZI/90/PN81/0a, 17.9/16.8, EF G34/3; oblique dorso-apical view of optical section (15), and ventro-antapical surface (16), operculum detached (E = equatorial processes); note a sexiform antapex and L-type ventral arrangement (16). 17, 18. MWGUW ZI/90/PN81/0a, 17.3/14.9, EF J33/0; ventral view of ventral surface showing details of tabulation in the sulcal area (E = equatorial process; fp = flagellar pore); note an L-type ventral arrangement.
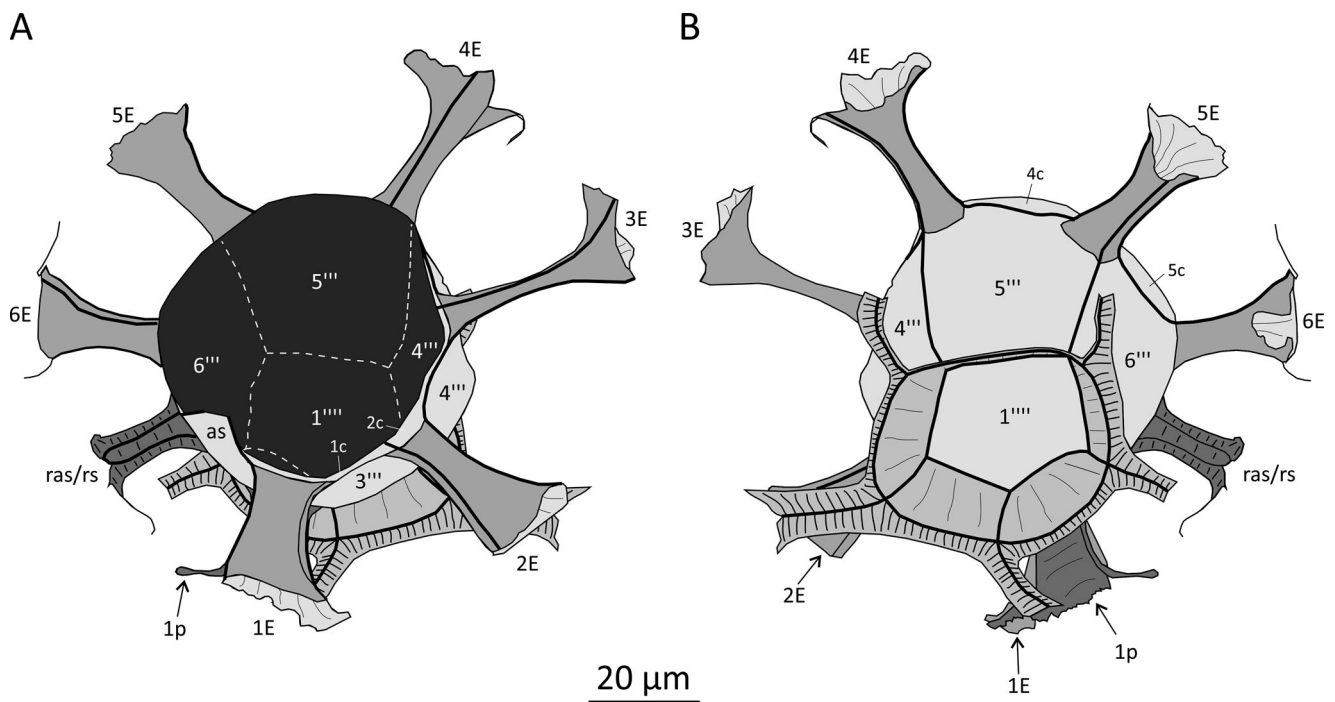
Figure 5. *Callaiosphaeridium bicoronatum* Niechwedowicz in Niechwedowicz & Walaszczyk 2021, drawing of a specimen lacking operculum illustrated in Plate 4, figures 12–15 (E = equatorial tubular processes). A, oblique ventro-apical view; B, oblique dorso-antapical view.

Recorded stratigraphical range. Middle upper Campanian–lowermost Maastrichtian, upper-third '*Inoceramus*' *inkermanensis* Zone–lower '*Inoceramus*' *redbirdensis* Zone (recorded from Kłudzie North, Kłudzie South, Piotrawin, Podole, Raj, and Raj North).

Genus *Oligosphaeridium* Davey & Williams 1966

Synonymy.
1966 *Oligosphaeridium* Davey & Williams: p. 70, 71.
2009 *Oligosphaeridium* Davey & Williams 1966 – Fensome, Williams, & MacRae: p. 47.
2016 *Oligosphaeridium* Davey & Williams 1966 – Fensome, Williams, & Nøhr-Hansen: p. 57.

Type. White 1842, pl. 4, fig. 11, as *Xanthidium tubiferum* var. *complex* (original type). Neotype: Davey & Williams 1966, pl. 7, fig. 1, as *Oligosphaeridium complex*, designated by Davey & Williams (1966, p. 71).

Oligosphaeridium araneum sp. nov.
Figure 6; Plate 6

Synonymy.
1998 *Oligosphaeridium pulcherrimum* (Deflandre & Cookson 1955) Davey & Williams 1966 – Herngreen, Schuurman, Verbeek, Brinkhuis, Burnett, Felder, & Kedves: pl. 4, fig. 2.
2021 *Oligosphaeridium* sp. A – Niechwedowicz & Walaszczyk: pl. 4, fig. 11.

Derivation of name. From Latin *araneum* = cobweb, spider's web; with reference to the perforate or fenestrate appearance of the distal process terminations.

Holotype. Plate 6, figures 1–4; Kłudzie South section, sample KS3; slide MWGUW ZI/90/KS3/0; slide coordinates: 2.1/11.7, EF N18/0; housed at the S.J. Thugutt Geological Museum, Faculty of Geology, University of Warsaw, Warsaw, Poland.

Type locality and horizon. Kłudzie South section, central Poland (51°09′09″N, 21°46′44″E), 0.5 m above the 'boundary marl'; lowermost Maastrichtian (middle '*Inoceramus*' *redbirdensis* Zone).

Diagnosis. A species of *Oligosphaeridium* with relatively slim and long (equal to, or slightly longer than, central body diameter) processes. Terminations of the processes are short (branching occurs in their distalmost portion), and wide, significantly expanded laterally, forming perforate or fenestrate platforms.

Description. The central body is subspheroidal, and consists of relatively thin (c. 0.5–1 μm) and homogeneous wall with rugulate outer surface; wall layering is not distinguishable, except at the centre of the plates where the periphragm forms the mesotabular processes, endophragm and periphram appressed elsewhere. The processes are relatively robust, slim, and long (up to c. 4/3 of central body diameter), hollow with round cross-sections; the process stems are long (c. 85% of total process length), approximately constant in width or slightly tapering. The process terminations are short (branching occurs in distal c. 15% of the processes), but wide, distinctly expanded laterally (process termination width = c. 50% of total process length), forming perforate or fenestrate platforms that consist of networks of simple, branched, or interconnected spines, distally united by continuous trabecular ring bearing 5–9 short (c. 3–6 μm) free spines, perpendicular to process stems or slightly curved towards the central body (Figure 6; Plate 6, figures 3, 10, 11). The processes are generally comparable in size and shape, but apical, ps, and 1p processes are commonly slimmer; the process formula is 4′, 6′′, 5′′′, 1p, ps, 1′′′′. The archaeopyle is apical (type $A_{1-4'}$) with angular margin, operculum is usually free.
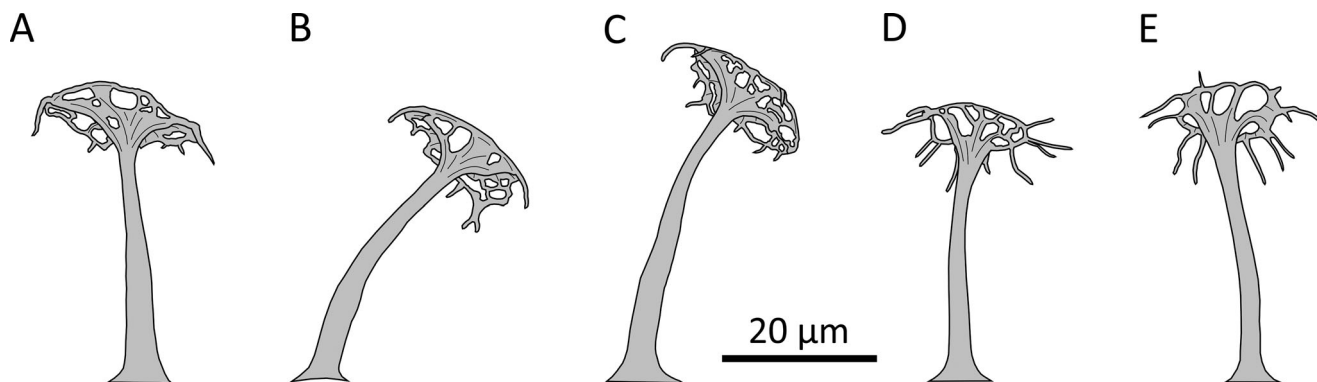
Figure 6. Morphological variability of the processes in *Oligosphaeridium araneum* sp. nov. A–C, processes of the holotype (see Plate 6, figures 1–4); D, E, processes of the specimen illustrated in Plate 6, figures 9, 10.

Dimensions.

Holotype. Central body width: 36 μm, total process length: 44 μm, process base width: 6 μm, minimal process stem width: 2 μm, process termination length: 6 μm, process termination width: 23 μm, total process length/central body width ratio: 1.22, process termination length/total process length ratio: 0.14.

Range (minimum (mean) maximum). Central body length (without operculum): 29 (33.6) 38 μm, central body width: 30 (36.5) 45 μm, total process length: 31 (40.6) 58 μm, process base width: 3 (5.5) 9 μm, minimal process stem width: 2 (2.1) 3 μm, process termination length: 3 (6.7) 12 μm, process termination width: 17 (21.5) 26 μm, total process length/central body width ratio: 0.82 (1.1) 1.3, process termination length/total process length ratio: 0.07 (0.16) 0.3 (31 specimens measured).

Remarks. To date, surface tabulation of the central body in the genus *Oligosphaeridium* has only been recognised in *O. abaculum* Davey 1979. Its tabulation corresponds to the formula pr, 4′, 6′′, 6c, 6′′′, 1p, 5 s, 1′′′′ (Davey 1979, p. 430). As in *O. abaculum*, the process formula in *O. araneum* sp. nov. does not reflect the full tabulation: some processes are absent (pr, 1′′′, all of the cingular and most sulcal processes; see Plate 6). The outer surface of the periphragm in *O. araneum* sp. nov. is finely rugulate (Plate 6, figure 16), but the rugulate nature of the ornament is only clearly visible under SEM (the wall surface may appear smooth to finely granular under TLM).

Oligosphaeridium pulcherrimum in Herngreen et al. (1998, pl. 4, fig. 2) has slim, relatively long processes, the distal extremities of which terminate with a regular trabecular margin bearing short spines. These features do not correspond to the original concept of *O. pulcherrimum* (see Deflandre and Cookson 1955, p. 270, 271, pl. 1, fig. 8, text-figs 21, 22); instead, the specimen probably belongs to *O. araneum* sp. nov.

Comparison. *Oligosphaeridium araneum* sp. nov. is easily distinguished from other species of the genus by its slim and long process stems and characteristic process terminations. The most comparable species are *O. pulcherrimum* (Deflandre & Cookson 1955) Davey & Williams 1966, *O. perforatum* (Gocht 1959) Davey & Williams 1969, and *O. perforatum*? subsp. *colum* Duxbury 1983. The processes in *O. pulcherrimum* are generally shorter than the central body diameter, with wider and shorter stems and a pronounced branching of processes starting at c. 1/2–2/3 of the total process length. Furthermore, while process extremities in both species are fenestrate, in *O. pulcherrimum* they terminate with an irregular margin, rather than with ring-shaped trabeculae as in the new species. *Oligosphaeridium perforatum* (see Plate 7, figures 9, 10) has relatively short processes, with their distal tips in the form of irregularly perforated platforms with a ragged margin devoid of spines. The processes in *O. perforatum*? *colum* have relatively short stems, and their distal extremities are significantly more expanded and highly fenestrated.

Recorded stratigraphical range. Middle upper Campanian–lowermost Maastrichtian, '*Inoceramus*' *altus* Zone–lower *Endocostea typica* Zone (species recorded in all sections studied).

Other occurrences. The Netherlands: Curfs quarry, sample RGD08 (lowermost Danian) – as *Oligosphaeridium pulcherrimum* in Herngreen et al. (1998, pl. 4, fig. 2).

Subfamily **CRIBROPERIDINIOIDEAE** Fensome et al. 1993

Genus ***Samlandia*** Eisenack 1954

Synonymy.
1954 *Samlandia* Eisenack: p. 76.
1954 *Palmnickia* Eisenack: p. 69.
1978 *Samlandia* Eisenack 1954 – Stover & Evitt: p. 185, 186.

Type. *Samlandia chlamydophora* Eisenack 1954.

Remarks. The inner cyst wall in *Samlandia* may be very thick (up to 6 μm in the type species; see Eisenack 1954), and is described as either one wall (e.g. Eisenack 1954; Stover and Evitt 1978 specified it as autophragm), or as two wall layers (endo- and periphragm; e.g. May 1980; McMinn 1988). The inner wall in *S. mayi*, when observed in cross-sectional view under TLM, appears to consist of two layers (Plate 10, figures 10, 11), but in *S. carnarvonensis* a SEM study revealed the presence of only one layer (Plate 10, figures 17, 18), referred to here as an autophragm. The ectophragm in *Samlandia* is thin and fragile, and may be discontinuous (see Stover and Evitt 1978; Damassa 1984; McMinn 1988).

The nature of archaeopyle formation in *Samlandia* species studied herein (*S. carnarvonensis*, *S. mayi*, *S.* cf.
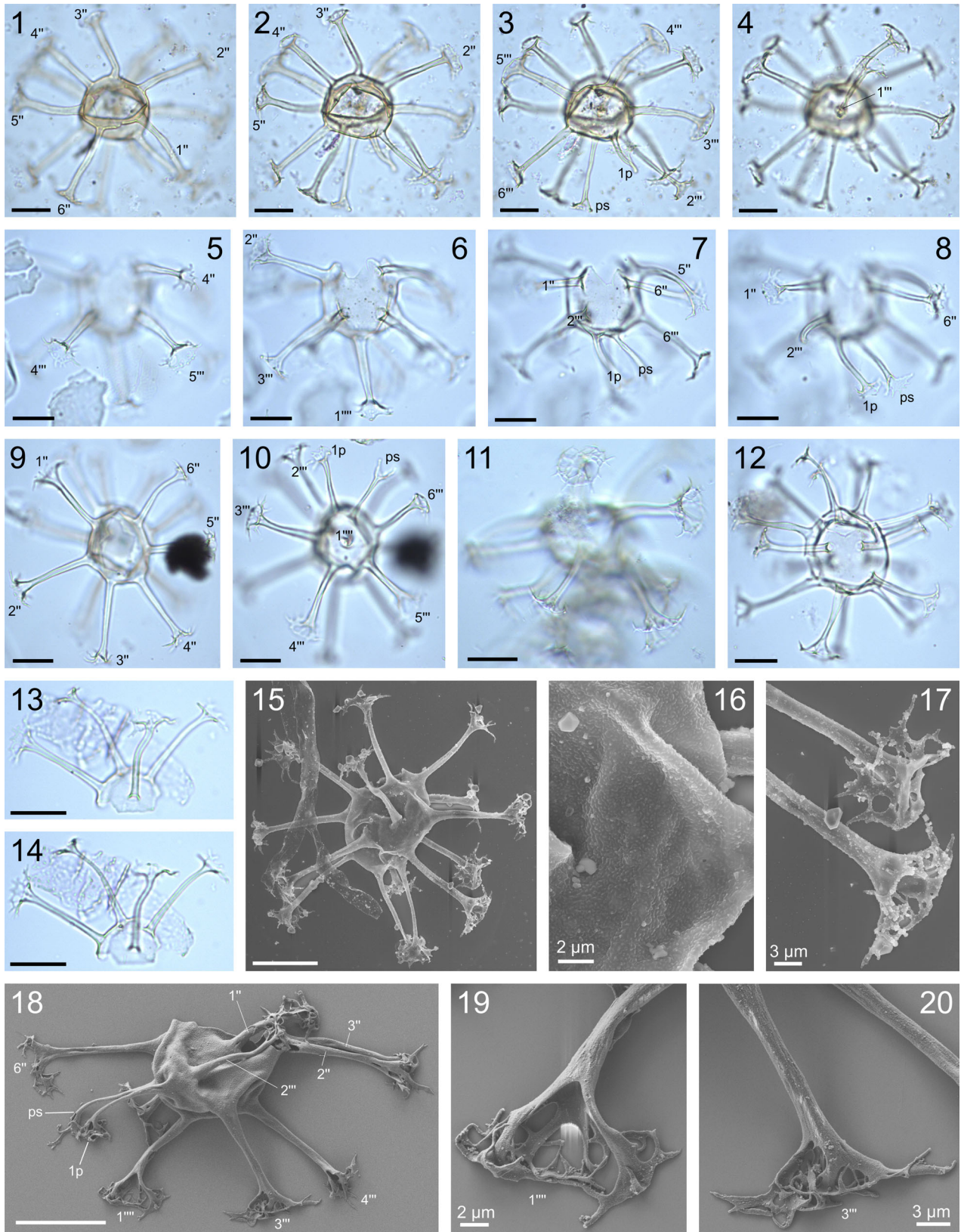
vermicularia) is similar to that in *Samlandia paucitabulata* Niechwedowicz in Niechwedowicz & Walaszczyk 2021 (see Niechwedowicz and Walaszczyk 2021, pl. 1, figs 9, 10). The ectophragmal piece of the operculum ('ectoperculum') is smaller than a part of the operculum formed from the inner cyst wall (Plate 11, figures 17–22). Similarly, the ectophragmal edges of the 'ectoarchaeopyle' form a smaller opening than that formed in the inner cyst wall. Consequently, the ectophragmal edges of the archaeopyle are usually collapsed into the cyst (Plate 10, figures 7, 16–18; Plate 11, figure 4), making the observation of wall structure at the archaeopyle edge difficult.

The genus is atabulate, with the tabulation expressed exclusively by the archaeopyle, but occasionally higher ornamentation developed in the equatorial cyst area may indicate cingulum (see Stover and Evitt 1978, p. 186; McMinn 1988, p. 152). Rare finds (e.g. Damassa 1984, p. 61, pl. 6, figs 4, 5) revealed a partially expressed dorsal tabulation, which enabled the assignment of *Samlandia* to the subfamily Cribroperidinioideae (Fensome et al. 1993, p. 91).

Stratigraphical comments. Among the Cretaceous species of the genus, *Samlandia carnarvonensis* and *S. mayi* were geographically widespread (e.g. May 1980; McMinn 1988; Antonescu et al. 2001a; Schiøler and Wilson 2001; Slimani 2001; Aleksandrova et al. 2012; Niechwedowicz and Walaszczyk 2021) and critical dinoflagellate cyst stratigraphical markers for the Campanian–Maastrichtian boundary: indeed, they constitute part of the definition of the GSSP level in Tercis les Bains, disappearing in the Lower Maastrichtian (Antonescu et al. 2001b; Odin and Lamaurelle 2001).

Samlandia carnarvonensis McMinn 1988
Plate 10, figures 13–19; Plate 11, figures 1–14, 19, 20

Synonymy.
1988 *Samlandia carnarvonensis* McMinn: p. 150, figs 7A–C.
1997 *Apteodinium* sp. A – Mohr and Mao: p. 58, pl. 2, fig. 5.
?2001 *Pyxidinopsis bakonyensis* (Góczán 1962) Stover & Evitt 1978 – Siegl-Farkas: pl. 1, figs 10–12.
2001 *Samlandia carnarvonensis* McMinn 1988 – Schiøler & Wilson: pl. 3, figs 51, 52.
?2001a *Pyxidinopsis bakonyensis* (Góczán 1962) Stover & Evitt 1978 – Antonescu, Foucher, & Odin: pl. 2, figs 41–44.

Dimensions (minimum (mean) maximum).
Autocyst length: 39 (44.9) 53 µm, autocyst width: 32 (38.7) 49 µm, total length (without apical horn): 42 (51.9) 61 µm, total width: 36 (45.1) 58 µm, ectocoel height: 3 (4.9) 6 µm, apical horn length 4 (5.2) 6 µm (17 specimens measured). Isolated operculum (length × width): 25 × 23 µm.

Remarks. The inner wall in *Samlandia carnarvonensis* is relatively thick (c. 1.5–2 µm) and homogeneous, and appears to consists of an autophragm (Plate 10, figures 17, 18). Its outer surface is shagreenate to very finely granular, giving the wall a smooth appearance under TLM. The autophragm ornamentation consists of a dense network of low (c. 1–2 µm high) non-tabular crests and short pillars or processes (c. 1–3 µm high) arising from the crests (the total ornament height is c. 2–5 µm) and supporting the ectophragm (Plate 10, figure 19; Plate 11, figures 11, 12). The ectophragm is very thin (c. 0.1–0.2 µm) and fragile (e.g. Plate 10, figures 14, 16–19) and homogeneous to finely spongy, with a densely granular outer surface (granulae c. 0.1–0.2 µm in diameter; see Plate 11, figure 6). The apical horn is commonly present and well developed (4–6 µm in length; Plate 10, figures 14–18; Plate 11, figures 2, 4, 5). The cyst ornament in the equatorial area may occasionally be higher (Plate 11, figure 2), which suggests the position of the cingulum; however, no indications of a paratabular ornament alignment were observed.

The connection between the ectophragm and its supporting structures appears to be rather weak, since the species was occasionally found with partially or completely, possibly mechanically (?), detached ectophragms (Plate 11, figures 7–14). Such forms are very similar to *Pyxidinopsis bakonyensis* (Góczán 1962) Stover & Evitt 1978; *Pyxidinopsis* Habib 1976 differs from *Samlandia* in the absence of the ectophragm and the apical horn (see e.g. Stover and Evitt 1978). The ectophragm in *S. carnarvonensis* is located very close to the autophragm; consequently, it may be difficult to differentiate under TLM. The issues associated with distinguishing between *Pyxidinopsis* and *Samlandia* have been discussed in previous works (Antonescu et al. 2001a, p. 239; Antonescu et al. 2001b, p. 258, 259). In light of the above considerations and the original illustrations, the forms assigned to *Pyxidinopsis bakonyensis* by Siegl-Farkas (2001, pl. 1, figs 10–12) and Antonescu et al. (2001a, pl. 2, figs 41–44) could possibly be conspecific with *S. carnarvonensis*. One of the specimens illustrated by Siegl-Farkas (2001, pl. 1, fig. 12) appears to possess an apical horn. *P. bakonyensis* was originally described from the upper Maastrichtian – as opposed to the Campanian–Maastrichtian boundary interval – which may further reinforce the proposed reinterpretation.

Samlandia carnarvonensis can be distinguished from *S. mayi* by its smaller size and – usually – the presence of a well-expressed apical horn. The ornament covering the inner wall in *S. carnarvonensis* forms a finer and almost regular

Plate 6. Dinoflagellate cysts from the upper Campanian–lowermost Maastrichtian of the Middle Vistula River section, central Poland. Photomicrographs 1–14 taken with a transmitted light microscope; 15–20 taken by scanning electron microscopy; scale bars = 20 µm (unless otherwise specified). 1–20. *Oligosphaeridium araneum* sp. nov. 1–4. Holotype, MWGUW ZI/90/KS3/0, 2.1/11.7, EF N18/0; apical view of apical (1) and antapical (4) surfaces, and optical section (2, 3). 5–8. MWGUW ZI/90/Po11/0a, 17.4/12.8, EF M33/2; dorsal view of dorsal (5, 6) and ventral (7, 8) surfaces. 9, 10. MWGUW ZI/90/Po12/0, 6.6/11.7, EF N22/2; apical view of apical (9) and antapical (10) surfaces. 11. MWGUW ZI/90/RN(-7)/0a, 17.1/2.1, EF X33/4; left lateral? view, focused on the fenestrate terminations of processes. 12. MWGUW ZI/90/RN(-2)/0a, 14.1/3.4, EF V31/3; right lateral view of left lateral surface, operculum attached. 13, 14. MWGUW ZI/90/Po11/0, 19.8/16.8, EF G35/4; isolated operculum. 15–17. MWGUW ZI/90/Po12/SEM/8, EF B30/4; oblique right lateral? view, operculum attached; note the rugulate wall ornament (16) and details of the perforate/fenestrate terminations of processes (17). 18–20. MWGUW ZI/90/Po12/SEM/1, EF U36/1; left lateral view; note the details of the fenestrate terminations of processes (19, 20).
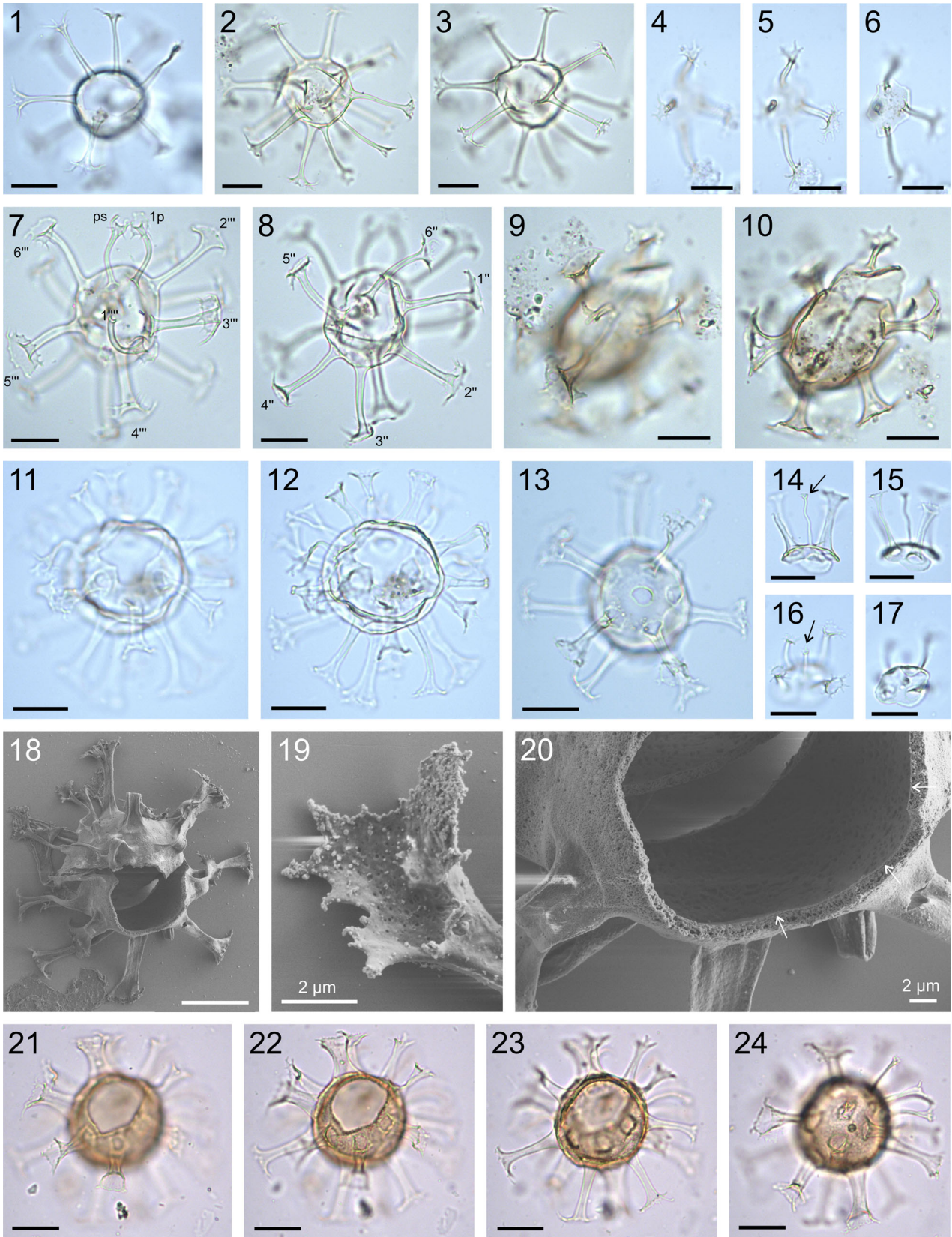
reticulum. It is relatively low: therefore, the ectophragm lies distinctly closer to the autophragm.

Recorded stratigraphical range. Middle upper Campanian–lowermost Maastrichtian, '*Inoceramus*' *altus* Zone–lower *Endocostea typica* Zone (species recorded in all sections studied, except for Raj North).

Samlandia mayi McMinn 1988
Plate 10, figures 1–12; Plate 11, figures 17, 18

Synonymy.
1980 *Samlandia angustivela* (Deflandre & Cookson 1955) Eisenack 1963a – May: p. 61, pl. 6, figs 1–5.
1988 *Samlandia mayi* McMinn: p. 150–152, figs 7D–F.
2001 *Samlandia mayi* McMinn 1988 – Schiøler & Wilson: pl. 3, fig. 53.
2001a *Samlandia mayi* McMinn 1988 – Antonescu, Foucher, & Odin: pl. 2, fig. 46.
2012 *Samlandia mayi* McMinn 1988 – Aleksandrova, Beniamovskii, Vishnevskaya, & Zastrozhnov: pl. VII, figs 12, 13 (only).
2013 *Samlandia mayi* McMinn 1988 – Surlyk, Rasmussen, Boussaha, Schiøler, Schovsbo, Sheldon, Stemmerik, & Thibault: fig. 9D.

Dimensions (minimum (mean) maximum).
Inner body length: 41 (48) 60 μm, inner body width: 34 (41.8) 52 μm, total length (without apical horn): 54 (65.3) 80 μm, total width: 46 (58.4) 70 μm, ectocoel height: 6 (9.9) 13 μm, apical horn length 1 (3) 5 μm (29 specimens measured). Isolated operculum (length × width): 26 (28) 30 × 24 (24.3) 25 μm (three opercula measured).

Remarks. The inner cyst wall is thick (2–3 μm) and composed of either autophragm or appressed endo- and periphragm; further SEM study is needed to solve this issue. TLM preliminarily suggests that the endo- and periphragm are present, with the endophragm thinner (c. 1 μm) and homogeneous, and the periphragm thicker (c. 1.5–2 μm) and less homogeneous in structure (Plate 10, figures 10, 11), giving the wall a smooth appearance. The ectophragm is homogeneous to finely spongy in structure, with a smooth to shagreenate outer surface; it is very thin (c. 0.2–0.5 μm), fragile, and prone to folding (see Plate 10, figures 7–9). It is relatively distant from the inner cyst wall, and it is supported by irregularly arranged, c. 6–10 μm high, homogeneous to finely spongy discontinuous muri and processes, distally connected by an arch-shaped trabecula. As a result, the thin ectophragm has an irregularly wavy appearance (Plate 10, figures 2, 6, 7). The nature of the holocavate wall structure in *S. mayi* commonly gives the cyst a raspberry-like appearance under TLM (Plate 10, figures 1, 2, 12). The processes may be membranous or connected proximally (Plate 10, figures 8, 9), but unlike *S. carnarvonensis* the ornamentation does not form a regular reticulum covering the inner cyst wall. The ectocoel cavations are generally of uniform height, but occasionally may be higher at the apex, antapex, and equatorial area (Plate 10, figures 2, 3). The greater height of cyst ornamentation in the equatorial area may suggest the position of the cingulum, but no signs of paratabular ornament alignment were observed. As in other *Samlandia* species, the only feature indicating the tabulation is the archaeopyle (operculum free or attached). The apical horn is rarely distinguishable (Plate 10, figure 12), although its presence may be obscured by the characteristic nature of holocavation in this species.

In overall morphology, *Samlandia mayi* is most comparable to *S. paucitabulata*. The latter can be distinguished from *S. mayi* by its reticulate wall appearance, sutural alignment of wall ornament (signs of tabulation), and thicker ectophragm, which is robust and more regular in outline.

Recorded stratigraphical range. Middle upper Campanian–lowermost Maastrichtian, '*Inoceramus*' *altus* Zone–lower *Endocostea typica* Zone (species recorded in Piotrawin, Raj, Podole, Kłudzie North, and Dziurków).

Samlandia cf. *vermicularia* McMinn 1988
Plate 11, figures 15, 16, 21, 22

Synonymy.
2021 *Samlandia* cf. *vermicularia* McMinn – Niechwedowicz & Walaszczyk: pl. 2, figs 15, 16.

Dimensions (minimum (mean) maximum).
Inner body length: 44 (53.5) 62 μm, inner body width: 40 (47) 56 μm, total length (without apical horn): 58 (66.5) 75 μm, total width: 51 (60.2) 70 μm, ectocoel height: 4 (6.3) 9 μm (seven specimens measured). Isolated operculum (length × width): 27 (28.6) 30 × 24 (25.3) 27 μm (three opercula measured).

Remarks. The inner homogeneous wall layer (either endo- and periphragm, or autophragm only?; 2–3 μm thick) bears ornamentation consisting of relatively wide (2–5 μm) and 4–9 μm high vermicular ridges, forming a network enclosing a polygonal to circular area. The ridges support a very thin and occasionally discontinuous ectophragm. Complete specimens are very rare in the present material, and a vermiculate
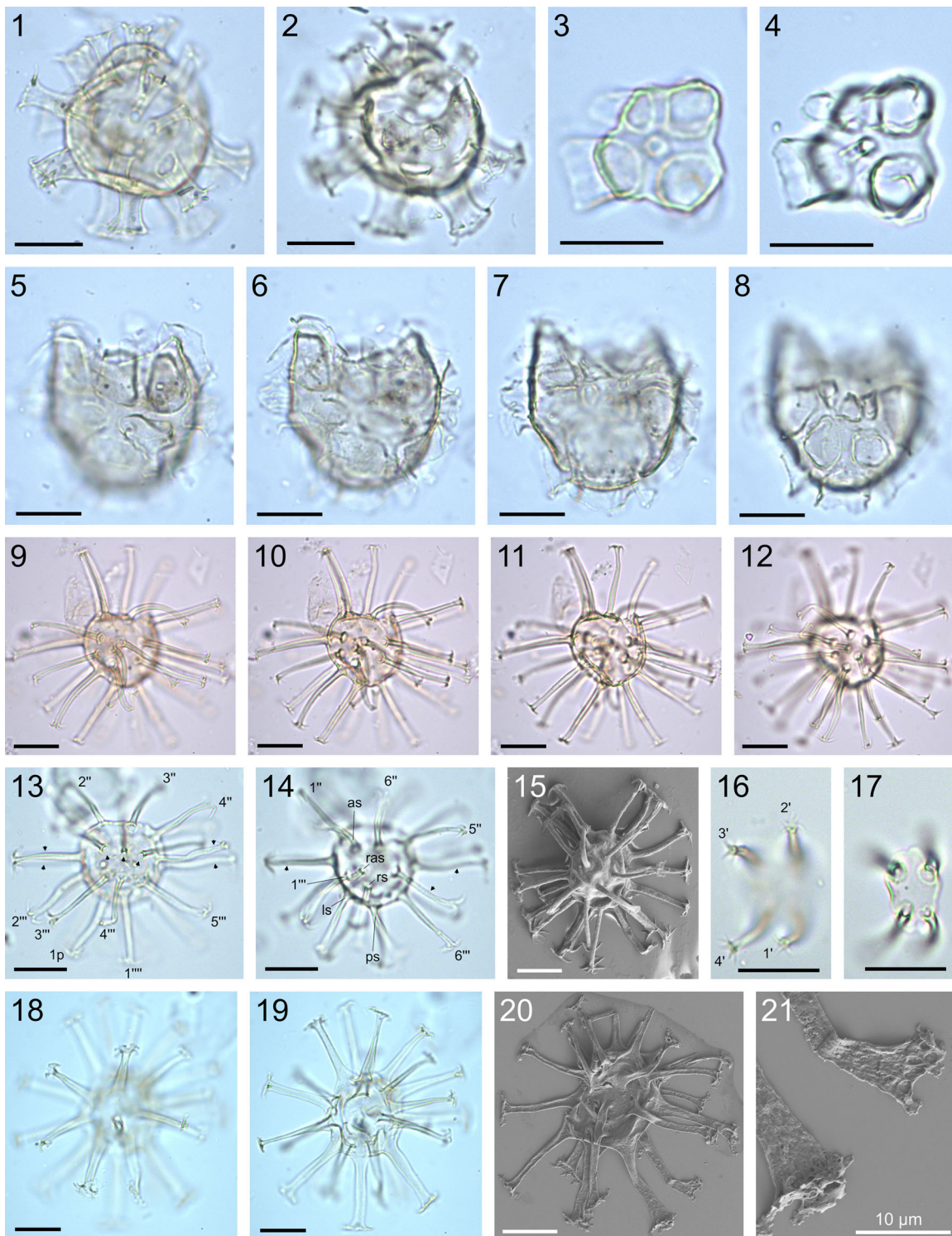
Plate 7. Dinoflagellate cysts from the upper Campanian–lowermost Maastrichtian of the Middle Vistula River section, central Poland. Photomicrographs 1–17, 21–24 taken with a transmitted light microscope; 18–20 taken by scanning electron microscopy; scale bars = 20 μm (unless otherwise specified). 1–6. *Oligosphaeridium complex* (White 1842) Davey & Williams 1966. 1. MWGUW ZI/90/Dz33/0, 7.4/16.2, EF H22/4; oblique antapical view of apical surface. 2, 3. MWGUW ZI/90/R4/0, 8.5/15.6, EF J25/2; oblique antapical view of optical section (2), and apical surface (3). 4–6. MWGUW ZI/90/Dz33/0, 4.8/3.3, EF V20/3; isolated operculum; external view of process terminations (4, 5) and central body surface (6). 7, 8. *Oligosphaeridium intermedium* Corradini 1973, MWGUW ZI/90/R24/0, 11.8/0.5, EF Z27/2; antapical view of antapical (7) and apical (8) surfaces. 9, 10. *Oligosphaeridium perforatum* (Gocht 1959) Davey & Williams 1969 (reworked), MWGUW ZI/90/R22/0, 4.6/8.2, EF Q20/0. 11–20. *Hystrichosphaeridium tubiferum* (Ehrenberg 1837) Deflandre 1937. 11, 12. MWGUW ZI/90/Po11/0a, 19.6/13.6, EF L36/0; oblique left lateral view of left lateral surface (11), and optical section (12). 13. MWGUW ZI/90/Po1/1, 12.2/13.9, EF L17/1; antapical view of antapical surface. 14, 15. MWGUW ZI/90/Po11/0, 4/15.8, EF H19/4; isolated operculum; lateral view; note that the pr process (indicated by an arrow) is mostly solid, hollow only in its distalmost portion. 16, 17. MWGUW ZI/90/Po11/0a, 6/5.5, EF T22/3; isolated operculum; external view of process terminations (16) and central body surface (17); note that the pr process (indicated by an arrow) is mostly solid, with hollow base and distalmost portion. 18–20. MWGUW ZI/90/Po12/SEM/1, EF T25/2; oblique apical view; close-ups show the details of process termination (19), and wall structure (20); note the very thin and homogeneous internal wall layer (?endophragm, indicated by arrows), and thicker and spongy external layer (?periphragm). 21–24. *Hystrichosphaeridium salpingophorum* Deflandre 1935 ex Deflandre 1937, MWGUW ZI/90/Dz5/0, 7.6/5.1, EF T23/3; oblique apical view of apical (21, 22) and antapical (24) surfaces, and optical section (23); note the subquadrate bases and terminations of pre- and postcingular processes.
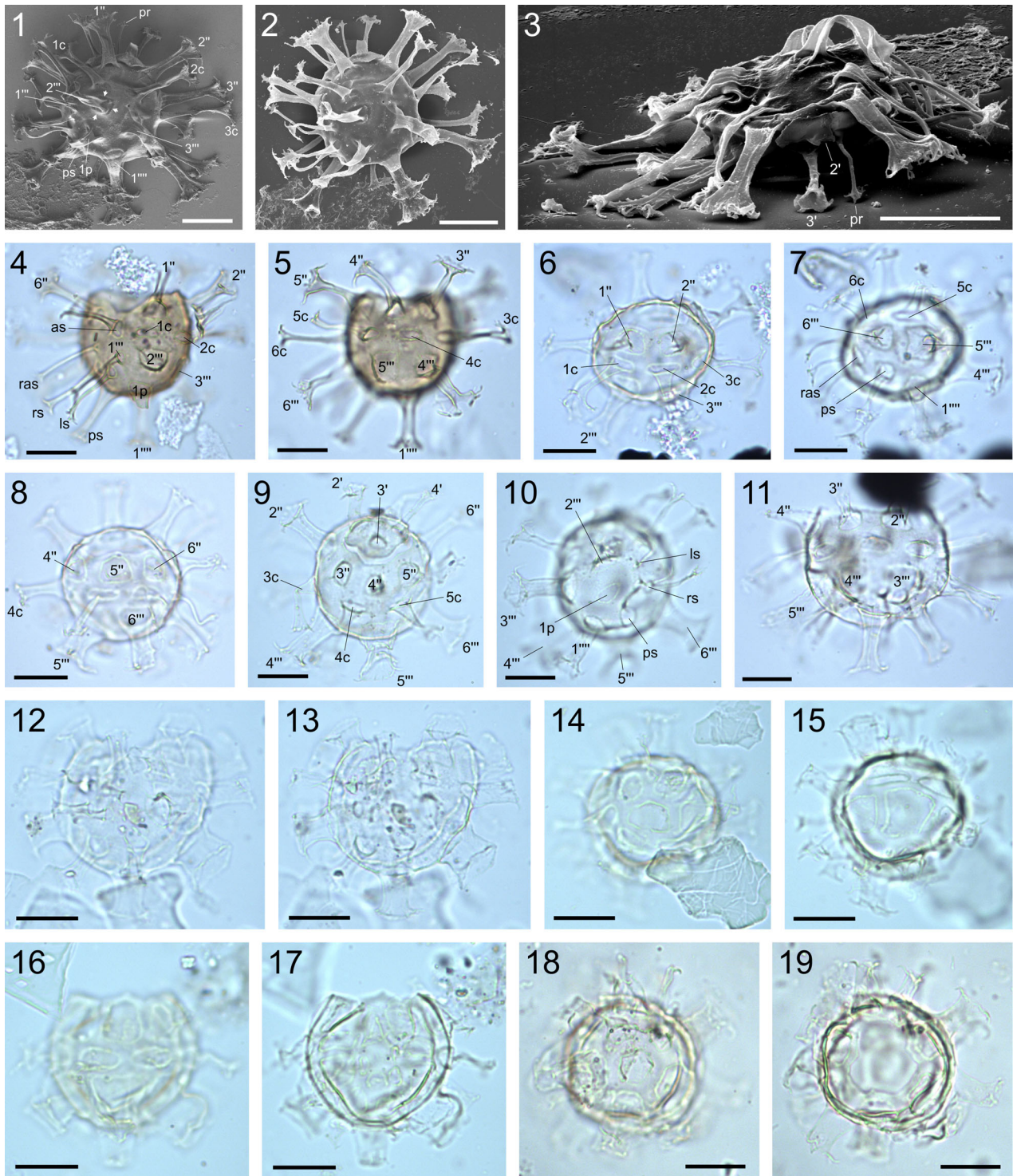
Plate 8. Dinoflagellate cysts from the upper Campanian–lowermost Maastrichtian of the Middle Vistula River section, central Poland. Photomicrographs 1–3 taken by scanning electron microscopy; 4–19 taken with a transmitted light microscope; scale bars = 20 μm. 1–5. *Hystrichosphaeridium salpingophorum* Deflandre 1935 ex Deflandre 1937. 1–3. MWGUW ZI/90/Po12/SEM/5, EF J27/2; left lateral view, operculum attached; note the subquadrate base of process 2‴ (indicated by arrowheads). 4, 5. MWGUW ZI/90/Dz9/0, 10.7/14.4, EF K27/3; oblique ventral view of ventral (4) and dorsal (5) surfaces; note a neutral torsion of the hypocyst (sutures between plates 3″/4″ and 4‴/5‴ are more or less in line). 6–11. *Hystrichosphaeridium proprium* Marheinecke 1992. 6, 7. MWGUW ZI/90/KN17/0a, 7.5/12.8, EF M23/2; oblique left lateral view of left lateral (6) and right lateral (7) surfaces; note the subquadrate bases of pre- and postcingular processes, and the ellipsoidal bases of cingular processes. 8. MWGUW ZI/90/Po2/0, 19/12.7, EF M36/3; right lateral view of right lateral surface; note the subquadrate bases of pre- and postcingular processes, and the ellipsoidal bases of cingular processes. 9, 10. MWGUW ZI/90/Po12/0a, 6.5/17, EF H23/1; oblique dorsal view of dorso-apical (9) and ventro-antapical (10) surfaces, operculum attached; note a neutral torsion of the hypocyst (sutures between plates 3″/4″ and 4‴/5‴ are more or less in line), and a quinqueform pattern (plate 1‴‴ is not in contact with plate 6‴). 11. MWGUW ZI/90/Po12/0, 10.3/5.5, EF T26/4; oblique ventral view of dorsal surface. 12–19. *Hystrichosphaeridium brevispinum* (Davey & Williams 1966) stat. nov., morphotype B. 12, 13. MWGUW ZI/90/PN(a)2/0, 8/16.4, EF H23/4; oblique ventral view of ventral surface (12), and optical section (13); note the subquadrate terminations of pre- and postcingular processes. 14, 15. MWGUW ZI/90/Po22/0, 6.4/1.6, EF X22/0; oblique left lateral view of left lateral (14) and right lateral (15) surfaces, operculum attached; note the subquadrate bases of pre- and postcingular processes. 16, 17. MWGUW ZI/90/KN11/0, 16.1/18, EF G33/1; dorsal view of dorsal (16) and ventral (17) surfaces. 18, 19. MWGUW ZI/90/Dz20/0a, 11.3/3.1, EF V27/0; antapical view of antapical (18) and apical (19) surfaces.

Plate 9. Dinoflagellate cysts from the upper Campanian–lowermost Maastrichtian of the Middle Vistula River section, central Poland. Photomicrographs 1–14, 16–19 taken with a transmitted light microscope; 15, 20, 21 taken by scanning electron microscopy; scale bars = 20 μm (unless otherwise specified). 1, 2. *Hystrichosphaeridium brevispinum* (Davey & Williams 1966) stat. nov., morphotype A, MWGUW ZI/90/Dz5/0, 17/12.7, EF L32/4; oblique ventral view of ventral (1) and dorsal (2) surfaces, operculum attached; note the round bases of pre- and postcingular processes. 3, 4. *Hystrichosphaeridium brevispinum* (Davey & Williams 1966) stat. nov., MWGUW ZI/90/Po11/0, 2.6/12, EF M18/3; isolated operculum; internal view of central body surface (3) and process terminations (4). 5–8. *Alisocysta circumtabulata* (Drugg 1967) Stover & Evitt 1978, MWGUW ZI/90/RN(-6)/0, 14.7/13.2, EF L32/4; dorsal view of dorsal (5, 6) and ventral (8) surfaces, and optical section (7). 9–17. *Hystrichosphaeridium? recurvatum* (White 1842) Lejeune-Carpentier 1940. 9–12. MWGUW ZI/90/P1/0, 8/1.2, EF X24/3; note the uniform process development. 13, 14. MWGUW ZI/90/R26/0, 16.8/11.9, EF N33/1; dorsal view of dorsal (13) and ventral (14) surfaces; note that cingular processes (indicated by arrowheads) are more numerous and densely arranged on the dorsal cyst surface, as compared with the few present on the ventral side. 15. MWGUW ZI/90/Po12/SEM/6, EF X33/4; operculum attached. 16, 17. MWGUW ZI/90/PN(a)5/0, 0.5/13.9, EF L15/2; isolated operculum; external view of process terminations (16) and central body surface (17); note the lack of pr process. 18–21. *Kleithriasphaeridium loffrense* Davey & Verdier 1976. 18, 19. MWGUW ZI/90/Po10/0, 13.5/11.2, EF N29/0. 20, 21. MWGUW ZI/90/Po12/SEM/6, EF E22/4; note the fragile nature of the central body and process walls, close-up (21) shows the details of the process terminations.
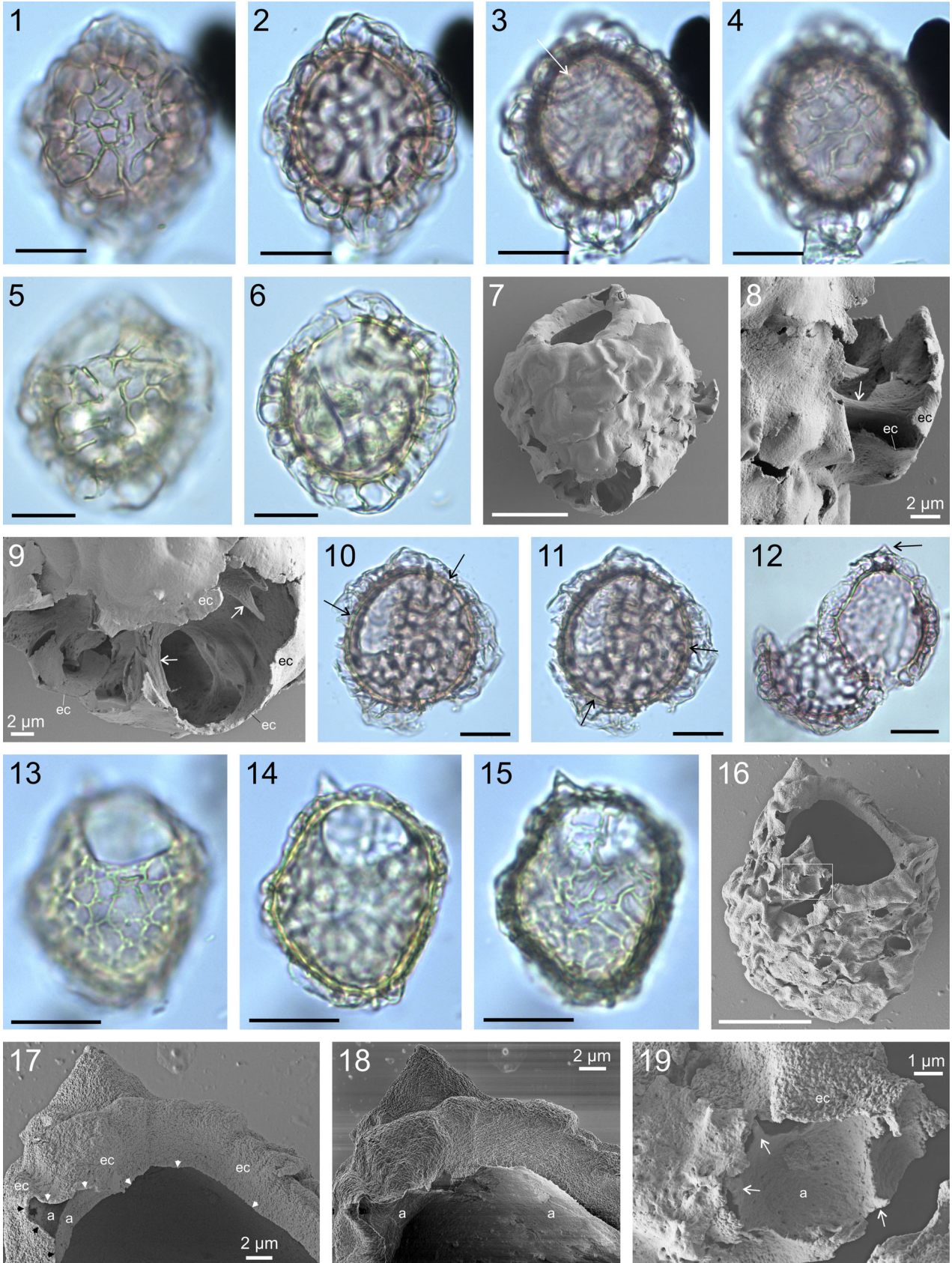
or globular ornament, characteristic of *Samlandia vermicularia* (see McMinn 1988, p. 152, figs 7G–I), is best recognisable on operculum (Plate 11, figures 16, 21, 22), while the ornament on the cyst surface is commonly unclear (Plate 11, figure 15). Consequently, the species is referred to here as *Samlandia* cf. *vermicularia*.

Samlandia cf. *vermicularia* is similar to *S. mayi*, but differs from the latter in the lower height of its ectocoel cavations and the nature of its cyst ornamentation. *Samlandia carnarvonensis* differs from *S.* cf. *vermicularia* in the type and height of its wall sculpture (see above).

Recorded stratigraphical range. Middle upper Campanian–lowermost Maastrichtian, 'Inoceramus' altus Zone–lower *Endocostea typica* Zone (species recorded in Piotrawin, Podole, and Dziurków).

<div align="center">

Family **AREOLIGERACEAE** Evitt 1963b
Genus ***Glaphyrocysta*** Stover & Evitt 1978

</div>

Synonymy.
1978 *Glaphyrocysta* Stover & Evitt: p. 49, 50.
2009 *Glaphyrocysta* Stover & Evitt 1978 – Fensome, Williams, & MacRae: p. 32.

Type. *Glaphyrocysta retiintexta* (Cookson 1965a) Stover & Evitt 1978.

<div align="center">

Glaphyrocysta expansa (Corradini 1973) Roncaglia &
Corradini 1997
Plate 12, figures 1–6

</div>

Synonymy.
1973 *Cyclonephelium expansum* Corradini: p. 161, 162, pl. 24, figs 8a, b, text-fig. 7.
1992 *Cyclonephelium*? *castelcasiense* subsp. *prominentum* Marheinecke: p. 73, 74, pl. 15, figs 1–4.
1997 *Glaphyrocysta expansa* (Corradini 1973) Roncaglia & Corradini: p. 187, 189, pl. 4, figs 5, 7–9.
?2001 *Glaphyrocysta* cf. *perforata* Hultberg & Malmgren 1985 – Schiøler & Wilson: pl. 2, fig. 25.
2004 *Glaphyrocysta castelcasiense* subsp. *promimentum* (Marheinecke 1992) Michoux & Soncini in Fauconnier & Masure: p. 245, pl. 30, figs 8–10.
2021 *Glaphyrocysta expansa* (Corradini 1973) Roncaglia & Corradini 1997 – Niechwedowicz & Walaszczyk: pl. 7, figs 5, 6.

Dimensions (minimum (mean) maximum).
Central body length (without operculum): 48 (60.2) 75 μm, central body width: 52 (66.9) 88 μm, total length (without operculum): 62 (91) 112 μm, total width: 105 (139.1) 163 μm,

maximal length of membrane: 42 (49.6) 62 μm, process length: up to 20 μm (16 specimens measured).

Remarks. *Glaphyrocysta expansa* is characterised by a wide membrane that arises from the lateral and antapical cyst margins; it is distinctly expanded antapically and laterally, but is commonly widest near the archaeopyle edge (Plate 12, figures 2, 5). The membrane is generally smooth, which is most evident at its distal portion (Plate 12, figures 2, 3, 6), although the membrane may be foveolate proximally, near the contact with the central body. The membrane is supported by the acuminate processes, which are apparently incorporated within it; the processes taper distally and gradually become lost in the membrane. The central body commonly bears two antapical lobes, of which the left one is often more expressed (Plate 12, figure 3). The cyst surface is finely granular, usually with a denser granulation found on the dorsal side along the plate boundaries (Plate 12, figure 1). Corradini's illustration (1973, text-fig. 7) of the paratype is probably the best figure to elucidate the most distinctive features of this species. *Glaphyrocysta perforata* Hultberg & Malmgren 1985 also possesses signs of tabulation on the dorsal surface of the central body and a smooth membrane. However, its membrane usually bears large perforations (holes) that are regularly distributed – that is to say, they only occur proximally at the contact of the membrane with the central body. If the perforations are numerous, the membrane appears to be connected to the central body by short simple or membranous processes.

Glaphyrocysta castelcasiensis prominenta (Marheinecke 1992) Michoux & Soncini in Fauconnier & Masure 2004, based on the description and illustrations of Marheinecke (1992), is a junior synonym of *G. expansa*. Marheinecke (1992, p. 74) compared the two species, but the differences he listed (degree of membrane expansion and its ornamentation, outline of antapex), while not inaccurate, are probably not substantial enough to differentiate these forms. For instance, *G. expansa* may also have a bilobated and asymmetrical antapex, in contrast to his suggestions (compare Corradini 1973, p. 161, 162).

Although *G. expansa* is similar to *Glaphyrocysta pala* comb. nov., it differs from the latter by possessing a smooth, unperforated membrane, which is distinctly expanded laterally (for a full comparison, see below).

Recorded stratigraphical range. Uppermost Campanian–lowermost Maastrichtian, 'Inoceramus' redbirdensis Zone–lower *Endocostea typica* Zone (recorded in Podole, Raj North, Kłudzie North, Kłudzie South, and Dziurków).

Plate 10. Dinoflagellate cysts from the upper Campanian–lowermost Maastrichtian of the Middle Vistula River section, central Poland. Photomicrographs 1–6, 10–15 taken with a transmitted light microscope; 7–9, 16–19 taken by scanning electron microscopy; scale bars = 20 μm (unless otherwise specified). 1–12. *Samlandia mayi* McMinn 1988. 1–4. MWGUW ZI/90/P9/0, 15.5/7.6, EF R31/4; oblique ventral view of ventral (1) and dorsal (4) surfaces, and optical section (2, 3), operculum attached (indicated by an arrow); note the raspberry-like cyst appearance. 5–9. MWGUW ZI/90/P9/SEM/2, EF H18/3; oblique dorsal view of dorso-antapical surface (5, 7), and optical section (6); close-ups (8, 9) show the wall structure; note the lack of any tabulation features other than the archaeopyle, and the fragile and wavy nature of the thin ectophragm (ec) supported by processes and discontinuous muri (indicated by arrows). 10, 11. MWGUW ZI/90/Dz5/0d, 12/3.5, EF V29/0; oblique dorsal view of optical section; note the two-layered? inner wall structure (indicated by arrows). 12. MWGUW ZI/90/P9/0, 3.5/1.1, EF Y19/0; damaged specimen, optical section; note the apical horn (indicated by an arrow). 13–19. *Samlandia carnarvonensis* McMinn 1988, MWGUW ZI/90/P9/SEM/1, EF M36/0; dorsal view of dorsal (13, 16) and ventral (15) surfaces, and optical section (14); close-ups (17–19) show the wall structure; note the lack of any tabulation features other than the archaeopyle, the distinct apical horn, and the homogeneous nature of the autophragm (a); arrows indicate processes supporting the very thin and fragile ectophragm (ec); arrowheads indicate ectophragm edge.

Glaphyrocysta pala (Kirsch 1991) comb. nov.
Plate 12, figures 7–16

Synonymy.

1991 *Riculacysta*? *pala* Kirsch: p. 128, 129, pl. 32, figs 11–13, pl. 33, figs 2–4, 7, 8, text-fig. 61a–c.

2004 *Riculacysta*? *pala* Kirsch 1991 – Fauconnier in Fauconnier & Masure: p. 473, pl. 67, figs 1–6.

2004 *Glaphyrocysta expansa* (Corradini 1973) Roncaglia & Corradini 1997 – Landman, Johnson, & Edwards: fig. 8I–K.

2021 *Riculacysta*? *pala* Kirsch 1991 – Niechwedowicz & Walaszczyk: pl. 7, figs 7, 8.

Dimensions (minimum (mean) maximum).

Central body length (without operculum): 48 (55.2) 63 µm, central body width: 60 (68.2) 80 µm, total length (without operculum): 72 (97.5) 118 µm, total width: 111 (134.1)
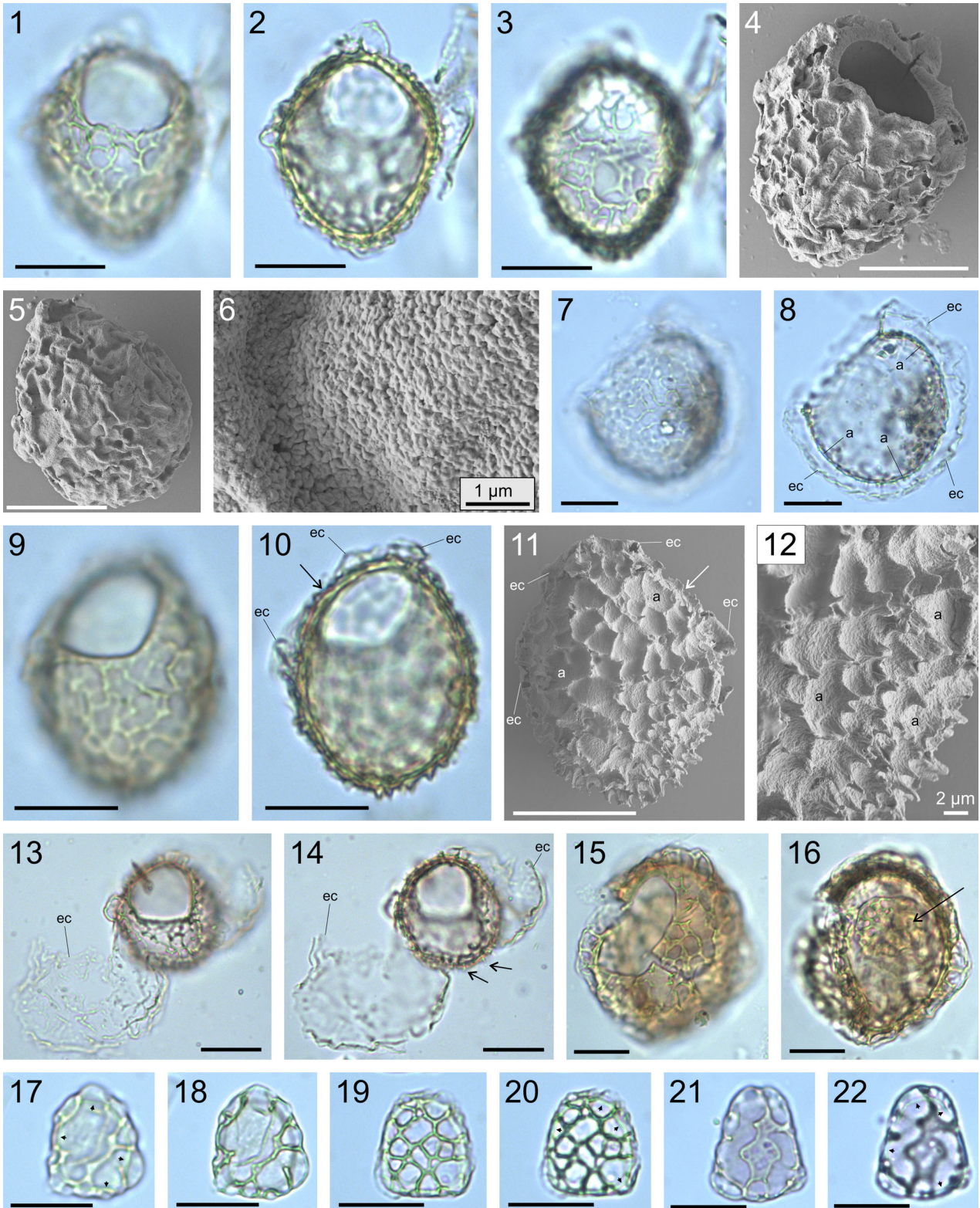
165 μm, maximal length of membrane: 37 (51.5) 68 μm, process length: up to 10 (15.7) 25 μm (22 specimens measured).

Remarks. Kirsch (1991, p. 128) questionably referred this species to the genus *Riculacysta*; however, he did not specify what his concerns were with his tentative assignment. Fauconnier (in Fauconnier and Masure 2004, p. 473) suggested it was based on the dorso-ventral compression of the central body in his species. The central body in *Riculacysta* is subspheroidal, and connected with the membrane by processes arising from the antapical, lateral, and mid-ventral cyst areas (see Stover 1977, p. 76, 77, pl. 2, figs 22, 25, 28). In contrast, *Glaphyrocysta* has generally marginate processes and/or membranes occupying the antapical and lateral periphery of a dorso-ventrally compressed central body (Fensome et al. 2009, p. 32). The present specimens are quite comparable with Kirsch's (1991) material, and confirm that *Glaphyrocysta pala* comb. nov. has a lenticular central body. Its antapical and lateral peripheries are connected with the membrane by short processes, but it lacks the processes on the mid-ventral cyst area. Consequently, it is transferred to the genus *Glaphyrocysta*.

Comparison. *Glaphyrocysta pala* comb. nov. is most comparable with *Glaphyrocysta expansa* (Corradini 1973) Roncaglia & Corradini 1997 and *Glaphyrocysta semitecta* (Bujak in Bujak et al. 1980) Lentin & Williams 1981. *Glaphyrocysta expansa* differs in having a smooth, unperforated membrane expanded antapically and laterally. In *G. pala* comb. nov., the membrane arises from the dorsal cyst side as in *G. semitecta*, and is typically shovel-shaped (not expanded near the archaeopyle edge; see Plate 12, figures 8, 9) and clearly perforate, with perforations irregular in size, shape and distribution (see Plate 12, figures 11, 13, 16). Additionally, *G. pala* comb. nov. has a characteristically low membranous flange surrounding the dorsal edge of the archaeopyle (Plate 12, figure 10). The dorsal surface of the central body is reticulate and generally lacks any sign of tabulation – only the cingulum is rarely discernible. The perforations in the membrane are a characteristic feature of *G. pala* comb. nov., and are similar to those present in *G. semitecta*, although in the latter the perforations are typically larger. Moreover, in *G. semitecta* the distalmost portion of the membrane is connected with the central body through long processes arising from the antapical and lateral cyst peripheries. *Glaphyrocysta pseudoreticulata* Vieira et al. 2017 differs from *G. pala* comb. nov. in

lacking a well-developed membrane, and in possessing more numerous processes, that are grouped into linear or arcuate complexes, usually connected distally by irregular trabeculae.

Stratigraphical comments. *Glaphyrocysta pala* comb. nov. first appeared in the latest Campanian with some other species of the genus (*G. expansa*, *G.* aff. *semitecta*, and *Glaphyrocysta* sp. A; Niechwedowicz and Walaszczyk 2021). This event illustrates the earliest significant radiation of the genus, which otherwise is more typical of the Paleogene (e.g. Fensome et al. 2016, 2019b). The wide geographical distribution of *G. pala* comb. nov. (see, e.g. Kirsch 1991; Slimani 2001; Torricelli and Amore 2003; Mohamed and Wagreich 2013) suggests it possesses considerable biostratigraphical value.

Recorded stratigraphical range. Uppermost Campanian–lowermost Maastrichtian, '*Inoceramus*' *redbirdensis* Zone–lower *Endocostea typica* Zone (recorded in Podole, Raj North, Kłudzie North, Kłudzie South, and Dziurków).

Glaphyrocysta aff. *semitecta* (Bujak in Bujak et al. 1980) Lentin & Williams 1981
Plate 12, figures 17–20

Synonymy.
2021 *Glaphyrocysta* aff. *semitecta* (Bujak in Bujak et al. 1980) Lentin & Williams 1981 – Niechwedowicz & Walaszczyk: pl. 7, figs 9, 10.

Dimensions (minimum (mean) maximum).
Central body length (operculum attached): 68 (72.3) 78 μm, central body width: 72 (75) 78 μm, total length (operculum attached): 118 (127.3) 144 μm, total width: 133 (140.5) 148 μm, maximal length of membrane: 50 (53.7) 59 μm, process length: up to 28 (34.3) 41 μm (four specimens measured).

Remarks. Some of the *Glaphyrocysta* specimens studied herein strongly resemble *G. semitecta* (Bujak in Bujak et al. 1980) Lentin & Williams 1981. Such forms have a significantly dorso-ventrally compressed central body, which is circular in outline (with an absence of antapical or apical lobes), and is distinctly reticulate on both the ventral and dorsal surfaces. The perforate membrane appears to arise from the dorsal cyst surface and turn towards the ventral cyst side. Its distal portion is connected with the central body by long processes (Plate 12, figures 17, 18). The studied specimens generally differ in having an attached operculum. *Glaphyrocysta semitecta*


Plate 11. Dinoflagellate cysts from the upper Campanian–lowermost Maastrichtian of the Middle Vistula River section, central Poland. Photomicrographs 1–3, 7–10, 13–22 taken with a transmitted light microscope; 4–6, 11, 12 taken by scanning electron microscopy; scale bars = 20 μm (unless otherwise specified). 1–14. *Samlandia carnarvonensis* McMinn 1988. 1–4. MWGUW ZI/90/P9/SEM/2, EF G27/2; dorsal view of dorsal (1, 4) and ventral (3) surfaces, and optical section (2); note the lack of any tabulation features other than the archaeopyle, and the distinct apical horn. 5, 6. MWGUW ZI/90/P9/SEM/1, EF K36/0; dorsal view; note the lack of any tabulation features; close-up (6) shows the ornament of the outer surface of the ectophragm. 7, 8. MWGUW ZI/90/P29/0e, 18.5/0.2, EF Z34/0; damaged specimen; right lateral view of right lateral surface (7), and optical section (8); note the lack of contact between the ectophragm (ec) and the processes arising from the autophragm (a). 9–12. MWGUW ZI/90/P9/SEM/2, EF E18/1; damaged specimen; oblique dorsal view of dorsal surface (9) and optical section (10), and oblique ventral view of ventral surface (11); close-up (12) shows the ornament of the outer surface of the autophragm (a dense and regular network of low muri and short processes); note the almost complete lack of ectophragm (ec), only partially preserved; note also the lack of any tabulation features other than the archaeopyle (indicated by arrows). 13, 14. MWGUW ZI/90/P29/0c, 13.6/14.1, EF K30/1; damaged specimen; dorsal view of dorsal surface (13), and optical section (14); note the almost complete mechanical separation of the ectophragm (ec); processes arising from the autophragm (ec) are indicated by arrows. 15, 16. *Samlandia* cf. *vermicularia* McMinn 1988, MWGUW ZI/90/Dz20/0a, 7.7/6.9, EF R23/4; oblique dorsal view of dorsal surface (15), and optical section (16); note the operculum (indicated by an arrow) placed inside the cyst. 17, 18. *Samlandia mayi* McMinn 1988, MWGUW ZI/90/P9/0j, 5.6/17, EF G22/0; isolated operculum; external view of external (17) and internal (18) surfaces; arrowheads indicate ectophragm edge. 19, 20. *Samlandia carnarvonensis* McMinn 1988, MWGUW ZI/90/P9/0m, 9.3/10.8, EF N28/0; isolated operculum; internal view of internal (19) and external (20) surfaces; arrowheads indicate ectophragm edge. 21, 22. *Samlandia* cf. *vermicularia* McMinn 1988, MWGUW ZI/90/P9/0d, 4.6/16.7, EF H20/1; isolated operculum; internal view of internal (21) and external (22) surfaces; arrowheads indicate ectophragm edge.

is a characteristic Eocene–Oligocene species (e.g. Bujak et al. 1980; Williams et al. 2004). The present specimens either prove that (i) *G. semitecta* first appeared in the Campanian (see also Mohamed and Wagreich 2013), or (ii) constitute a

separate, although similar species. The latter option seems to be more reasonable in the presented estimation.

Recorded stratigraphical range. Uppermost Campanian–lowermost Maastrichtian, '*Inoceramus*'
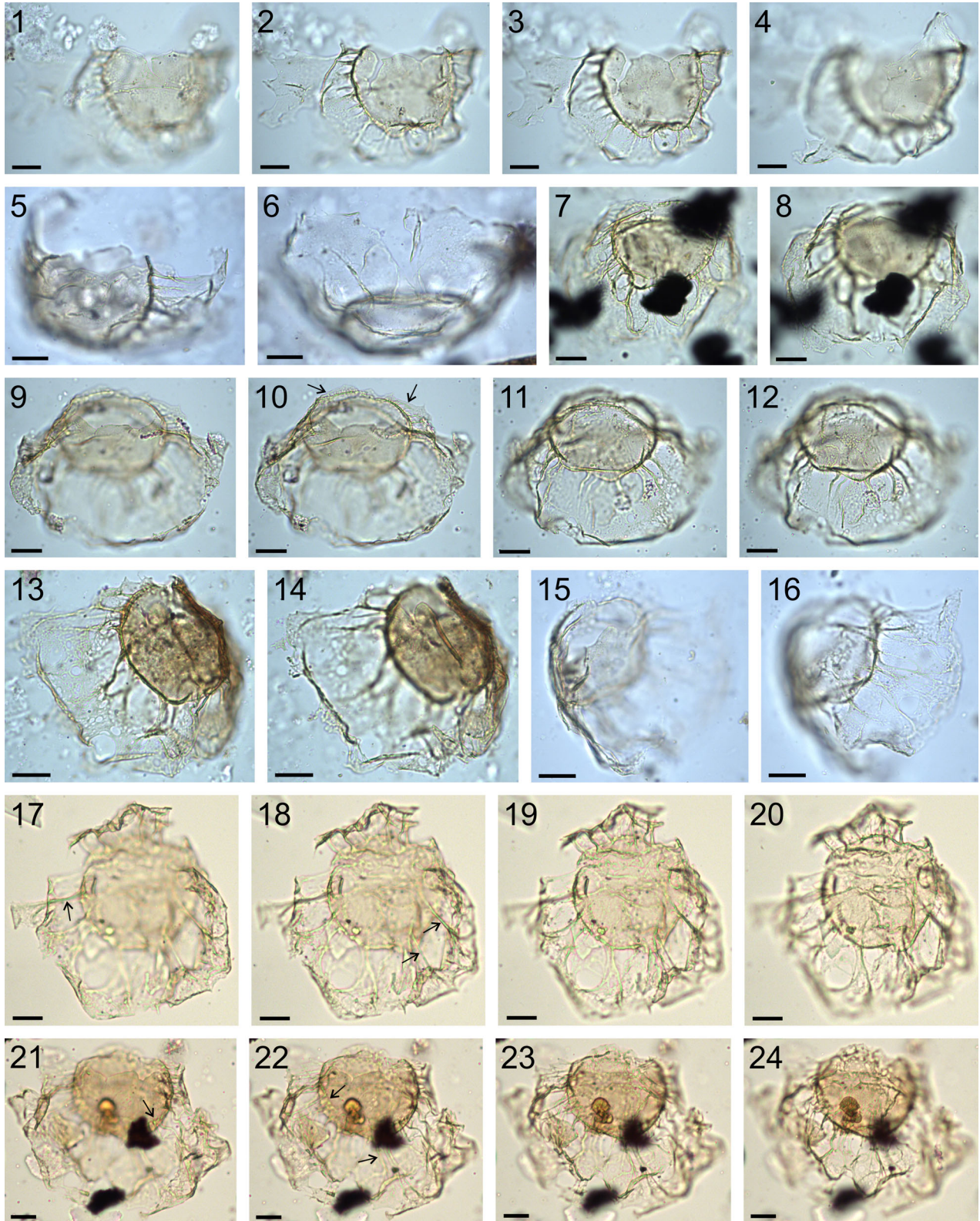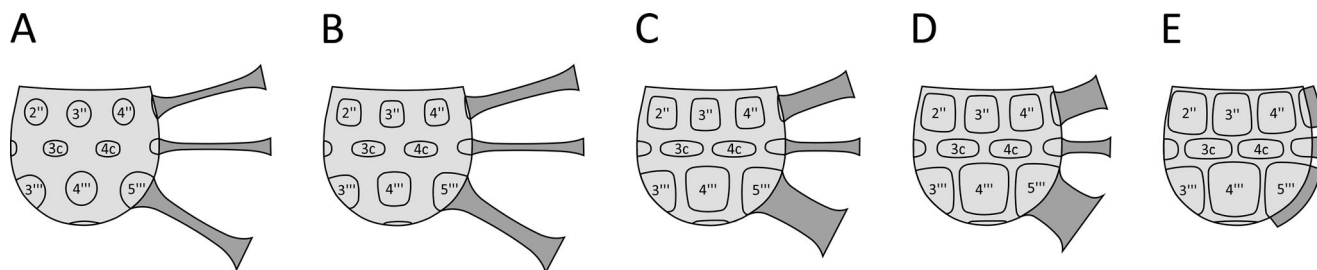
Figure 7. Schematic drawings showing the distribution and morphology (base shape and width, and relative length) of the dorsal projections in selected pyrodinioid species. A, *Hystrichosphaeridium tubiferum*; B, *Hystrichosphaeridium salpingophorum*; C, *Hystrichosphaeridium proprium*; D, *Hystrichosphaeridium brevispinum* stat. nov. (morphotype B); E, *Alisocysta circumtabulata*.

redbirdensis Zone–lower *Endocostea typica* Zone (recorded in Podole, Raj North, Kłudzie North, and Dziurków).

Glaphyrocysta sp. A
Plate 12, figures 21–24

Dimensions (minimum (mean) maximum).
Central body length (without operculum): 70 μm, central body width: 80 μm, total length (without operculum): 140 μm, total width: 179 μm, maximal length of membrane: 64 μm, process length: up to 55 μm.

Remarks. A single specimen from the collection studied represents a form different from all of the other known species of the genus, and is referred to here in open nomenclature as *Glaphyrocysta* sp. A. Its central body is circular in outline, with one weakly marked asymmetrical (left) indentation. It has a wide, highly perforate membrane similar to *Glaphyrocysta semitecta*, arising from a transverse furrow present on the dorsal surface of the central body, likely representing the cingulum. The membrane originates from the lower margin of the dorsal transverse furrow, surrounds the cyst antapex, and turns towards the ventral side, where it is the most distant from the central body. As in *G. semitecta*, the distal portion of the membrane is connected to the antapical and lateral cyst peripheries by long processes; however, in contrast to *G. semitecta* the connection is not formed by single processes, but by linear complexes composed of 3–5 solid processes (Plate 12, figures 21, 22). The membrane arising from the upper margin of the dorsal transverse furrow runs towards the dorsal archaeopyle edge, where it forms a membranous flange (Plate 12, figure 23) analagous to that present in *G. pala* comb. nov. or *G. semitecta*. The process complexes in *Glaphyrocysta* sp. A are probably penitabular and arise from the posterior and lateral margins of pre- and postcingular plates, partially reflecting the tabulation.

Recorded stratigraphical range. Lowermost Maastrichtian, middle part of the '*Inoceramus*' *redbirdensis* Zone (recorded in Kłudzie North, sample KN16).

Suborder **GONIODOMINEAE** Fensome et al. 1993
Family **GONIODOMACEAE** Lindemann 1928
Subfamily **PYRODINIOIDEAE** Fensome et al. 1993

Genus ***Hystrichosphaeridium*** Deflandre 1937

Synonymy.
1937 *Hystrichosphaeridium* Deflandre: p. 68.
1966 *Hystrichosphaeridium* Deflandre 1937 – Davey & Williams: p. 55, 56.

Type. *Hystrichosphaeridium tubiferum* (Ehrenberg 1837) Deflandre 1937.

Remarks. The tabulation formula of the genus (1pr, 4′, 6″, 6c, 6‴, 1p, 5 s, 1‴′) is clearly reflected in the arrangement of the processes (one mesotabular process per plate), distinguishable in all species of the genus except for *H*? *recurvatum* (see below). The operculum bears five processes, the slimmest of which is located at its centre and likely corresponds to the preapical plate (see also Lejeune-Carpentier 1940, text-fig. 4, re-illustrated by Evitt 1961, pl. 5, fig. 12; Morgenroth 1968, pl. 45, fig. 6, illustrated as *Hystrichokolpoma bulbosum*; Evitt 1985, fig. 11.4D). The preapical process in *Hystrichosphaeridium* may be developed to a variable extent, but is always present. It may be hollow and relatively wide, as in *H. brevispinum* stat. nov. (Plate 9, figures 3, 4), or may have a hollow base and tip with a solid process stem, as in *H. tubiferum* (Plate 7, figures 14–17).

In contrast to the description of Fensome et al. (2016, p. 50), the processes in *Hystrichosphaeridium* may proximally cover most of the underlying plate, which is exemplified by

Plate 12. Dinoflagellate cysts from the upper Campanian–lowermost Maastrichtian of the Middle Vistula River section, central Poland. All photomicrographs taken with a transmitted light microscope; scale bars = 20 μm. 1–6. *Glaphyrocysta expansa* (Corradini 1973) Roncaglia & Corradini 1997. 1–4. MWGUW ZI/90/Dz33/0a, 16.5/14, EF K32/0; oblique dorsal view of dorsal (1) and ventral (4) surfaces, and optical section (2, 3); note the signs of tabulation on the dorsal surface, and the smooth and laterally expanded membrane. 5. MWGUW ZI/90/Po42/0, 6.5/18.1, EF F23/0; oblique ventral view of dorsal surface. 6. MWGUW ZI/90/Po42/0a, 11.5/13.6, EF L28/2; apical view of antapical surface; note the smooth membrane. 7–16. *Glaphyrocysta pala* (Kirsch 1991) comb. nov. 7, 8. MWGUW ZI/90/Dz1/0, 19.8/7.1, EF S22/1; dorsal view of optical section (7) and ventral surface (8). 9–12. MWGUW ZI/90/KN16/0, 11.9/18.3, EF F27/0; oblique ventral view of ventral (9, 10) and dorsal (11, 12) surfaces; note the shovel-like shape of the membrane (it is not expanded laterally at the archaeopyle edge); the membranous flange surrounding the dorsal edge of archaeopyle is indicated by arrows. 13, 14. MWGUW ZI/90/KS3/0, 3.3/5.5, EF T19/3; oblique left lateral view of left lateral (13) and right lateral (14) surfaces; note the nature of the perforations (irregular in size, shape and distribution) in the membrane. 15, 16. MWGUW ZI/90/KS5/0b, 15/11, EF O32/0; oblique right lateral view of right lateral (15) and left lateral (16) surfaces; note the dorso-ventral compression of the central body, and the nature of the perforations in the membrane. 17–20. *Glaphyrocysta* aff. *semitecta* (Bujak in Bujak et al. 1980) Lentin & Williams 1981, MWGUW ZI/90/Po22/0a, 17.4/1.2, EF Y33/2; ventral view of ventral (17, 18) and dorsal (20) surfaces, and optical section (19), operculum attached; note the long processes (indicated by arrows) connecting the distal portion of the membrane with the central body periphery. 21–24. *Glaphyrocysta* sp. A, MWGUW ZI/90/KN16/0b, 7.3/16.9, EF G22/4; ventral view of ventral (21, 22) and dorsal (23, 24) surfaces; note the process complexes (indicated by arrows) connecting the distal portion of the membrane with the central body periphery.

the nature of process development in *H. brevispinum* stat. nov. and *H. proprium* (see Plate 8, figures 6–9, 14–16).

Hystrichosphaeridium brevispinum (Davey & Williams 1966) stat. nov.
Plate 8, figures 12–19; Plate 9, figures 1–4

Synonymy.
1966 *Hystrichosphaeridium tubiferum* (Ehrenberg 1837) Deflandre 1937 var. *brevispinum* Davey & Williams: p. 58, pl. 10, fig. 10.
1973 *Hystrichosphaeridium tubiferum* subsp. *brevispinum* (Davey & Williams 1966) Lentin & Williams: p. 80.
1992 *Hystrichosphaeridium proprium* subsp. *brevispinum* (Davey & Williams 1966) Marheinecke: p. 61, pl. 11, figs 7, 8.
1993 *Hystrichosphaeridium tubiferum* subsp. *brevispinum* (Davey & Williams 1966) Lentin & Williams 1973 – Lentin & Williams: p. 336.

Dimensions (minimum (mean) maximum).
Central body length (without operculum): 42 (42.7) 43 μm, central body width: 39 (43.3) 49 μm, process length: 12 (14.1) 16 μm, base width of dorsal postcingular processes: 11 (13.9) 17 μm, process length/central body width ratio: 0.3 (0.33) 0.35 (10 specimens measured).

Remarks. This species was originally designated as a variety of *Hystrichosphaeridium tubiferum* (Ehrenberg 1837) Deflandre 1937, and was subsequently treated as a subspecies (Lentin and Williams 1973). Marheinecke (1992, p. 61) proposed a new combination of this taxon (as *Hystrichosphaeridium proprium* subsp. *brevispinum*), arguing it had a considerable morphological resemblance to his *Hystrichosphaeridium proprium*, particularly in the shape of its processes. It is worth noting *H. proprium* was transferred to *Hystrichokolpoma* by Foucher in Fauconnier and Masure (2004, p. 283, 284); however, it is retained in *Hystrichosphaeridium* here (see below).

Hystrichosphaeridium brevispinum (Davey & Williams 1966) stat. nov. bears very characteristic processes, which are short (c. 1/3 of central body width) but relatively wide. These are the primary feature distinguishing between this species and *H. tubiferum*. The morphological distinction between these two species is even greater than that between *H. tubiferum* and *H. salpingophorum*, or between *H. salpingophorum* and *H. proprium* (see e.g. Marheinecke 1992, p. 58). There seem to be no objective reasons to treat this taxon a subspecies of *H. tubiferum*: consequently, it is raised here to species rank.

According to its original description (Davey and Williams 1966, p. 58), *H. brevispinum* stat. nov. differs from *H. tubiferum* due to its distinctly shorter processes. However, two morphological types have been attributed to *H. brevispinum* stat. nov., as observed by Ioannides (1986, p. 25). In the first morphotype, all of the processes have rounded cross sections (e.g. Ioannides 1986, p. 25; Kirsch 1991, p. 78), whereas in the second morphotype most of the processes are subangular (e.g. Ioannides 1986, p. 25; Marheinecke 1992, p. 61, pl. 11, figs 7, 8; Nøhr-Hansen 1996, pl. 16, figs 4–6). In the latter case, the cross-sections of precingular, postcingular, and cingular processes resemble the plate shapes, while the others (preapical, apical, antapical, and sulcal) are nearly rounded.

In the present material, both morphological varieties – rounded (morphotype A herein; Plate 9, figures 1, 2) and subangular (morphotype B herein; (Figure 7D; Plate 8, figures 12–19) – were encountered, although the latter were more frequent. *Hystrichosphaeridium brevispinum* stat. nov. morphotype B seems to be comparable to *Hystrichokolpoma mentitum* McLean 1974. They have the same appearance, and apparently the same tabulation (compare McLean 1974, p. 68, 69, pl. 8, figs 1–5, text-fig.1B). Intriguingly, the diagnosis of *H. mentitum* highlights its similarity to the genus *Eisenackia* Deflandre & Cookson 1955 (see McLean 1974, p. 69), which has pyrodinioid tabulation (e.g. Fensome et al. 1993). The generic assignment of McLean's (1974) species is likely incorrect, as previously noted by Damassa (1979b, p. 196), who suggested that McLean's specimens instead exhibit a hypocystal tabulation identical to that of *Alisocysta* Stover & Evitt 1978 (which also is a pyrodinioid genus).

The two morphotypes of *H. brevispinum* stat. nov. differ significantly from each other: they represent either two separate species (see also Ioannides 1986, p. 25) or considerable intraspecific variation. Davey and Williams (1966, p. 58) did not provide a detailed description of *H. brevispinum* stat. nov., and the shape of the process cross-sections cannot be clearly inferred from illustrations of the holotype alone (Davey and Williams 1966, pl. 10, fig. 10; Bujak et al. 1980, pl. 8, figs 10–12; Fauconnier and Masure 2004, pl. 47, figs 1–4). A more thorough examination of the type material is needed before a final taxonomic decision is reached.

Recorded stratigraphical range. Middle upper Campanian–lowermost Maastrichtian, '*Inoceramus*' *altus* Zone–lower *Endocostea typica* Zone (recorded in all sections studied except for Kłudzie South).

Hystrichosphaeridium proprium Marheinecke 1992
Plate 8, figures 6–11

Synonymy.
1968 *Hystrichokolpoma bulbosum* (Ehrenberg 1837) Morgenroth: pl. 45, fig. 1 (only).
?1985 *Hystrichosphaeridium* sp. cf. *tubiferum* (Ehrenberg 1837) Deflandre 1937 – Evitt: fig. 11.4 l.
1992 *Hystrichosphaeridium proprium* subsp. *proprium* Marheinecke: p. 60, pl. 11, figs 4–6.
1996 *Hystrichosphaeridium proprium* subsp. *proprium* Marheinecke 1992 – Nøhr-Hansen: pl. 16, figs 1–3.
2004 *Hystrichokolpoma proprium* (Marheinecke 1992) Foucher in Fauconnier & Masure: p. 283, 284, pl. 40, figs 1–7.

Dimensions (minimum (mean) maximum).
Central body length (without operculum): 34 (41.5) 52 μm, central body width: 36 (45.5) 58 μm, process length: 19 (22) 28 μm, base width of dorsal postcingular processes: 10 (12.7) 16 μm, process length/central body width ratio: 0.44 (0.48) 0.55 (23 specimens measured).

Remarks. This species was originally referred to the genus *Hystrichosphaeridium*. It was subsequently transferred to *Hystrichokolpoma* (by Foucher in Fauconnier and Masure 2004, p. 281), based on the presence of distally closed processes. In *Hystrichokolpoma* the processes may be open or

closed distally (e.g. Williams and Downie 1966, p. 176; Foucher in Fauconnier and Masure 2004, p. 281), whereas *Hystrichosphaeridium* is believed to have only open processes (e.g. Stover and Evitt 1978, p. 55; Pearce and Williams 2018, p. 18). However, it is worth noting the processes in *Hystrichosphaeridium* may also be closed distally by a thin membrane (see Evitt 1985, p. 253).

Basically, the two genera possess a very similar tabulation. The process formula in *Hystrichosphaeridium proprium* is 1pr, 4′, 6′′, 6c, 6′′′, 1p, 5 s, 1′′′′ (five sulcal processes correspond to plates ps, rs, ls, ras, as), and it is the same in *Hystrichosphaeridium tubiferum*, the type species of the genus. *Hystrichokolpoma* possibly lacks the pr process (see Williams and Downie 1966, p. 176; Stover and Evitt 1978, p. 54; Foucher in Fauconnier and Masure 2004, p. 281). The morphology of the processes in *Hystrichosphaeridium proprium* is characteristic of the other species of the genus (e.g. *H. salpingophorum* and *H. tubiferum*), but different from that in species belonging to *Hystrichokolpoma*. In *Hystrichokolpoma*, most of the pre- and postcingular processes are significantly wider than the cingular and sulcal processes (e.g. Stover and Evitt 1978; Fensome et al. 2009). In addition, as in other cribroperidinioids the process corresponding to plate 6′′ is significantly smaller than the other precingular processes in *Hystrichokolpoma*, and the processes arising from plates 1′′′ and 2′′′ are smaller than the other processes of this series (see e.g. Damassa 1979a, text-figs 4, 5A; Evitt 1985, fig. 7.5H). In contrast, in *Hystrichosphaeridium proprium* – and in other species of the genus, such as *H. salpingophorum* and *H. tubiferum* – all of the precingular processes and the 2′′′–6′′′ postcingular processes are roughly comparable in size, while the processes of the cingular and of the sulcal series are only slightly slimmer (see Figure 7). However, the most important difference between the two genera is in their respective plate arrangements. The configuration of plates in *H. proprium* indicates a largely neutral torsion of the hypocyst (the boundaries between plates 3′′/4′′ and 4′′′/5′′′ are nearly in line; see Plate 8, figures 9, 11), which can also be seen in the holotype (Marheinecke 1992, pl. 11, fig. 5; Fauconnier and Masure 2004, pl. 40, figs 1, 2). In contrast, *Hystrichokolpoma* – and other representatives of the subfamily Cribroperidinioideae – is characterised by a dextral torsion (see e.g. Damassa 1979a, text-fig. 5B; Fensome et al. 1993). Furthermore, *Hystrichosphaeridium proprium* has a typical goniodominean (quinqueform) hyposome (plate 1′′′′ is not in contact with plate 6′′′; see Plate 8, figure 10), while that in *Hystrichokolpoma* is sexiform (see Fensome et al. 1993). These differences in tabulation pattern are fundamental attributes of the underlying taxonomy. As such, the combination proposed by Foucher (in Fauconnier and Masure 2004) is here rejected, and this species is retained in the genus *Hystrichosphaeridium*.

Hystrichosphaeridium proprium is distinguishable from the other species of the genus by the shape and size of its processes (see Figure 7). The morphology of *H. proprium* falls between that of *H. salpingophorum* Deflandre 1935 ex Deflandre 1937 and *H. brevispinum* (Davey & Williams 1966) stat. nov. morphotype B. These three taxa have processes with subangular bases that roughly reflect the shape of the plates. *Hystrichosphaeridium proprium* differs from *H. salpingophorum* in having slightly shorter processes (in *H. proprium*, process length- = c. 1/2 of central body width) with wider bases and a better expressed subangularity. In general, the processes in *H. proprium* cover most of the underlying plate areas (see Plate 8, figures 6–9); for example, process bases of pre-, postcingular and cingular processes are visibly wider than the distances between particular processes of that plate series. In *H. brevispinum* stat. nov. morphotype B, the processes may be only slightly wider than those in *H. proprium*; however, they are distinctly shorter.

Recorded stratigraphical range. Middle upper Campanian–lowermost Maastrichtian, 'Inoceramus' altus Zone–lower *Endocostea typica* Zone (species recorded in all sections studied).

Hystrichosphaeridium? *recurvatum* (White 1842) Lejeune-Carpentier 1940
Plate 9, figures 9–17

Synonymy.
1842 *Xanthidium tubiferum* var. *recurvatum* White: p. 39, pl. 4, fig. 12.
1842 *Xanthidium tubiferum* var. *palmatum* White: p. 39, 40, pl. 4, fig. 12.
?1937 *Hystrichosphaeridium tubiferum* (Ehrenberg 1837) Deflandre: pl. 13 (also labelled pl. 10), fig. 2.
1940 *Hystrichosphaeridium recurvatum* (White 1842) Lejeune-Carpentier: p. B221–B222.
1965 *Hystrichosphaeridium palmatum* (White 1842) Downie & Sarjeant: p. 121 (combination illegitimate, according to Fensome et al. 2019a).
1980 *Hystrichosphaeridium recurvatum* (White 1842) Lejeune-Carpentier 1940 – May: p. 55, pl. 3, figs 18–20.
1989 *Hystrichosphaeridium duplum* Lentin & Williams: p. 181 (illegitimate name, according to Fensome et al. 2019a).
1991 *Hystrichosphaeridium duplum* Lentin & Williams 1989 – Kirsch: p. 77, 78, pl. 5, figs 7, 8.
1992 *Hystrichosphaeridium duplum* Lentin & Williams 1989 – Marheinecke: p. 62, pl. 11, fig. 9.
2016 *Hystrichosphaeridium recurvatum* (White 1842) Lejeune-Carpentier 1940 – Machalski, Vellekoop, Dubicka, Peryt, & Harasimiuk: fig. 6I.
2018 *Hystrichosphaeridium tubiferum* (Ehrenberg 1837) Deflandre 1937 – FitzPatrick, Forber, & Hart: fig. 6D.
2018 *Hystrichosphaeridium recurvatum* (White 1842) Lejeune-Carpentier 1940 – Pearce & Williams, pl. 1, figs 1, 5.

Dimensions (minimum (mean) maximum).
Central body length (without operculum): 27 (31.1) 38 μm, central body width: 25 (28.7) 36 μm, process length: 24 (27.7) 32 μm, process base width: 3 (4.1) 6 μm, process length/central body width ratio: 0.8 (0.97) 1.1 (19 specimens measured). Isolated operculum: process length: 24 μm, process base width: 4 μm (two opercula measured).

Remarks. Although similar in overall appearance to other *Hystrichosphaeridium* species, this taxon diverges from them in some key morphological aspects. In *H*? *recurvatum*, all the processes are comparable in size and morphology: they have

circular bases, constant width and length (the latter roughly equal to the central body diameter), and terminate with 5–6 short (c. 5 μm) spines commonly curved towards the central body. The monotonous process development distinguishes *H? recurvatum* from *H. tubiferum*, *H. proprium*, and *H. salpingophorum*, in which the cingular, sulcal, and apical processes are slightly slimmer than the others; the difference is especially evident in comparison with the dorsal postcingular processes. Furthermore, *H? recurvatum* differs from other *Hystrichosphaeridium* in the number of processes. It may have more processes in particular latitudinal series, but the pr process is absent (Plate 9, figures 16, 17). In *H? recurvatum*, cingular processes are commonly more densely spaced on the dorsal cyst side (Plate 9, figure 13), while those on the ventral side (Plate 9, figure 14) are sparsely arranged, which may suggest the presence of two processes per cingular plate or a variable number of processes per plate (the process formula of the specimen illustrated in Plate 9, figures 13, 14 is 4′, 6′′, 8c, 6′′′, 1p, 5 s, 1′′′′). The number of processes in other plate series may also be higher (the specimen lacking operculum, illustrated in Plate 9, figures 9–12, has 35 processes). In *Hystrichosphaeridium*, all of the processes are mesotabular (one per plate), and their number is invariant from specimen to specimen. *Hystrichosphaeridium? recurvatum* is also very similar to *Fetchamium prolixispinosum* (Davey & Williams 1966) Pearce & Williams 2018 in overall morphology: the latter also has processes of uniform size and morphology, but with a reduced number of cingular and sulcal processes (0–4c, 1–3 s; see Pearce and Williams 2018, p. 19). Consequently, *H? recurvatum* is questionably left here in *Hystrichosphaeridium*.

Recorded stratigraphical range. Middle upper Campanian–lowermost Maastrichtian, '*Inoceramus*' *altus* Zone–lower *Endocostea typica* Zone (species recorded in all sections studied).

Hystrichosphaeridium salpingophorum Deflandre 1935 ex Deflandre 1937
Plate 7, figures 21–24; Plate 8, figures 1–5

Synonymy.
1935 *Hystrichosphaera salpingophora* Deflandre: p. 232, pl. 9, fig. 1.
1937 *Hystrichosphaeridium salpingophorum* Deflandre: p. 70, pl. 13 (also labelled pl. 10), figs 1, 3.
1966 *Hystrichosphaeridium salpingophorum* Deflandre 1935 ex Deflandre 1937 – Davey & Williams: p. 61, 62.
1968 *Hystrichokolpoma bulbosum* (Ehrenberg 1837) Morgenroth: pl. 44, figs 6, 7 (only).
?1985 *Hystrichosphaeridium* sp. cf. *tubiferum* (Ehrenberg 1837) Deflandre 1937 – Evitt: fig. 11.4 l.
1988 *Hystrichosphaeridium salpingophorum* Deflandre 1935 ex Deflandre 1937 – Wrenn & Hart: p. 355.
1991 *Hystrichosphaeridium salpingophorum* Deflandre 1935 ex Deflandre 1937 – Kirsch: p. 78, pl. 4, figs 10, 11.
1992 *Hystrichosphaeridium salpingophorum* Deflandre 1935 ex Deflandre 1937 – Marheinecke: p. 63, pl. 12, fig. 3.
2016 *Hystrichosphaeridium tubiferum* (Ehrenberg 1837) Deflandre 1937 – Riding & Lucas-Clark, pl. 7, figs 3, 4.

Dimensions (minimum (mean) maximum).
Central body length (without operculum): 28 (38.3) 47 μm, central body width: 27 (38.6) 50 μm, process length: 20 (25.2) 32 μm, base width of dorsal postcingular processes: 6 (9.6) 12 μm, process length/central body width ratio: 0.57 (0.65) 0.79 (31 specimens measured).

Remarks. *Hystrichosphaeridium salpingophorum* has a subspheroidal to ovoidal central body. The processes are mesotabular, with expanded bases and tips; in individual specimens, they are comparable in length (c. 2/3 of central body width) but variable in width (as in *H. tubiferum* or *H. proprium*). The process width generally depends on the plate series from which they derive. The slimmest are the processes of the sulcal, cingular, and apical series (especially 1′ and 4′), as well as the processes corresponding to plates 1′′′ and pr. The rest of the postcingular and precingular processes are roughly comparable in width (3′′′–5′′′ are usually the widest processes; see Plate 8, figure 5). The shapes of the process bases and terminations roughly reflect the shapes of the plates, so the pre- and postcingular processes are subangular or subquadrate, while the cingular processes have oval cross-sections (Figure 7B; Plate 8, figure 5). Distally, the processes bear spines that are prolonged from the faint longitudinal striae, with the most prominent spines (3–5 μm in length) arising from the corners of subquadrate process termination (Plate 7, figures 21, 24).

The main feature that differentiates this species from *H. tubiferum* is the subquadrate termination of some of its processes (e.g. Deflandre 1937; Deflandre and Cookson 1955; Davey and Williams 1966; Ioannides 1986; Kirsch 1991), although the distinction may not necessarily be obvious (see Davey and Williams 1966, p. 62; Ioannides 1986, p. 26). In the present material, the process stems and terminations were commonly deformed (withered in appearance) in both species, which obscures their true shape and renders their differentiation impossible. In this respect, the material studied here is quite comparable with that of Marheinecke (1992). However, the illustration of the holotype [Deflandre 1937, pl. 13 (also labelled pl. 10), fig. 1] clearly indicates that the process bases and terminations are of the same shape. The pre- and postcingular processes in *H. salpingophorum* have subquadrate or subangular bases, whereas they are rounded in *H. tubiferum* (Figure 7A,B). Thus, the shape of process bases is considered here the most valuable feature in distinguishing between these two species (compare also Wrenn and Hart 1988, p. 355; Marheinecke 1992, p. 59, 63).

Morgenroth (1968) significantly widened the concept of *Hystrichokolpoma bulbosum* (Ehrenberg 1837) Morgenroth 1968, including into it several forms showing distinct morphological variability of the processes. But most of the specimens illustrated by Morgenroth as *H. bulbosum* are clearly *Hystrichosphaeridium* species, and referable to *H. tubiferum* (Morgenroth 1968, pl. 45, figs 4–6), *H. proprium* (Morgenroth 1968, pl. 45, fig. 1) and *H. salpingophorum* (Morgenroth 1968, pl. 44, figs 6, 7 (sic)). Moreover, Morgenroth (1968) designated a specimen conspecific with *Hystrichosphaeridium salpingophorum* as the neotype of *Hystrichokolpoma bulbosum* (Morgenroth 1968, pl. 44, fig. 6; according to Stover and Evitt

1978, p. 55, specimen referable to *H. tubiferum*). As a consequence of this emendation, Stover and Evitt (1978, p. 55) considered *H. bulbosum* a junior synonym of *H. tubiferum*, which was later rejected by Lentin and Williams (1981, p. 134).

Recorded stratigraphical range. Middle upper Campanian–lowermost Maastrichtian, '*Inoceramus*' *altus* Zone–lower *Endocostea typica* Zone (species recorded in all sections studied).

Hystrichosphaeridium tubiferum (Ehrenberg 1837) Deflandre 1937
Plate 7, figures 11–20

Synonymy.
1837 *Xanthidium tubiferum* Ehrenberg: pl. 1, fig. 16.
1937 *Hystrichosphaeridium tubiferum* (Ehrenberg 1837) Deflandre: p. 68.
1966 *Hystrichosphaeridium tubiferum* (Ehrenberg 1837) Deflandre 1937 – Davey & Williams: p. 56–58, pl. 6, figs 1, 2, text-fig. 13.
1968 *Hystrichokolpoma bulbosum* (Ehrenberg 1837) Morgenroth: pl. 45, figs 4–6 (only).
1980 *Hystrichosphaeridium tubiferum* (Ehrenberg 1837) Deflandre 1937 – May: p. 55, 56, pl. 3, figs 12–14.
1985 *Hystrichosphaeridium tubiferum* (Ehrenberg 1837) Deflandre 1937 – Evitt: figs 7.5G, 11.4 D–G.
1992 *Hystrichosphaeridium tubiferum* subsp. *tubiferum* (autonym) – Marheinecke: p. 59, pl. 11, figs 1–3.

Dimensions (minimum (mean) maximum).
Central body length (without operculum): 31 (36.5) 51 μm, central body width: 32 (38.6) 43 μm, process length: 19 (24) 29 μm, base width of dorsal postcingular processes: 6 (7.6) 9 μm, process length/central body width ratio: 0.58 (0.62) 0.67 (15 specimens measured).

Remarks. *Hystrichosphaeridium tubiferum* is very similar to *H. salpingophorum*. Both species have processes of constant length, varying in width on a single specimen (see above) with expanded bases and tips: the main distinction is that all of the process bases (and terminations) in *H. tubiferum* are rounded (see Figure 7A). While the process bases are also rounded in *H*? *recurvatum*, its processes are relatively longer (as compared with the central body diameter), comparable in width, and have a different style of terminations. Furthermore, *H*? *recurvatum* differs in the number of processes and lacks the pr process (see above).

Under TLM, the central body wall of *H. tubiferum* is smooth to granular (as in *H. salpingophorum*), but SEM study proves that it is homogeneous to spongy in structure: it could be described either as an autophragm or as an endo- and periphragm. The innermost part of the central body wall (c. 0.1–0.2 μm) appears to be more homogeneous, forming a continuous level that could be referred to as endophragm (see Plate 7, figure 20). If this is the case, then the thin-walled (c. 0.2–0.5 μm) processes in *H. tubiferum* are not formed from the entire periphragm (c. 1–1.5 μm thick), but only from its outermost portion. In any case, the process walls in *H. tubiferum* are distinctly thinner than the central

body wall (compare, e.g. with the thickness of walls in *Kleithriasphaeridium loffrense*; Plate 9, figures 18–21).

Recorded stratigraphical range. Middle upper Campanian–lowermost Maastrichtian, '*Inoceramus*' *altus* Zone–lower *Endocostea typica* Zone (species recorded in all sections studied).

5. Conclusions

The new dinoflagellate cyst species *Oligosphaeridium araneum* sp. nov. is consistently present throughout the succession, appearing first in the middle upper Campanian ('*Inoceramus*' *altus* Zone). Outside central Poland, the species (illustrated as *Oligosphaeridium pulcherrimum* in Herngreen et al. 1998) is known from the lowermost Danian of the Netherlands and potentially has stratigraphical significance.

In the new combination *Glaphyrocysta pala* comb. nov., the species *pala* is transferred from the genus *Riculacysta* to *Glaphyrocysta*, based on its lenticular (dorso-ventrally compressed) central body and the absence of mid-ventral processes connecting the central body with the membrane. The lenticular shape of the central body was already noticed by Kirsch (1991, p. 128), apparently leading him to provisionally attribute the species to *Riculacysta* (Fauconnier in Fauconnier and Masure 2004, p. 473). Differentiating between *Samlandia carnarvonensis* and *S. mayi* has been troublesome to date (Antonescu et al. 2001a, 2001b). Using both TLM and SEM microscopy techniques, it is possible to identify the most evident features differentiating the two species: namely, the height of the ectocoel cavations and the inner cyst wall ornament. In *S. mayi*, the ectophragm is significantly more distant from the inner cyst wall (? endo- and periphragm, or an autophragm) and connected to it by the discontinuous muri and long processes distally joined by arch-shaped trabeculae, giving the impression of an imperfect (commonly discontinuous) and sparse reticulum. In contrast, the inner cyst wall (an autophragm) in *S. carnarvonensis* is covered by a dense network of low crests forming a clear and regular reticulum. The ectophragm, which in *S. carnarvonensis* is located distinctly closer to the autophragm (the holocavate nature of the wall structure may be difficult to recognise under TLM), is supported by thin and short processes arising from the muri. The connection between the ectophragm and the process tips in *S. carnarvonensis* is, however, rather weak. Consequently, the ectophragm can be mechanically separated. Such specimens lacking the ectophragm may be confused with *Pyxidinopsis bakonyensis*. *Samlandia mayi* is more similar to *Samlandia paucitabulata*, another taxon characteristic of the upper Campanian. *Samlandia paucitabulata* differs from *S. mayi* in having signs of tabulation reflected by the arrangement of wall features, while the latter is atabulate. Furthermore, *S. paucitabulata* possesses a distinctly thicker, more robust, and regularly outlined ectophragm.

The distribution of processes, sutural ridges, and septa in *Callaiosphaeridium*, documented here using TLM and SEM, revealed that the tabulation pattern in the genus is characterised by a sexiform antapex, L-type ventral configuration, and neutral torsion of hypocyst, which enables the

attribution of the genus to the subfamily Leptodinioideae. Moreover, all of the processes (including the tubular ones) in *Callaiosphaeridium* are shown to be gonal in position. A leptodinioid tabulation pattern was also recognised in *Amphorosphaeridium*, based on the distribution of the processes in *A. fenestratum*. *Amphorosphaeridium* and *Callaiosphaeridium*, and their type species, are emended accordingly.

An analysis of the genera *Hystrichosphaeridium* and *Hystrichokolpoma* suggests that the species *proprium* should be re-transferred back to *Hystrichosphaeridium*, which accords with the original affiliation proposed by Marheinecke (1992). The arrangement of processes in this species clearly reflects a pyrodinioid tabulation, rather than a cribroperidinioid pattern (the latter is typical for *Hystrichokolpoma*). Consequently, the transfer of *H. proprium* to *Hystrichokolpoma* proposed by Foucher (in Fauconnier and Masure 2004) is here rejected. Additionally, one new status, *H. brevispinum* stat. nov., is proposed. This taxon is raised to the species level on the basis of the distinct morphology of its processes, which concurs with features widely used to differentiate species within the genus. *Hystrichosphaeridium*? *recurvatum*, another morphologically related chorate species, is questionably left in *Hystrichosphaeridium*, although it possesses a variable number of processes between individual specimens, the common presence of more than one process per plate, and the lack of a preapical process. These features are not typical for *Hystrichosphaeridium*.

Acknowledgements

Disclosure statement

No potential conflict of interest was reported by the author.

Notes on contributor

MARIUSZ NIECHWEDOWICZ is a curator of the palaeontological collection at the S.J. Thugutt Geological Museum (Faculty of Geology, University of Warsaw, Poland). He obtained his MSc (stratigraphy and palaeontology) at the Faculty of Geology of the University of Warsaw in 2003. For several years he was involved in ammonoid palaeobiology and the palaeoenvironmental importance of this group. After being introduced to palynology in 2014, Mariusz started his PhD project on the systematics, biostratigraphy, and palaeoecological significance of the Campanian–Maastrichtian organic-walled dinoflagellate cysts of central Poland.

ORCID

Mariusz Niechwedowicz 🆔 http://orcid.org/0000-0002-1967-2945

References

Aleksandrova GN, Beniamovskii VN, Vishnevskaya VS, Zastrozhnov AS. 2012. New data on Upper Cretaceous biostratigraphy of the Lower Volga Region. Stratigraphy and Geological Correlation. 20(5):426–465.

Antonescu E, Foucher JC, Odin GS. 2001a. Les kystes de dinoflagellés de la carrière de Tercis les Bains (Landes, France). In: Odin GS, editor. The Campanian–Maastrichtian stage boundary: characterisation at Tercis les Bains (France) and correlation with Europe and other continents. IUGS special publication (monograph) series, 36. Developments in palaeontology and stratigraphy, Vol. 19; p. 235–252.

Antonescu E, Foucher JC, Odin GS, Schiøler P, Siegl-Farkas A, Wilson GJ. 2001b. Dinoflagellate cysts in the Campanian–Maastrichtian succession of Tercis Les Bains (Landes, France), a synthesis. In: Odin GS, editor. The Campanian–Maastrichtian stage boundary: characterisation at Tercis les Bains (France) and correlation with Europe and other continents. IUGS special publication (monograph) series, 36. Developments in palaeontology and stratigraphy, Vol. 19; p. 253–264.

Below R. 1981. Dinoflagellaten-Zysten aus dem oberen Hauterive bis unteren Cenoman Süd-West-Marokkos. Palaeontographica, Abteilung B. 176:1–145.

Bujak JP, Downie C, Eaton GL, Williams GL. 1980. Dinoflagellate cysts and acritarchs from the Eocene of Southern England. Special Papers in Palaeontology. 24:1–100.

Clarke RFA, Verdier J-P. 1967. An investigation of microplankton assemblages from the Chalk of the Isle of Wight, England. Verhandelingen der Koninklijke Nederlandse Akademie van Wetenschappen, Afdeeling Natuurkunde, Eerste Reeks. 24:1–96.

Corradini D. 1973. Non-calcareous microplankton from the Upper Cretaceous of the Northern Apennines. Bollettino Della Societá Paleontológica Italiana. 11:119–197.

Damassa SP. 1979a. Eocene dinoflagellates from the Coastal Belt of the Franciscan Complex, northern California. Journal of Paleontology. 53: 815–840.

Damassa SP. 1979b. Danian dinoflagellates from the Franciscan Complex, Mendocino County, California. Palynology. 3(1):191–207.

Damassa SP. 1984. Morphologic variability and paraplate configuration of the dinoflagellate genus *Danea* Morgenroth 1968. Palynology. 8(1): 51–69.

Davey RJ. 1969. The evolution of certain Upper Cretaceous hystrichospheres from South Africa. Palaeontologia Africana. 12:25–51.

Davey RJ. 1979. Two new Early Cretaceous dinocyst species from the northern North Sea. Palaeontology. 22:427–437.

Davey RJ, Williams GL. 1966. The genus *Hystrichosphaeridium* and its allies. In: Davey RJ, Downie C, Sarjeant WAS, Williams GL, editors. Studies on Mesozoic and Cainozoic dinoflagellate cysts. Bulletin of the British Museum (Natural History) Geology, Supplement. 3:53–106.

Deflandre G. 1935. Considérations biologiques sur les microorganismes d'origine planctonique conservés dans les silex de la craie. Bulletin Biologique de la France et de la Belgique. 69:213–244.

Deflandre G. 1937. Microfossiles des silex crétacés. Deuxième partie. Flagellés incertae sedis. Hystrichosphaeridés. Sarcodinés. Organismes divers. Annales de Paléontologie. 26:51–103.

Deflandre G, Cookson IC. 1955. Fossil microplankton from Australian Late Mesozoic and Tertiary sediments. Marine and Freshwater Research. 6(2):242–313.

Deflandre G, Courteville H. 1939. Note préliminaire sur les microfossiles des silex crétacés du Cambrésis. Bulletin de la société française de microscopie. 8:95–106.

Downie C, Sarjeant WAS. 1965. Bibliography and index of fossil dinoflagellates and acritarchs. Geological Society of America. Memoir. 94: 1–180. [cover date December, 1964, issue date January, 1965].

Dubicka Z, Peryt D. 2012. Latest Campanian and Maastrichtian palaeoenvironmental changes: implications from an epicontinental sea (SE Poland and western Ukraine). Cretaceous Research. 37:272–284.

Duxbury S. 1980. Barremian phytoplankton from Speeton, east Yorkshire. Palaeontographica, Abteilung B. 173:107–146.

Duxbury S. 1983. A study of dinoflagellate cysts and acritarchs from the Lower Greensand (Aptian to Lower Albian) of the Isle of Wight, southern England. Palaeontographica, Abteilung B. 186:18–80.

Ehrenberg CG. 1837. Über das Massenverhältniss der jetzt lebenden Kiesel-Infusorien und über ein neues Infusorien-Conglomerat als Polirschiefer von Jastraba in Ungarn. Abhandlungen der Königlichen Akademie der Wissenschaften zu Berlin, aus dem Jahre 1836, Physikalische Klasse, p. 109–135.

Eisenack A. 1954. Mikrofossilien aus Phosphoriten des samländischen Unteroligozäns und über die Einheitlichkeit der Hystrichosphaerideen. Palaeontographica, Abteilung A. 105:49–95.

Evitt WR. 1961. Observations on the morphology of fossil dinoflagellates. Micropaleontology. 7(4):385–420.

Evitt WR. 1985. Sporopollenin dinoflagellate cysts: their morphology and interpretation. Dallas (TX): American Association of Stratigraphic Palynologists; p. 1–333.

Fauconnier D, Masure E, co-ordinators. 2004. Les dinoflagellés fossile. Guide pratique de détermination. Les genres à processus et à archéopyle apical. Orléans: BRGM Editions; p. 1–602.

Fensome RA, Nøhr-Hansen H, Williams GL. 2016. Cretaceous and Cenozoic dinoflagellate cysts and other palynomorphs from the western and eastern margins of the Labrador–Baffin Seaway. Geus Bulletin. 36:1–143.

Fensome RA, Taylor FJR, Norris G, Sarjeant WAS, Wharton DI, Williams GL. 1993. A classification of fossil and living dinoflagellates. Micropaleontology Press Special Paper. 7:1–351.

Fensome RA, Williams GL, MacRae RA. 2009. Late Cretaceous and Cenozoic fossil dinoflagellates and other palynomorphs from the Scotian Margin, offshore Eastern Canada. Journal of Systematic Palaeontology. 7(1):1–79.

Fensome RA, Williams GL, MacRae RA. 2019a. The Lentin and Williams index of fossil dinoflagellates 2019 edition. American Association of Stratigraphic Palynologists, Contributions Series. 50:1–1173.

Fensome RA, Williams GL, Wood SEL, Riding JB. 2019b. A review of the areoligeracean dinoflagellate cyst Cyclonephelium and morphologically similar genera. Palynology. 43(sup1):1–71.

FitzPatrick MEJ, Forber DA, Hart MB. 2018. Dinocyst stratigraphy and palaeoenvironmental interpretation of the Cretaceous/Paleogene boundary at Stevns Klint. Cretaceous Research. 87:408–421.

González F. 2012. Software for universally relocating specific points of interest on microscope slides. Marine Micropaleontology. 96-97:63–65.

Habib D, Miller JA. 1989. Dinoflagellate species and organic facies evidence of marine transgression and regression in the Atlantic Coastal Plain. Palaeogeography, Palaeoclimatology, Palaeoecology. 74(1-2): 23–47.

Harding IC. 1990. A dinocyst calibration of the European Boreal Barremian. Palaeontographica, Abteilung B. 218:1–76.

Helenes J. 2000. Exochosphaeridium alisitosense n. sp., a new gonyaulacoid dinoflagellate from the Albian of Baja California. Micropaleontology. 46(2):135–142.

Herngreen GFW, Schuurrnan HAHM, Verbeek JW, Brinkhuis H, Burnett JA, Felder WM, Kedves M. 1998. Biostratigraphy of Cretaceous/Tertiary boundary strata in the Curfs quarry, the Netherlands. Mededelingen Nederlands Lnstituut Voor Toegepaste Geowetenschappen. 61:1–57.

Ioannides NS. 1986. Dinoflagellate cysts from Upper Cretaceous–Lower Tertiary sections, Bylot and Devon Islands, Arctic Archipelago. Geological Survey of Canada, Bulletin. 371:1–99.

Jurkowska A, Świerczewska-Gładysz E, Bąk M, Kowalik S. 2019. The role of biogenic silica in the formation of Upper Cretaceous pelagic carbonates and its palaeoecological implications. Cretaceous Research. 93: 170–187.

Keutgen N, Remin Z, Walaszczyk I. 2012. Early representatives of the belemnite genus Belemnella (Cephalopoda) from the uppermost Campanian–Lower Maastrichtian of the Middle Vistula River section, central Poland. Acta Geologica Polonica. 62(4):535–559.

Khowaja-Ateequzzaman, Garg R. 2004. Callaiosphaeridium scabratum sp. nov. – a new dinoflagellate cyst species from Early Turonian of the Cauvery Basin, India. Palaeobotanist. 53:97–103.

Kirsch K-H. 1991. Dinoflagellatenzysten aus der Oberkreide des Helvetikums und Nordultrahelvetikums von Oberbayern. Münchner Geowissenschaftliche Abhandlungen, Reihe A, Geologie Und Paläontologie. 22:1–306.

Kurita H, Mcintyre DJ. 1994. Dinoflagellate assemblages and depositional environments of the Campanian Bearpaw Formation, Alberta. Geological Survey of Canada, Bulletin. 479:67–83.

Landman NH, Johnson RO, Edwards LE. 2004. Cephalopods from the Cretaceous/Tertiary boundary interval on the Atlantic Coastal Plain, with a description of the highest ammonite zones in North America. Part 2. Northeastern Monmouth County, New Jersey. Bulletin of the American Museum of Natural History. 287:1–107.

Lejeune-Carpentier M. 1940. L'étude microscopique des silex. Systématique et morphologie des "tubifères". (Huitième note.). Annales de la Société géologique de Belgique. 63:B216–B236.

Lentin JK, Williams GL. 1973. Fossil dinoflagellates: index to genera and species. Geological Survey of Canada, Paper 73-42:1–176.

Lentin JK, Williams GL. 1981. Fossil dinoflagellates: index to genera and species, 1981 edition Bedford Institute of Oceanography, Report Series no. BI-R-81-12:1–345.

Lentin JK, Williams GL. 1989. Fossil dinoflagellates: index to genera and species, 1989 edition. American Association of Stratigraphic Palynologists, Contributions Series. 20:1–473.

Lentin JK, Williams GL. 1993. Fossil dinoflagellates: index to genera and species. 1993 edition. American Association of Stratigraphic Palynologists, Contributions Series. 28:1–856.

Machalski M. 2012a. Stratigraphically important ammonites from the Campanian–Maastrichtian boundary interval of the Middle Vistula River section, central Poland. Acta Geologica Polonica. 62(1):91–116.

Machalski M. 2012b. A new ammonite zonation for the Maastrichtian Stage in Poland. In: Jagt JWM, Jagt-Yazykova EA, editors. The Maastrichtian stage; the current concept, Natuurhistorisch Museum Maastricht/Centre Ceramique 6-8 September 2012, Workshop programme, abstracts and field guide. Natuurhistorisch Museum Maastricht, The Netherlands, p. 40–44.

Machalski M, Vellekoop J, Dubicka Z, Peryt D, Harasimiuk M. 2016. Late Maastrichtian cephalopods, dinoflagellate cysts and foraminifera from the Cretaceous-Paleogene succession at Lechówka, southeast Poland: stratigraphic and environmental implications. Cretaceous Research. 57:208–227.

Marcinowski R. 1980. Cenomanian ammonites from German Democratic Republic, Poland, and the Soviet Union. Acta Geologica Polonica. 30: 215–325.

Marcinowski R, Radwański A. 1983. The mid-Cretaceous transgression onto the Central Polish Uplands (marginal part of the Central European Basin). Zitteliana. 10:65–95.

Marheinecke U. 1992. Monographie der Dinozysten, Acritarcha und Chlorophyta des Maastrichtium von Hemmoor (Niedersachsen). Palaeontographica, Abteilung B. 227:1–173.

May FE. 1980. Dinoflagellate cysts of the Gymnodiniaceae. Peridiniaceae, and Gonyaulacaceae from the Upper Cretaceous Monmouth Group, Atlantic Highlands, New Jersey. Palaeontographica, Abteilung B 172:10–116.

McLean DM. 1974. Two new Paleocene dinoflagellates from Virginia and Maryland. Palaeontology. 17:65–70.

McMinn A. 1988. Outline of a Late Cretaceous dinoflagellate zonation of northwestern Australia. Alcheringa: An Australasian Journal of Palaeontology. 12(2):137–156.

Mohamed O, Wagreich M. 2013. Organic-walled dinoflagellate cyst biostratigraphy of the Well Höflein 6 in the Cretaceous–Paleogene Rhenodanubian Flysch Zone (Vienna Basin, Austria). Geologica Carpathica. 64(3):209–230.

Mohr BAR, Mao S. 1997. Maastrichtian dinocyst floras from Maud Rise and Georgia Basin (Southern Ocean): their stratigraphic and paleo-environmental implications. Palynology. 21(1):41–65.

Morgenroth P. 1968. Zur Kenntnis der Dinoflagellaten und Hystrichosphaeridien des Danien. Geologisches Jahrbuch. 86:533–578.

Niechwedowicz M. 2018a. *Odontochitina dilatata* sp. nov. from the Campanian (Upper Cretaceous) of Poland: the importance of wall structure in the taxonomy of selected ceratiacean dinoflagellate cysts. Palynology. 43(3):423–450.

Niechwedowicz M. 2018b. Dinoflagellate cyst assemblages as a tool in local biostratigraphic correlation: an example from the upper Campanian (Upper Cretaceous) of the Middle Vistula River section, central Poland. In: Pšenička J, Frojdová J, Svobodová A, Dašková J, editors. 19th Czech-Slovak-Polish Palaeontological Conference & Mikro 2018 workshop, abstract book. Folia, Special Volume 2018, p. 63.

Niechwedowicz M, Walaszczyk I. 2021. Dinoflagellate cysts of the upper Campanian–basal Maastrichtian (Upper Cretaceous) of the Middle Vistula River section (central Poland): stratigraphic succession, correlation potential and taxonomy. Newsletters on Stratigraphy. DOI:10.1127/nos/2021/0639.

Nøhr-Hansen H. 1996. Upper Cretaceous dinoflagellate cyst stratigraphy, onshore West Greenland. Grønlands Geologiske Undersøgelse Bulletin 170:1–104.

Odin GS, Lamaurelle MA. 2001. The global Campanian–Maastrichtian stage boundary. Episodes. 24(4):229–238.

Pearce MA, Williams GL. 2018. *Fetchamium prolixispinosum* gen. et comb. nov. (division Dinoflagellata). Journal of Micropalaeontology. 37(1):17–20.

Peyrot D. 2011. Late Cretaceous (Late Cenomanian–Early Turonian) dinoflagellate cysts from the Castilian Platform, northern Spain. Palynology. 35(2):267–300.

Plasota T, Nawrocki J, Walaszczyk I. 2015. Magnetostratigraphy of the Campanian/Maastrichtian boundary succession from the Middle Vistula River section, central Poland. Geological Quarterly. 59(4):831–842.

Pożaryski W. 1938. Stratygrafia senonu w przełomie Wisły między Rachowem i Puławami. Biuletyn Państwowego Instytutu Geologicznego. 6:1–94.

Pożaryski W. 1974. Tektonika, cz. 1. Niż Polski. In: Pożaryski W, editor. Budowa geologiczna Polski. Warszawa: Wydawnictwa Geologiczne; p. 2–34.

Remin Z. 2012. The *Belemnella* stratigraphy of the Campanian–Maastrichtian boundary; a new methodological and taxonomic approach. Acta Geologica Polonica. 62(4):495–533.

Remin Z. 2015. The *Belemnitella* stratigraphy of the Upper Campanian–basal Maastrichtian of the Middle Vistula section, central Poland. Geological Quarterly. 59(4):783–813.

Riding JB, Lucas-Clark J. 2016. The life and scientific work of William R. Evitt (1923–2009). Palynology. 40(sup1):2–131.

Roncaglia L, Corradini D. 1997. Correlation of key dinoflagellate events with calcareous nannoplankton and planktonic foraminiferal zones in the Solignano Formation (Maastrichtian, Late Cretaceous), northern Apennines, Italy. Review of Palaeobotany and Palynology. 97(1-2):177–196.

Schiøler P, Wilson GJ. 2001. Dinoflagellate biostratigraphy around the Campanian–Maastrichtian boundary at Tercis les Bains, southwest France. In: Odin GS, editor. The Campanian–Maastrichtian stage boundary: characterisation at Tercis les Bains (France) and correlation with Europe and other Continents. IUGS special publication (monograph) series, 36. Developments in palaeontology and stratigraphy, Vol. 19; 221–234.

Siegl-Farkas A. 2001. Palynological examination of samples from the Campanian–Maastrichtian succession at Tercis les Bains: a preliminary view on spores and pollen. In: Odin GS, editor. The Campanian–Maastrichtian stage boundary: characterisation at Tercis les Bains (France) and correlation with Europe and other Continents. IUGS special publication (monograph) series, 36. Developments in palaeontology and stratigraphy, Vol. 19; p. 187–191.

Skupien P, Mohamed O. 2008. Campanian to Maastrichtian palynofacies and dinoflagellate cysts of the Silesian Unit, Outer Western Carpathians, Czech Republic. Bulletin of Geosciences. 83:207–224.

Slimani H. 2000. Nouvelle zonation aux kystes de dinoflagellés du Campanien au Danien dans le nord et l'est de la Belgique et dans le sud-est des Pays-Bas. Memoirs of the Geological Survey of Belgium. 46:1–88.

Slimani H. 2001. Les kystes de dinoflagellés du Campanien au Danien dans la région de Maastricht (Belgique, Pays-Bas) et de Turnhout (Belgique): biozonation et corrélation avec d'autres régions en Europe occidentale. Geologica et Palaeontologica. 35:161–201.

Slimani H, Louwye S, Dusar M, Lagrou D. 2011. Connecting the Chalk Group of the Campine Basin to the dinoflagellate cyst biostratigraphy of the Campanian to Danian in borehole Meer (northern Belgium). Netherlands Journal of Geosciences - Geologie en Mijnbouw. 90(2-3):129–164.

Stover LE. 1977. Oligocene and Early Miocene dinoflagellates from Atlantic Corehole 5/5B, Blake Plateau. American Association of Stratigraphic Palynologists, Contributions Series 5A:66–89.

Stover LE, Evitt WR. 1978. Analyses of pre-Pleistocene organic-walled dinoflagellates. Stanford University Publications, Geological Sciences 15:1–300.

Surlyk F, Rasmussen SL, Boussaha M, Schiøler P, Schovsbo NH, Sheldon E, Stemmerik L, Thibault N. 2013. Upper Campanian–Maastrichtian holostratigraphy of the eastern Danish Basin. Cretaceous Research. 46:232–256.

Torricelli S, Amore MR. 2003. Dinoflagellate cysts and calcareous nannofossils from the Upper Cretaceous Saraceno Formation (Calabria, Italy): implications about the history of the Liguride Complex. Rivista Italiana di Paleontologia e Stratigrafia. 109:499–516.

Walaszczyk I. 1987. Mid-Cretaceous events at the marginal part of the Central European Basin (Annopol-on-Vistula section, central Poland). Acta Geologica Polonica. 37:61–74.

Walaszczyk I. 1992. Turonian through Santonian deposits of the Central Polish Uplands; their facies development, inoceramid palaeontology and stratigraphy. Acta Geologica Polonica. 42:1–122.

Walaszczyk I. 2004. Inoceramids and inoceramid biostratigraphy of the Upper Campanian to basal Maastrichtian of the Middle Vistula River section, central Poland. Acta Geologica Polonica. 54:95–168.

Walaszczyk I. 2012. Integrated stratigraphy of the Campanian–Maastrichtian boundary succession of the Middle Vistula River (central Poland) section; introduction. Acta Geologica Polonica. 62(4):485–493.

Walaszczyk I. 2015. Integrated stratigraphy of the Campanian/Maastrichtian boundary succession of the Middle Vistula River section, central Poland: part II. Geological Quarterly. 59(4):781–782.

Walaszczyk I, Dubicka Z, Olszewska-Nejbert D, Remin Z. 2016. Integrated biostratigraphy of the Santonian through Maastrichtian (Upper Cretaceous) of extra-Carpathian Poland. Acta Geologica Polonica. 66(3):321–350.

Walaszczyk I, Odin GS, Dhondt AV. 2002. Inoceramids from the Upper Campanian and Lower Maastrichtian of the Tercis section (SW France), the Global Stratotype Section and Point for the Campanian–Maastrichtian boundary; taxonomy, biostratigraphy and correlation potential. Acta Geologica Polonica. 52:269–305.

White HH. 1842. On fossil *Xanthidia*. Microscopical Journal, London. 11:35–40.

Williams GL, Brinkhuis H, Pearce MA, Fensome RA, Weegink JW. 2004. Southern Ocean and global dinoflagellate cyst events compared: index events for the Late Cretaceous–Neogene. In: Exon NF, Kennett JP, Malone MJ, editors. Proceedings of the Ocean Drilling Program, Scientific Results. 189:1–98.

Williams GL, Downie C. 1966. The genus *Hystrichokolpoma*. In: Davey RJ, Downie C, Sarjeant WAS, Williams GL, editors. Studies on Mesozoic and Cainozoic dinoflagellate cysts. Bulletin of the British Museum (Natural History) Geology, Supplement. 3:176–181.

Williams GL, Fensome RA, Miller MA, Sarjeant WAS. 2000. A glossary of the terminology applied to dinoflagellates, acritarchs and prasinophytes, with emphasis on fossils. American Association of Stratigraphic Palynologists, Contributions Series. 37:1–370.

Wrenn JH, Hart GF. 1988. Paleogene dinoflagellate cyst biostratigraphy of Seymour Island, Antarctica. Geological Society of America, Memoir. 169:321–447.

Appendix

List of genera and other taxa mentioned in this study, arranged in alphabetical order (*: illustrated taxa). References not provided here are given in Fensome et al. (2019a).

Actinotheca Cookson & Eisenack 1960a

Alisocysta Stover & Evitt 1978

* *Alisocysta circumtabulata* (Drugg 1967) Stover & Evitt 1978

Amphorosphaeridium Davey 1969

* *Amphorosphaeridium fenestratum* Davey 1969

Avellodinium Duxbury 1977

Callaiosphaeridium Davey & Williams 1966

* *Callaiosphaeridium asymmetricum* (Deflandre & Courteville 1939) Davey & Williams 1966

* *Callaiosphaeridium bicoronatum* Niechwedowicz in Niechwedowicz & Walaszczyk 2021

Callaiosphaeridium trycherium Duxbury 1980

Cladopyxidium McLean 1972

Cordosphaeridium Eisenack 1963b

Eisenackia Deflandre & Cookson 1955

Exochosphaeridium Davey et al. 1966

Exochosphaeridium alisitosense Helenes 2000

* *Exochosphaeridium majus* (Lejeune-Carpentier 1940) Peyrot 2011

Fetchamium Pearce & Williams 2018

Fetchamium prolixispinosum (Davey & Williams 1966) Pearce & Williams 2018

Fibrocysta Stover & Evitt 1978

Glaphyrocysta Stover & Evitt 1978

Glaphyrocysta castelcasiensis subsp. *prominenta* (Marheinecke 1992) Michoux & Soncini in Fauconnier & Masure 2004

* *Glaphyrocysta expansa* (Corradini 1973) Roncaglia & Corradini 1997

* *Glaphyrocysta pala* (Kirsch 1991) comb. nov.

Glaphyrocysta perforata Hultberg & Malmgren 1985

Glaphyrocysta pseudoreticulata Vieira et al. 2017

Glaphyrocysta retiintexta (Cookson 1965a) Stover & Evitt 1978

Glaphyrocysta semitecta (Bujak in Bujak et al. 1980) Lentin & Williams 1981

* *Glaphyrocysta* aff. *semitecta* (Bujak in Bujak et al. 1980) Lentin & Williams 1981

* *Glaphyrocysta* sp. A

Heslertonia Sarjeant 1966b

Hystrichokolpoma Klumpp 1953

Hystrichokolpoma bulbosum (Ehrenberg 1837) Morgenroth 1968

Hystrichokolpoma mentitum McLean 1974

Hystrichosphaeridium Deflandre 1937

* *Hystrichosphaeridium brevispinum* (Davey & Williams 1966) stat. nov. (morphotype A)

* *Hystrichosphaeridium brevispinum* (Davey & Williams 1966) stat. nov. (morphotype B)

* *Hystrichosphaeridium proprium* Marheinecke 1992

* *Hystrichosphaeridium? recurvatum* (White 1842) Lejeune-Carpentier 1940

* *Hystrichosphaeridium salpingophorum* Deflandre 1935 ex Deflandre 1937

* *Hystrichosphaeridium tubiferum* (Ehrenberg 1837) Deflandre 1937

* *Kleithriasphaeridium loffrense* Davey & Verdier 1976

Odontochitina Deflandre 1937

Odontochitina dilatata Niechwedowicz 2018a

Oligosphaeridium Davey & Williams 1966

Oligosphaeridium abaculum Davey 1979

* *Oligosphaeridium araneum* sp. nov.

* *Oligosphaeridium* complex (White 1842) Davey & Williams 1966

* *Oligosphaeridium intermedium* Corradini 1973

* *Oligosphaeridium perforatum* (Gocht 1959) Davey & Williams 1969

Oligosphaeridium perforatum? subsp. *colum* Duxbury 1983

Oligosphaeridium pulcherrimum (Deflandre & Cookson 1955) Davey & Williams 1966

Operculodinium Wall 1967

Pervosphaeridium Yun Hyesu 1981

* *Pervosphaeridium elegans* Louwye 1997

* *Pervosphaeridium tubuloaculeatum* Slimani 1994

Pyxidinopsis Habib 1976

Pyxidinopsis bakonyensis (Góczán 1962) Stover & Evitt 1978

Riculacysta Stover 1977

Samlandia Eisenack 1954

* *Samlandia carnarvonensis* McMinn 1988

Samlandia chlamydophora Eisenack 1954

* *Samlandia mayi* McMinn 1988

Samlandia paucitabulata Niechwedowicz in Niechwedowicz & Walaszczyk 2021

Samlandia vermicularia McMinn 1988

* *Samlandia* cf. *vermicularia* McMinn 1988

Spiniferites Mantell 1850

Spiniferites procerus Marheinecke 1992

Spiniferites pseudofurcatus (Klumpp 1953) Sarjeant 1970

Spiniferites ramosus (Ehrenberg 1837) Mantell 1854

Turbiosphaera Archangelsky 1969a

Xenascus Cookson & Eisenack 1969